Biochemical investigation of hyperforin-related prenyltransferases expressed in *Saccharomyces cerevisiae*

Von der Fakultät für Lebenswissenschaften

der Technischen Universität Carolo-Wilhelmina zu Braunschweig

zur Erlangung des Grades eines

Doktors der Naturwissenschaften

(Dr. rer. nat.)

genehmigte

D i s s e r t a t i o n

von Marco Grull
aus Eberswalde-Finow

1. Referent: Professor Dr. Ludger Beerhues
2. Referent: Professor Dr. Rainer Krull
eingereicht am: 19.02.2018
mündliche Prüfung (Disputation) am: 01.06.2018

Druckjahr 2018

Vorveröffentlichungen der Dissertation

Teilergebnisse aus dieser Arbeit wurden mit Genehmigung der Fakultät für Lebenswissenschaften, vertreten durch den Mentor der Arbeit, in folgenden Beiträgen vorab veröffentlicht:

Vorträge:

Grull M., Gaid M., Liu B., Fiesel T., Beuerle T., Ernst L., Beerhues L. **Metabolic engineering of *S. cerevisiae* for the recombinant production of hyperforin precursor molecules.**
Konferenz: SPhERe "Symposium on Pharmaceutical Engineering Research", 06.09 – 08.09.2017, Braunschweig, Deutschland.

Grull M., Liu B., Gaid M., Fiesel T., Beuerle T., Ernst L., Beerhues L. **Produktion von Hyperforin-Vorstufen in genetisch veränderter Hefe.**
Pharmazie-Seminar, 19.06.2017, Braunschweig, Deutschland

Poster:

Grull M., Gaid M., Liu B., Fiesel T., Beuerle T., Ernst L., Beerhues L. **Metabolic engineering of *S. cerevisiae* for the recombinant production of hyperforin precursor molecules.**
Konferenz: SPhERe "Symposium on Pharmaceutical Engineering Research", 06.09 – 08.09.2017, Braunschweig, Deutschland.

Grull M., Liu B., Gaid M., Fiesel T., Beuerle T., Ernst L., Beerhues L. **Metabolic engineering of *S. cerevisiae* for the recombinant production of hyperforin precursor molecules.**
Konferenz: „ProcessNet-Jahrestagung und 32. DECHEMA-Jahrestagung der Biotechnologen" 2016. 12.09 – 15.09.2016, Aachen, Deutschland.

Grull M., Fiesel T., Beuerle T., Gaid M., Beerhues L. **Expression of hyperforin-related prenyltransferases in yeast.**

Konferenz: SPhERe “Symposium on Pharmaceutical Engineering Research”, 19.10 – 20.10.2015, Braunschweig, Deutschland.

Grull M., Patz S., Fiesel T., Gaid M., Beerhues L. **Expression of plant-derived prenyltransferases in yeast for the production of hyperforin and related compounds.**

DECHEMA Summer school, “Quantitative Biology: Current concepts and tools for strain development”, 20.07 – 24.07.2015, Berlin, Deutschland.

„Die Neugier steht immer an erster Stelle eines Problems, das gelöst werden will.“

Galileo Galilei (1564 – 1642)

Die folgenden Personen wurden während dieser Promotion betreut. Diese Doktorarbeit enthält Ergebnisse aus den unten genannten angefertigten Arbeiten. Die unten aufgeführten Personen und Ergebnisse werden in den entsprechenden Paragraphen benannt.

1. Svenja Patz (Master-Student): Aktivitätsbasiertes Substratscreening einer episomal und genomintegrierten aromatischen Prenyltransferase aus *Hypericum perforatum* in Hefe. 09.2015

2. David Quast (Bachelor-Student): Biosynthese der Hyperforin-Vorstufe Phlorisobutyrophenon in *Saccharomyces cerevisiae*. 02.2016

3. Henning Ummethum (Bachelor-Student): Biosynthese der Hyperforin-Vorstufe Phlorisobutyrophenon in *Saccharomyces cerevisiae*. 08.2016

4. Sandra Grünhoff und Karna Meyer (Forschungspraktikantinnen): Optimierung und Expression von pflanzlichen Prenyltransferasen in Hefe zur Herstellung von Hyperforin. 08.2015

Acknowledgments

I would especially like to thank Prof. Ludger Beerhues for giving me the opportunity to work on such an interesting and challenging project. I would also like to thank him for his great support and scientific discussions during the last three years.

I would like to thank Prof. Krull for being the second referee of my PhD thesis. I would also like to thank him for giving me the opportunity to work in his well-equipped laboratory during the lab internship.

Another thanks goes to Prof. Ute Wittstock, who has agreed to be the head of the examination board.

Dr. Mariam Gaid is acknowledged for her tremendous scientific support during the entire PhD project. I am very grateful for her helpful discussions and advice, even though it was already Saturday evening. Thanks also for her great help in writing this thesis. Without you, the project would not have been so successful like it was.

I would also like to thank Dr. Benye Liu for his fruitful discussions and his support throughout the PhD project. Thanks for the friendly working atmosphere also with the students.

Dr. Till Beuerle is acknowledged for his support for the analytical work (MS). In the same context, thousand thanks to Prof. Luger Ernst for his professional effort to evaluate all NMR samples for this project.

I´m especially grateful to Svenja Patz, David Quast, Henning Ummethum, Sandra Grünhoff, and Karna Meyer for their great support. Thank you all for your great work.

Another thanks to Sebastian Tesche for the funny evenings we had. With and without the home-brewed. May IOTA brings us the desired island.
A big thank goes to Sarah Hinkel for the great time as a PhD speaker and the many house parties she organized. I really enjoyed working with her.

I would also like to say a big thank you to both working groups of the IPB for the great atmosphere. I really enjoyed working with all of you. Thanks to Ines Rahaus for all the funny conversations.

Thanks to all the colleagues of the µ-Props PhD program, I´m happy to have met you all. A big thank you to the state of Lower Saxony, which provided the financial resources for the program. In this context, I would like to sincerely thank Prof. Heike Bunjes and Prof. Dietzel, who launched the µ-Props program. I would also like to thank both for being able to join the µ-Props committee for three years. Thank you, it was a great experience. Dr. Gerlinde Benninger is acknowledged for giving me the opportunity to work in the PVZ. Thanks many times, I really learned a lot.

Of course, I would also like to thank my long-time friends Moritz, Julian, Lölö and Yenn for the exciting time in my life. I don´t want to miss the time with you.

I am also mentally with the relatives who unfortunately are no longer with us.

Last but not least, I would like to say thank you to the people who have been my faithful companions for some decades now. This is of course my whole family (mother, father and sister) and relatives. Thanks for all your support in the recent years. Special thanks goes to my grandmother, who send me almost every day new funny pictures at Whatsapp.

My last thanks go to my girlfriend Shohana for the exciting last three years and her patience with me. I hope we will experience many more years together. I'm looking forward to the new challenges that we will jointly meet. Thank you for being with me.

Abstract

Hypericum perforatum, known as St. John´s wort, is one of the most famous and best investigated medicinal plants. It is commonly used for the treatment of mild to moderate depression. Hyperforin was identified as an important constituent to be responsible for the major pharmaceutical effects of the extract. However, it is a light, oxygen, and temperature sensitive hydrophobic acylphloroglucinol derivative with one geranyl and several prenyl side chains. Its biosynthetic pathway is not yet completely understood. As proposed, the biosynthesis of hyperforin starts with the formation of the core structure, phlorisobutyrophenone (PIBP), catalyzed by a type III polyketide synthase. The subsequent decoration of PIBP with the prenyl and geranyl groups is catalyzed by membrane-bound aromatic prenyltransferase (PT) enzymes.

The aim of the present project was the identification and characterization of enzymes that are involved in hyperforin biosynthesis. Four consecutive enzymes encoding an acyl-CoA ligase (*Hp*IBCL), an isobutyrophenone synthase (*Hp*IBS) and two successive PTs were functionally expressed in *Saccharomyces cerevisiae.* The first step was the *de novo* biosynthesis of the hyperforin skeleton PIBP. Therefore, cDNAs encoding *Hp*IBCL and *Hp*IBS had been cloned from *H. perforatum*. Feeding isobutyric acid to *S. cerevisiae* harboring either episomal or genome-integrated *Hp*IBCL and *Hp*IBS resulted in the formation of intracellular and extracellular PIBP.

In total, twelve PTs were individually expressed in *S. cerevisiae*. One PT (*Hp*PT2) was identified to catalyze the GPP-dependent geranylation of acylphloroglucinol derivatives, preferably PIBP and 2-methylbutyrophenone (2-MBP). A second PT (*Hp*PT6) catalyzed the addition of one prenyl group to the *Hp*PT2 product, forming the hyperforin precursor 3-geranyl-5-prenyl-PIBP. The biochemical properties of both PTs were further characterized. They showed typical characteristics of plant-derived PTs, such as dependency on divalent cations, alkaline pH optimum, and the relatively broad acceptor substrate specificity. The K_M values of *Hp*PT2 for 2-MBP and PIBP were 85 ± 15 µM and 124 ± 19 µM, respectively. The K_M values of *Hp*PT6 for 3-geranyl-2-MBP, 3-geranyl-PIVP, and 3-geranyl-PIBP were 73 ± 10, 78 ± 8.6, and 181 ± 218, respectively. These results confirm the identification of the first PT enzymes involved in hyperforin biosynthesis. Formation of the hyperforin precursor by *Hp*PT2 and *Hp*PT6 in *S. cerevisiae* stimulates further research efforts into this promising approach.

Table of content

1. Introduction

1.1. White and red biotechnology, the new era

Biotechnology involves the application of organisms such as bacteria, yeast cells and plants to manufacture and/or modify products for commercial purposes. Biotechnological production processes have many advantages compared to chemical manufacturing processes. Especially the usability of renewable resources instead of fossil raw materials is expected to completely change many future manufacturing processes [1].

Many different industrial branches discover and elevate the potential of e.g. microbial fermentation processes to produce nutraceuticals, cosmetics, flavors, fragrances, lubricants, fuels, and polymers [2–6]. The use of microbial biocatalyst has many attractive advantages compared to chemical catalysis. This involves environmentally friendly reaction conditions such as low temperature, atmospheric pressure and neutral pH. Additionally, microorganisms can produce highly valuable and complex structures, which would require multiple reaction steps in chemical synthesis processes. The major bottleneck using microbial production processes is still the low product yield. The commonly used microbial production hosts are *Escherichia coli* (*E. coli*) and the baker´s yeast (*Saccharomyces cerevisiae*) [7].

S. cerevisiae is one of the most interesting and most commonly used eukaryotic organisms for industrial production processes. It belongs to the best-investigated organisms regarding its metabolic profile, molecular genetic tools, and experience with cultivation methods. Furthermore, it is tolerant against low pH and stable against autolysis [8]. This enables cultivations at low pH to reduce the risk of contamination and facilitates long cultivation processes. Nowadays, *S. cerevisiae* is used for the production of a large variety of different compounds such as proteins, foods, beverages, bulk chemicals, biofuels, pharmaceuticals, and plant secondary metabolites [9].

1.2. Plant secondary metabolites

Many plant secondary metabolites are useful and highly valuable compounds with a broad range of applications as pharma- and nutraceuticals [10]. They are divided into three main classes based on their biosynthetic pathways: 1) (poly-) phenols derived from the malonate (polyketide) pathway and/or shikimate pathway, 2) terpenoids derived from the mevalonic acid (MVA) pathway and/or the methylerythritol phosphate (MEP) pathway, and 3) nitrogen-containing constituents (alkaloids) derived from either aliphatic amino acids (tricarboxylic acid cycle) or aromatic acids (shikimic acid pathway) (Figure 1) [11].

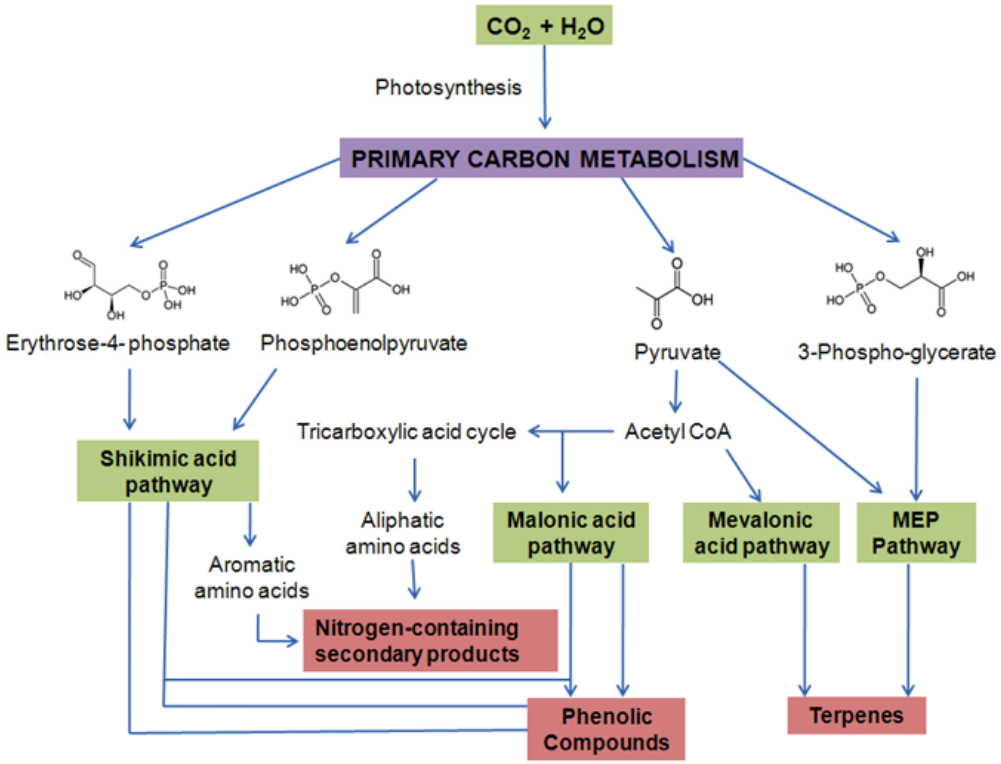

Figure 1. Overview of the biosynthesis of plant secondary metabolites. The biosynthesis starts with the primary carbon metabolism, which involves important routes, such as the shikimic acid, malonic acid, mevalonic acid, and MEP pathways. The major classes of plant secondary metabolites are formed *via* the latter pathways (Chaturvedi 2012) [155].

One branch of plant secondary metabolism leads to acylphloroglucinols and xanthones, which exhibit various pharmacologically interesting effects and applications and are substituted by C_5 – C_{20} isoprene units [12]. The isoprenoid substitution of the aromatic ring system increases the lipophilicity, thereby increasing the penetration tendency of the molecules through biological membranes [13]. The mentioned plant

secondary metabolites are discovered widely distributed throughout the plant kingdom including Guttiferae (Clusiaceae), Leguminosae (Fabaceae), Cannabaceae, and Hypericaceae [13].

A broad range of biological activities has been reported for (poly)prenylated (poly)phenols, e.g., anti-tumor, anti-bacterial, anti-viral, anti-oxidant, anti-tyrosinase, and estrogenic properties as well as sulfotransferases, nitric oxide, and phospholipase inhibitory activities[14]. The isolation of plant constituents is still very challenging, and the product yield obtained from the native production system is commonly low. Natural upscaling of plant systems requires large areas and long developing phases (up to one year). Furthermore, the reproducible production of the required product is expected to be environmentally dependent.

The transfer of plant biosynthetic pathways into heterologous expression systems is very promising for future production processes of plant secondary metabolites. Metabolic engineering of the target host can overcome the upscaling challenges using plant systems to enable the recombinant production of plant constituents. Yeasts have been already genetically modified for the production of plant secondary metabolites, such as terpenoid taxadiene as a precursor molecule for the production of taxol [15]; fragrances and flavors like vanillin [16,17]; artemisinic acid as the precursor of the antimalarial artemisinin, [18]; the polyphenolic heart-protective compound resveratrol [19,20]; carotenoids as vitamin A precursors with coloring and antioxidant properties [21]; sulfur-rich amino acid-derived indolylglucosinolate as potential anti-cancer agent [10]; the anti-inflammatory, antiviral, and antitumoral compound naringenine [22], as well as long-chain fatty acids utilized as high value compounds, e.g. lubricants, detergents, and polymers [23].

1.3. *Hypericum perforatum*, the medicinal plant

The genus *Hypericum* belongs to the family of the Hypericaceae, which comprises 496 species including trees, shrubs, and herbs [24,25]. The most famous species known is the herb *Hypericum perforatum* (*H. perforatum*), also known as St. John´s wort. The latter name was given due to traditional reasons because it is flowering and harvested on the St John´s Day (24th of June, Figure 4). *H. perforatum* is one of the best investigated medicinal plants worldwide. It can be found all over the world, but it is majorily originated in parts of Europe and Asia. The typical herb size ranges from 15 to 100 cm, having an erected stem that branches in the upper part. The leaves are oblong in shape, yellow-green in color, and 1–2 cm long. The leaves look like "perforated" due to the transparent translucent glands containing essential oil, giving the plant its Latin species name. The flowers are colored in bright yellow and about 2-3 cm in diameter [26].

In 2014, the plant was selected medicinal plant of the year due to its traditional and topically diverse medical applications [156]. Since hundreds of years, it is used in the form of tinctures and oils for either oral or external admission. Medical applications include the treatment of skin injuries, sunburns, cramps, and diarrhea. Recent research also identified effects such as antimicrobial, antioxidant, photosensitization, anti-inflammatory and anti-cancer activities [27]. The broad range of applications is due to the synergistic effects of the wide variety of constituents within the plant [28]. The most common medical application is the treatment of patients suffering from mild to moderate depression [29].

Figure 2. The medicinal plant *Hypericum perforatum*. (A) plant, (B): open flower, (C): leave.

1.4. *Hypericum perforatum*, the constituents

H. perforatum contains a diverse and complex mixture of pharmacologically active secondary metabolites such as phenylpropanes, flavonoids, biflavones, tannins, proanthocyanidins, naphthodianthrones, essential oil, amino acids, xanthones and, phloroglucinol derivatives [27,28,30,31].

The essential oil consists mainly of monoterpenes and sesquiterpenes. Also, the presence of long-chain alcohols like alkanes and alkanols is known, which are mainly found within the translucent glands of the leaves. The sedative transmitter substance γ-aminobutyric acid has been identified at low concentrations. However, the overall concentration of this constituent is too low to have a significant impact as antidepressant [32].

Phenylpropanes have been shown to have weak spasmolytic and antimicrobial activities. Typical constituents found are chlorogenic, caffeic, and *p*-coumaric acids in low concentrations [31,33].

Flavonol glycosides are one of the major constituents ranging from 2-4% in *H. perforatum.* They were found to have spasmolytic and antidepressant activities (*in vitro* MAO-inhibiting properties). Typical compounds are quercetin (small amounts) besides rutin, quercitrin, hyperoside, and isoquercitrin [31,32].

Naphthodianthrones such as protohypericin and protopseudohypericin, which are converted to hypericin, pseudohypericin and cyclopseudohypericin upon exposure to light, are also present in *H. perforatum*. Pharmaceutical effects like inhibition of the MAO enzyme (antidepressant) and antiretroviral activity were discovered. The compounds have an intense red color, phototoxic properties and are mainly formed in sepals, petals, and stamens within the plant [31,32].

Xanthones were identified to show strong inhibition of the MAO enzyme, but the concentration in *H. perforatum* is too low to have antidepressant activity. Besides this antidepressant activity, also effects against Alzheimer have been reported [34]. Xanthone derivatives can be found in trace concentrations in all parts of the plant including root, stem, and flower [31,32].

Phloroglucinol derivatives such as hyperforin and adhyperforin are very lipophilic structures, mainly found in the reproductive parts of the plant such as the flowers, buds, and leaves. Adhyperforin increases from about 0.2 % in the flower to about 1.8 % in the ripe fruits and makes up 1/10 compared to the hyperforin content. During flower

development, the hyperforin content increases from 2.5 % (first bud phase) to 6.6 % (flower opening phase). The highest hyperforin concentration can be found in the fruits, reaching up to 8.5 % [31,35]. The hyperforins are the best investigated and major constituents responsible for the pharmaceutical activity against depression [24,25,30,36].

1.5. Pharmacological application of hyperforin

The most common pharmacological use of hyperforin is the treatment of mild to moderate depression. Roughly, about 350 million people worldwide and about 4 million in Germany are suffering from depression [157]. Depression is a mental disorder leading to e.g. loss of interest, low energy, erectile dysfunction and even suicide due to the low mood. The emotional disorder typically stays for weeks up to several years. The major causes are believed to be genetically innate, environmental, and/or psychological factors [37]. Depression can be treated by psychotherapy, electroconvulsive therapy or by pharmaceutical medication. Besides psychotherapy, synthetic pharmaceuticals represent the most common way to treat depression. The major target is to increase the synaptic neurotransmitter concentration by blocking the transporter and therefore preventing the reuptake. The three major classes of synthetic antidepressants are serotonin selective reuptake inhibitors (SSRIs), tricyclic antidepressants (TCAs) and monoamine oxidase inhibitors (MAOIs) [37]. TCAs inhibit simultaneously the reuptake of serotonin, (nor)adrenalin and dopamine by blocking the relevant transporters. Selective reuptake inhibitors are specific for one neurotransmitter such as serotonin and dopamine. MAO inhibitors reduce the activity of the MAO enzyme, which is responsible for the degradation of intraneuronal neurotransmitters, leading to an increase of the synaptic neurotransmitter concentration [37]. Typical side effects caused by synthetic pharmaceuticals vary individually and may involve dizziness, blood pressure fluctuations, stomach discomfort, digestive disorders, fatigue, sleep disorder, lack of appetite and sexual dysfunction [38]. Undesired effects are less with phytopharmaceuticals used for treatment of mild to moderate depression, e.g. extracts from the medicinal plant St. John´s wort containing hyperforin, which has been identified as a major active constituent. [24,39].

The mode of action of hyperforin is not completely understood yet. Until today, there are two major principles described; the more recent one describes the discovery of

hyperforin acting as a protonophore. The second principle describes the interaction of hyperforin with the neurotransmitter receptor TRPC6, thereby increasing the synaptic neurotransmitter concentration [36,39,40].

1.6. The hyperforin biosynthesis, still a secret

Hyperforin is a lipophilic bicyclic polyprenylated acylphloroglucinol (PPAP) derivative consisting of a mixture of interconverting tautomers leading to poor resolutions of ^{1}H and ^{13}C NMR measurements [24,30,31,41,42]. Its unstability against light, oxygen, temperature and non-polar solvent is due to the enolized β-dicarbonyl system [24,30,31,41]. Stabilization was achieved using the dicyclohexylammonium salt [24]. Due to the highly complex structure of hyperforin, the total synthesis could be achieved by chemical reactions ranging from 10 to 35 steps. However, the chemical synthesis approaches are very laborious, ending in low yield insufficient for further medical research [43–46].

The biosynthetic pathway is not yet completely understood. As proposed by Beerhues (2006), the biosynthesis of hyperforin (Figure. 3) starts with the formation of the core skeleton, phlorisobutyrophenone (PIBP), by the condensation of 3 molecules of malonyl-CoA and one molecule of isobutyryl-CoA. This reaction is catalyzed by a type III polyketide synthase (PKS), referred to as phlorisobutyrophenone synthase [47,48]. The subsequent decoration of PIBP occurs with residues that are derived from the non-mevalonate (MEP) pathway. These side chains include dimethylallyl pyrophosphate (DMAPP)-derived prenyl groups and geranyl pyrophosphate (GPP)-derived geranyl groups, which are attached by membrane-bound aromatic prenyltransferase (PT) enzymes, giving the hydrophobic properties [24,30,49].

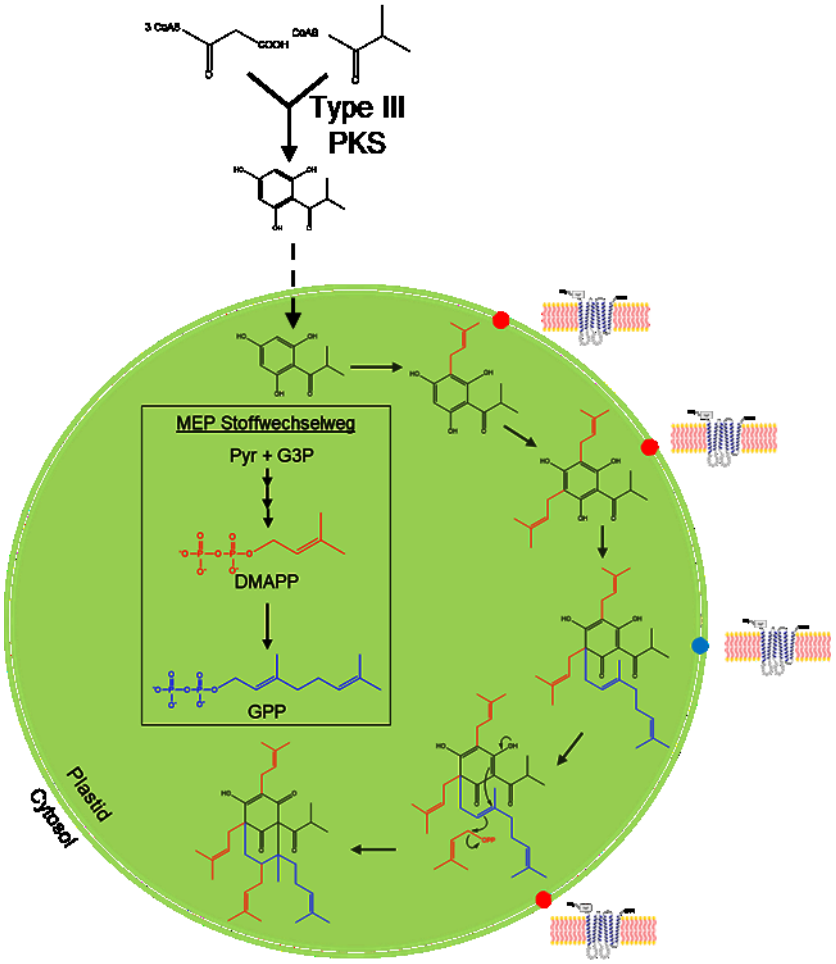

Figure. 3 Proposed hyperforin biosynthesis. Modified from Beerhues (2006) [24].

1.7. Acyl-CoA ligases, the starting point

Acyl-CoA ligases are widely distributed throughout the plant kingdom. They are involved in the biosynthesis of many plant secondary metabolites such as bitter acids, xanthones, flavonoids, and guaiacyl-lignin [48,50,51]. In the hyperforin biosynthetic pathway, these enzymes catalyze the enzymatic conversion of carboxylic acid derivatives including isobutyric, 2-methylbutyric, and isovaleric acids to their CoA esters (Figure 4). The latter substrates are derived from the degradation of the branched-chain alpha acids, including valine to form isobutyryl-CoA, leucine to form isovaleryl-CoA and isoleucine and/or threonine to form 2-methylbutyrl-CoA [48]. Isovaleryl-CoA is involved in the biosynthesis of phlorisovalerophenone (PIVP), the core skeleton of β-bitter acid derived from hop [48,52,53]. In contrast, isobutyryl-CoA and

2-methylbutyryl-CoA are involved in the biosynthesis of hyperforin and adhyperforin, respectively [24,54].

The reaction mechanism of acyl-CoA ligases is catalyzed in two steps (Figure 4). The first step is the adenylation of the carboxylic acid group of isobutyric acid to form an acyl-AMP intermediate. The second step involves the displacement of AMP with CoA to form the corresponding isobutyryl-CoA product (Figure 4).

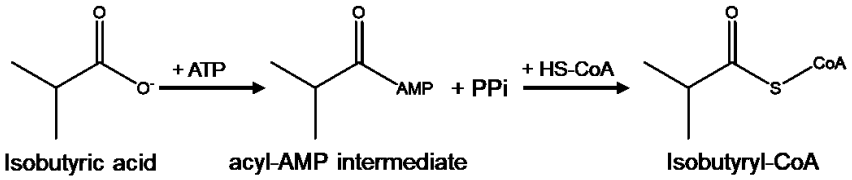

Figure 4. Formation of isobutyryl-CoA. Adenylation of isobutyric acid to form an acyl-AMP intermediate, followed by displacement of AMP with CoA to form isobutyryl-CoA.

1.8. Polyketide synthases, with tremendous catalytic features

Polyketides are a very large group of natural products, which can be found in all kingdoms of life including plants, bacteria, fungi and other eukaryotic organisms [55–57]. They show a large spectrum of pharmacological activities such as antibiotic, anticancer, and immunosuppressive activities. Within plant species, they are produced for UV protection, disease resistance, and against microbial invasion and insects [57–59].

Polyketide synthases can be divided into three different types. Type I polyketide synthases (modular type) are large and highly modular proteins with several domains. These domains contain a ketosynthase domain, acyl carrier protein (ACP) domain, and an acyltransferase domain. Ketosynthases belong to the family of thiolases, converting acetyl-CoA to acetoacetyl-CoA in the mevalonate pathway. This is carried out by a Claisen condensation following a carbon-carbon bond formation while releasing the thiol-CoA group. The acyl carrier protein binds the thioester group of the CoA ester [60]. Type II polyketide synthases (subunit type) are aggregates of the heterodimeric ketosynthase domain and ACP [61].

Type III polyketide synthases are homodimers, only consisting of a single ketosynthase domain with a small size of about 40 – 45 kDa (Structure/Function) [62].

This single ketosynthase domain performs all reactions alone as found in type I and type II PKSs [63]. The reaction itself is divided into two reactions: the first step is the condensation of the starter substrate with several extender substrates. The extender substrate is typically malonyl-CoA while the starter substrates are variable. The variable starter substrates are divided into three different types based on the acyl-CoA nature: 1) aromatic acyl-CoA such as p-coumaroyl-CoA, benzoyl-CoA, cinnamoyl-CoA, 2) short-chain acyl-CoA, e.g. isovaleryl-CoA, isobutyryl-CoA, and hexanoyl-CoA, and 3) long chain-CoA such as cerotyl-CoA. A linear polyketide intermediate is formed which is finally cyclized to form the aromatic structure (Figure 5).

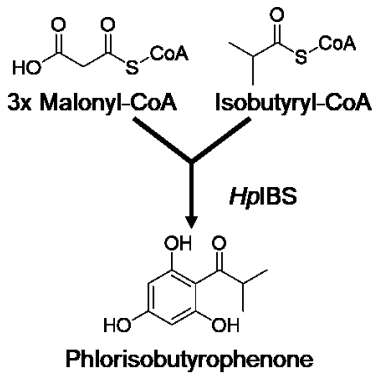

Figure 5. Biosynthesis of phlorisobutyrophenone (PIBP). Condensation of three molecules of malonyl-CoA with one molecule of isobutyryl-CoA to form PIBP.

In general, PKSs have a broad substrate specificity for the starter molecules. Therefore, plant PKSs are responsible for the biosynthesis of a wide variety of plant secondary metabolite backbones. The first type found was a chalcone synthase, which is involved in the biosynthesis of naringenin chalcone in parsley. Also, the biosynthesis of stilbenes, phloroglucinols, resorcinols, benzophenones, pyrones, and even more has been reported [59,62–70]. Many PKS products serve as core skeletons for the formation of further plant constituents. Benzophenone derivatives, for example, are further converted to xanthone derivatives catalyzed by P450 monooxygenase [71]. Also, high molecular weight structures such as oktaketides (hypericins), which are present in *Hypericum* species and provide the red pigment, are formed by PKS [72].

1.9. Prenyltransferases, the key enzymes

Prenyltransferases (PTs) are involved in the biosynthesis of a vast number of primary and secondary metabolites. They are divided into two groups classified by their natural function and named as prenyl diphosphate synthases and aromatic prenyltransferases. Both belong to the class of enzymes that transfer (homo)allylic prenyl groups, e.g. DMAPP-derived C_5, to different acceptor molecules [12,73,74].

Prenyl diphosphate synthases are involved in the biosynthesis of different terpenoids and in the posttranslational modification of peptides, proteins, and tRNA. The terpenoid biosynthesis starts with the condensation of DMAPP (C_5) as prenyl acceptor and IPP (C_5) as donor molecule [75]. These precursor molecules are members of a large molecule family, which plays a crucial role in the biosynthesis of many secondary metabolites such as pigments and hormones. Protein prenyltransferases transfer either FPP (C_{15}) or GGPP (C_{20}) to peptides or proteins serving as acceptor molecules [74]. The latter posttranslational modifications are responsible for correct protein localization and activity. Additionally, tRNA is prenylated, which is required for translational regulation [75]. Prenyl diphosphate synthases can be found in all living organisms and are known to be soluble proteins, with some being divalent cation-dependent [12,74,75].

Many aromatic prenyltransferase (PT) enzymes have been isolated and biochemically characterized throughout the living kingdoms of fungi, bacteria and plants [12,74,75]. PTs isolated from fungi and bacteria occur as soluble proteins, whereas plant-derived PTs are membrane-bound enzymes [75].

Plant-derived aromatic PTs transfer prenyl moieties derived from the MEP pathway (C_5, isopentenyl; C_{10}, geranyl; C_{15}, farnesyl; C_{20}, geranylgeranyl) onto its acceptor, while forming C-C, C-N or C-O bonds (Figure 6) [74,76].

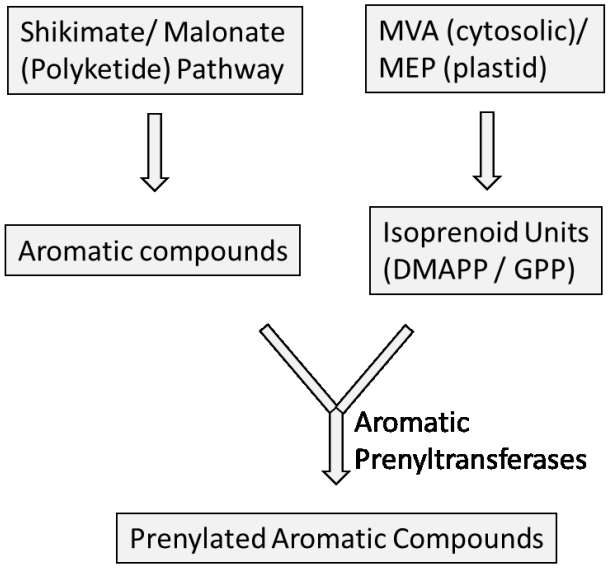

Figure 6. Combination of the shikimate/malonate and isoprenoid pathways to form aromatic PT substrates. The isoprenoid moieties are formed in the cytosolic mevalonate (MVA) pathway and the plastid-localized methyl erythritol phosphate (MEP) pathway. Modified from Yazaki 2009 [12].

The acceptors are very diverse and include phenols, flavonoids, phenolic acids, coumarins, naphthalenes [25]. The most abundant compounds carry isopentenyl or geranyl side chains rather than farnesyl or geranylgeranyl side chains [77].

Plant-derived aromatic PT enzymes are involved in the biosynthesis of secondary metabolites and are mainly located in the membrane of plastids. They also contain aspartate-rich motifs, e.g., NDxxDxxxD, and are strongly dependent on divalent cations [12,25,74,75]. Recent studies have shown that plant-derived membrane-bound aromatic prenyltransferases are involved in the biosynthesis of a number of different biosynthesis pathways and in the prenylation of various aromatic compounds such as xanthones, benzoic acid derivatives, (iso)flavonoids, coumarins and phloroglucinol derivatives [34,77–95].

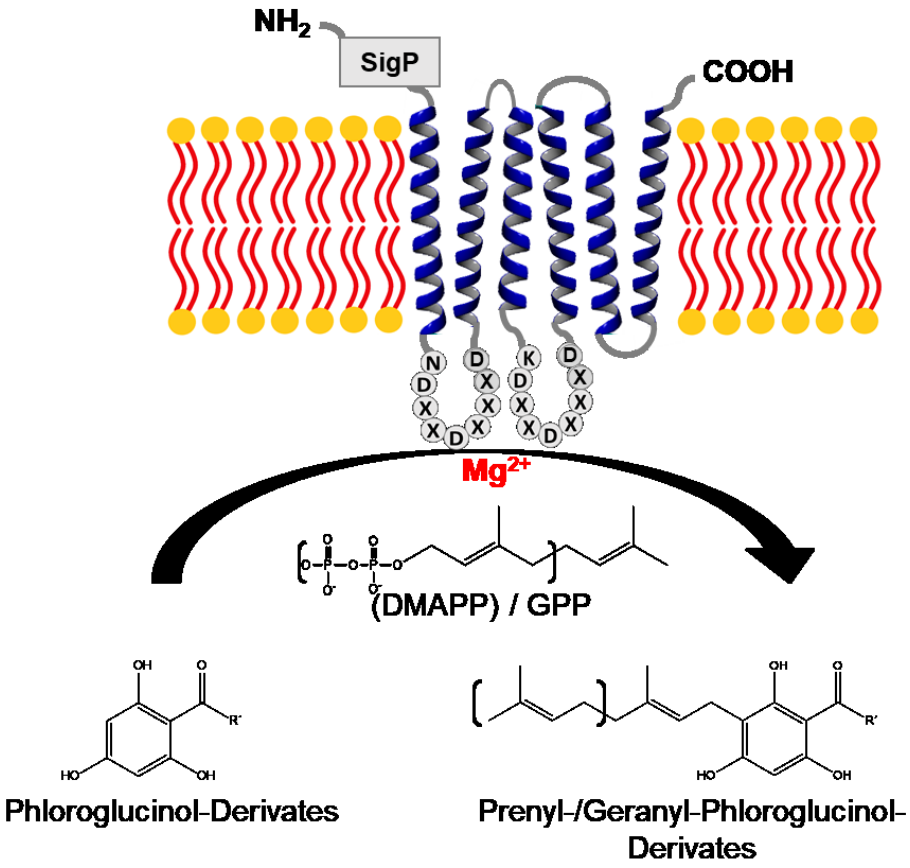

Figure 7: Reaction of aromatic prenyltransferases. Membrane-bound aromatic PTs have conserved aspartate-rich motifs located in the cytosolic loops (L1 and L3) and an N-terminal transit peptide (TP). Acceptor molecules such as phloroglucinol-derivatives are prenylated or geranylated to form the corresponding derivatives. R = H or OH, R´ = $(CH_3)_2$; $CH_2 – CH – (CH_3)_2$; $(CH_3)_2 – CH_3$; C_6H_5. Modified from Gaid et. al. 2017.

Prenylated compounds demonstrate a large variety of biological activities and are therefore promising high-potential candidates for future drug development [77]. Due to their lipophilic character, the bio-barrier penetration of the molecules is supported, which facilitates the pharmacological effects [96]. Thus, there is a growing interest to provide further research for the production of polyprenylated aromatic compounds as perspective candidates for future medical applications.

1.10. Objectives

Hyperforin is identified as a major constituent of St. John's wort, which is responsible for many pharmacologically interesting effects, such as antidepressant, antibacterial, anti-inflammatory, and antitumoral properties. Due to the versatile applications of hyperforin-rich extract, hyperforin is considered as a promising herbal metabolite. However, the extraction of hyperforin from the plant is difficult. The instability to normal environmental conditions makes the standardisation of the extract challenging. In addition, the hyperforin concentrations vary in St. John's herb from plant to plant but also between various plant organs. All the aforementioned critical parameters increase the market price of hyperforin to currently around 200 € per mg. The chemical synthesis of hyperforin has already been achieved by several approaches. Nevertheless, at least 10 steps are currently required for the total chemical synthesis.

Due to the low yields achieved by chemical synthesis, a commercial large-scale synthesis is not economic. One possibility to obtain cost-effective yields would be the heterologous production in fast-growing organisms, such as tobacco and yeast. However, the full biosynthetic pathway is not yet fully understood, making the complete heterologous expression impossible. The postulated hyperforin biosynthesis is based on at least six enzymes. Due to this high number of enzymes to be expressed, a genome integration protocol for the production organism is required.

The aims of the present work are as follows.

1. Functional expression in yeast of previously isolated acyl-CoA ligase and polyketide synthase.
2. Functional expression and full characterization of previously isolated prenyltransferase genes.
3. Establishment of a yeast genome integration protocol for multiple gene integrations.

2. Materials and Methods

2.1. Chemicals

Unless stated otherwise, all chemicals used were of analytical grade and purchased from Carl Roth GmbH (Karlsruhe, Germany), Sigma Aldrich (Steinheim, Germany), Fluka (Neu-Ulm, Germany), AppliChem (Darmstadt, Germany), Merck (Darmstadt, Germany), Thermo Fischer Scientific (Darmstadt, Germany), Becton Dickinson (Heidelberg, Germany), Bio-Rad (München, Germany), J.T. Baker (München, Germany), Nippon Genetics (Düren, Germany), Cayman Chemical (Michigan, USA), VWR (Darmstadt, Germany) and Qiagen (Hilden, Germany). The following chemicals used in this study were chemically synthesized: DMAPP, PIBP, PIVP, 2-MBP, 3-g-PIBP, 3-g-PIVP, 3-g-PAP, 3-g-PBP, and 3-g-2-MBP.

2.2. Enzymes and PCR components

Phusion Hot Start II DNA Polymerase (2 U/µL), Phusion U Hot Start DNA Polymerase, dNTPs, Restriction enzymes (10 U/µL), Alkaline Phosphatase (1 U/µL), and T4 DNA Ligase (5 Weiss U/µL) were purchased from Thermo Fischer Scientific (Darmstadt, Germany). peqGOLD *Taq* DNA Polymerases (5 U/µL) was obtained from VWR (Peqlab, Darmstadt, Germany). Oligonucleotides used for standard PCRs and USER-cloning were synthesized either at Eurofins MWG Operon (Ebersberg, Germany) or Microsynth (Balgach, Switzerland) and produced at high purity salt-free (HPSF) grade.

2.3. Kits

The following kits were used for the molecular biological and microbiological works.

Table 1. Kits

Kit	Application	Manufacturer
InnuPREP DOUBLEpure	PCR product purification	Analytic Jena
S.c. EasyComp™	Preparation of competent	Thermo Fischer Scientific

Transformation Kit	yeast cells and transformation	
Yeast DNA Extraction Kit	Extraction of genomic DNA	Thermo Fischer Scientific

2.4. Equipment, Software

The following equipment and software were used during this study.

Table 2. Equipment

Device	Model	Manufacturer
Autoclave	Vx-120	Systec GmbH
Clean bench	LaminAir HLB 2472	Heraeus
DASGIP Bioreactor	Bioblock (CWD 4)	Eppendorf
Electrophoresis chamber		BioRad
Filters 0.2 µm	Acrodisc syringe filter	PALL Life sciences
Glas beads	425-600 µm	Sigma-Aldrich
Heating block	DriBlock DB 3D	Techne
HPLC (Agilent Technologies)	1260 Infinity	Agilent Technologies
HPLC (VWR-Hitachi)	Elite LaChrom series, Diode Array Detector (L-2455),	VWR-Hitachi
Imager	Infinity 3026	Peqlab
Incubator	HT Minitron / HT Multitron	Infors HT
LED-Transilluminator		Nippon Genetics
Mass spectrometer	3200 Q TRAP LC/MS/MS System	Applied Biosystems Sciex
MilliQ water Purification System	Arium 611	Satorius
NanoDrop	SimpliNano	GE Healthcare

PCR Cycler	T Professional Basic Gradient	Biometra
PCR cycler	T Professional	Biometra
pH-Meter	Digital pH Meter 325	WTW
Power supply (agarose gel electrophoresis)	power-pack 300	BioRad
Scale	LA230S	Sartorius
Shaker	Minitron	Infors HT
Spectrophotometer	Ultrospec 1000	Pharmacia Biotech
Steril Werkbank	HLB 2472	Heraeus
Sterile filter	Millex®-Filtereinheiten (0.22 µm, PE5 Membran)	Roth
Ultrasonic Cell-Disrupter	Sonifier 250	Branson (G. Heinemann)
Vortexer	Vortex Genie 2	Scientific Industries
Water bath	MW4	Julabo
Centrifuge(s)	Biofuge pico	Heraeus
	Universal 32R	Hettich Zentrifugen
	Avanti®-J-E Centrifuge	Beckman Coulter
	Biofuge 13	Heraeus Sepatech
	Sigma 1-15K	Sigma
	Universal 32R	Hettich

Table 3. Software

Name	Version	Manufacturer
Agilent ChemStation for LC 3D systems	Rev. B.04.03(16)	Agilent Technologies, Inc.
ChemDraw Professional	15.1.0.144	PerkinElmer Informatics, Inc.
Hyper32	1.0.0	John S. Easterby http://hyper32.software.informer.com/Sicherer-download/
LSM Image Browser	3.5.0.223	Carl Zeiss GmbH
OriginPro	Version 2016G	OriginLab Corporation

2.5. Organisms

Molecular cloning and plasmid amplification were performed with the *E. coli* DH5α strain. Recombinant protein expression was carried out using the *S. cerevisiae* INVSc1 strain. The genotype of each strain is shown in Table 4.

Table 4. Organisms

Organisms	Application	Genotype
E. coli DH5α	Plasmid amplification	*F'φ80δlacZ9M15endA1hsdR17(rk-mk+)supE44thi-1λ-gyrA96relA19(lacZYA-argFV169) deoR*
S. cerevisiae INVSc1	Rec. protein expression	*MATa his3D1 leu2 trp1-289 ura3-52 MAT His3D1 leu2 trp1-289 ura3-52*

2.6. Cultivation media

The LB-medium (Table 5) was used for the cultivation of the *E. coli* DH5α strain. *S. cerevisiae* pre-cultures were prepared in SGI-medium and the main-cultures in YPSE-medium.

Table 5. Cultivation media

Medium	Components	Concentration
LB-medium*	Casein peptone	10 g/L
	NaCl	10 g/L
	Yeast extract	5 g/L
SGI-medium*	Bacto Casamino Acids	1 g/L
	Yeast nitrogen base (without amino acids)	6.7 g/L
	Glucose	20 g/L
YPSE-medium	Yeast extract	10 g/L
	Bacto-peptone	10 g/L
	Sucrose	5 g/L
	Ethanol	30 mL/L

* gar (15 g/L) was added for obtaining solid medium

2.7. Molecular Biological Methods

2.7.1. Oligonucleotides

PCR and sequencing primers were designed by the following primer criteria for successful PCR amplification: GC Range: 50 to 60 %, T_m Range: 55 to 70 °C, GC clamp at the 3´end, avoiding primer dimers and hairpins.

Criteria for sequencing primers: same as for PCR primers, except that T_m was chosen to have about 55 °C. Sequencing data were analyzed by the Clone Manager software. The primer tables can be found in the appendix 6.4. Oligonucleotides, page 138.

2.7.2. Polymerase chain reaction (PCR)

Polymerase chain reaction (PCR) was carried out for all *in vitro* DNA amplifications using either Phusion Hot Start II DNA Polymerase or peqGOLD Taq DNA Polymerases. The Phusion Hot Start II DNA Polymerase was exclusively used for the amplification of amplicons required for recombinant protein expression in *S. cerevisiae*. This enzyme provides no or very low mutational errors (4.4×10^{-7} single nucleotide polymorphisms = SNPs) due to its 3´→ 5´ exonuclease activity (proof reading activity). PeqGOLD Taq DNA Polymerases was mainly used (if not stated otherwise) for colony PCR (Table 21, page 32). The standard reaction volume was 25 µL and the composition prepared as described in Table 6.

Table 6. PCR setup using Phusion Hot Start II High-Fidelity DNA Polymerase

Component	Quantity
5x Phusion HF-buffer	5.0 µL
dNTPs (2 mM)	2.5 µL
Template DNA	0.1-10 ng
Forward Primer (5 µM)	2.5 µL
Reverse Primer (5 µM)	2.5 µL
Phusion polymerase	0.25 µL
ddH_2O ad.	25 µL

A typical PCR program used for the amplification of the GOI is shown in Table 7. The annealing temperature depends on the primer pairs and was adjusted according to the T_m calculated by Clone manager. The time of DNA amplification depends on the polymerase used in the PCR reaction. For the Phusion Hot Start II High-Fidelity polymerase 15-30 s/kb (Table 7) and for the peqGOLD *Taq* DNA Polymerases 60 s/kb were used (Table 22, page 33).

Table 7. Thermocycler program for DNA amplification using Phusion Hot Start II DNA Polymerase

Step	Temperature (°C)	Time (min:sec)
1. Initial Denaturation	98	00:30
2. Denaturation	98	00:10
3. Annealing	55 - 65	00:30
4. Extension*	72	00:15 – 00:30 per kb
5. Final Extension	72	04:00
6. Hold	4	-

* 25 - 30 cycles from step 1 - 4.

2.7.3. Restriction digestion

Restriction enzymes were mainly used for:

1. Template degradation after PCR amplification of target genes using *Dpn*I.

2. Generation of compatible ends of plasmid DNA and PCR fragments for molecular cloning.

2.7.3.1. Template degradation after PCR amplification of target genes using *Dpn*I

Plasmid DNA isolated from *E. coli* DH5α, which was used as a template in the PCR reaction, is methylated and can, therefore, be digested with the restriction enzyme *Dpn*I. The recognition sequence is GATC with the base adenine being methylated. The following procedure reduces the background of colonies containing only template DNA. In the following Table 8 a standard *Dpn*I digestion is shown, taking the PCR reaction mixture from Table 6, page 20.

Table 8. Components of the *Dpn*I restriction digestion

Component	Quantity
PCR Reaction Mixture	25 µL
*Dpn*I Enzyme	1.0 µL
10x Tango Buffer	5.0 µL
ddH_2O ad.	19.0 µL
Incubation time and temp.	1 – 2 h at 37 °C

After the *Dpn*I digestion, the innuPREP DOUBLEpure kit was used for the purification of the PCR DNA. The purification was done according to the manual, except that the elution was done twice with 20 µL of elution buffer.

2.7.3.2. Generation of compatible ends of plasmid DNA and PCR fragments for molecular cloning

For cloning a standard gene into an e.g. pESC_URA vector, the sticky end cloning method was mainly used. To check whether a double digest can be performed, the double digest finder (press: **Link**) from Thermo Fischer Scientific was used. In Table 9 a double digest is shown as an example for plasmid DNA and in Table 10, page 23 for the GOI.

Table 9. Restriction digestion of the plasmid DNA

Component	Quantity
Plasmid DNA	2 – 10 µg
10x Enzyme Buffer	5.0 µL
Restriction Enzyme 1	1.0 µL
Restriction Enzyme 2	1.0 µL
Alkaline Phosphatase (AP)	1.0 µL
ddH_2O ad.	50 µL
Incubation time and temp.	1 – 2 h at 37 °C

Table 10. Restriction digestion of the PCR fragment

Component	Quantity
PCR fragment (µg)	variable
10x Enzyme Buffer	5.0 µL
Restriction Enzyme 1	1.0 µL
Restriction Enzyme 2	1.0 µL
ddH_2O ad.	50 µL
Incubation time and temp.	1 – 2 h at 37 °C

2.7.4. Ligation

For the ligation of linearized plasmid DNA with previously amplified and digested PCR fragments, the T4 DNA Ligase was used. A typical ligation reaction composition can be reviewed in Table 11. Depending on the vector and insert size, the molar ratio was chosen between 1:1 to 1:5.

The amount of insert used was calculated by the following formula:

$$Amount\ insert\ [ng] = \frac{Amount\ Vector\ \ [ng] * Size\ Insert\ [kb]}{Size\ Vector\ [kb]} * Molar\ ratio\ \frac{Insert}{Vector}$$

Figure 8. Formula to calculate vector/insert ratio

Table 11. Composition of a typical ligation reaction using T4 DNA Ligase

Component	Quantity
T4 DNA Ligase	1 µL
Vector (100 ng/µL)	1 µL
Insert	a molar ratio to vector (1:1 to 1:5)
10X T4 DNA Ligase Buffer	2 µL
ddH_2O ad.	20 µL
Incubation time and temp.	overnight at 16 °C

In case no proper restriction enzymes were found to perform the sticky end cloning method, the blunt cloning method was chosen. A standard blunt end cloning composition is shown in the following Table 12.

Table 12. Composition of a typical blunt end ligation reaction using T4 DNA Ligase

Component	Quantity
Plasmid DNA	200 ng
PCR fragment	180 ng
10x T4 Ligase Buffer	2.0 µL
T4 Ligase Enzyme	1.0 µL
*Sma*I/*Srf*I Enzyme	1.0 µL
ddH_2O ad.	20 µL
Incubation time and temp.	overnight at 16 °C

2.7.5. Agarose gel electrophoresis

Agarose gel electrophoresis was used as an analytical method to separate DNA fragments according to their differences in size. All agarose gels were prepared by dissolving 1 % (w/v) agarose (peqGold Universal Agarose, Peqlab, Germany) in 1x TAE-buffer (Table 13, page 25). For DNA staining, 5 µL Midori Green (Nippon Genetics Europe GmbH, Düren, Germany) per 100 mL agarose was added after agarose was dissolved. A proper amount of DNA samples was mixed with 6x loading dye (Figure 9, page 25) and run between 90 to 120 V until an appropriate separation was obtained. GeneRuler 1 kb DNA Ladder (100 to 10,000 bp) (Figure 9, page 25) was used as a marker to estimate sample DNA size. DNA visualization was achieved using a UV transilluminator**,** which illuminates fluorophores at a wavelength of 312 nm (UV-B).

If necessary, linearized plasmid DNA or PCR fragments were extracted from the agarose gel by cutting out the required band. To prevent mutations within the DNA strands caused by the UV light, a LED transilluminator (Nippon genetics) was used. Finally, the DNA was purified using the innuPREP DOUBLEpure kit. The procedure

was followed according to the manual, except that the elution was done twice with 20 µL of elution buffer.

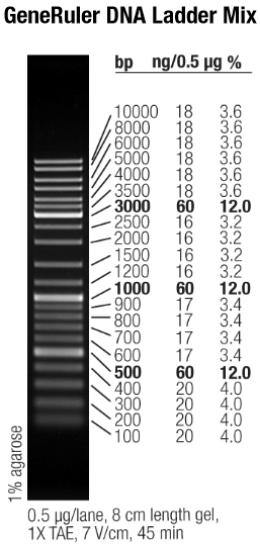

Figure 9: GeneRuler 1 kb DNA ladder (Thermo Fischer Scientific).

Table 13. Buffer for agarose gel electrophoresis and Loading Dye

Buffer	Composition	Quantity
50 x TAE	Tris-HCl	2.0 M
	Acetic Acid	1.0 M
	EDTA	0.05 M
	pH 8.0	
6x Loading Dye	Tris-HCl pH 7.5	10 mM
	EDTA	60 mM
	Glycerol	60 % (v/v)
	Bromophenol Blue	0.03 % (w/v)
	Xylene Cyanol FF	0.03 % (w/v)

2.7.6. Plasmid isolation from *E. coli*

For the propagation of plasmid DNA, the corresponding plasmids were first transformed into *E. coli* DH5α (Table 4, page 18), which were then cultivated on LB-agar plates containing the appropriate antibiotic. One single colony was picked,

transferred into 5 mL LB-medium (Table 5, page 19) and grown overnight at 37 °C and 220 rpm. Thereafter, 1.5 mL cell culture was centrifuged for 20 sec. The pellet was resuspended in 150 µL buffer 1 (Table 14) and let sit for 5 min at room temperature. 150 µL buffer 2 (Table 14) was added, mixed (invert) and placed on ice for 5 min. Afterwards, 150 µL buffer 3 (Table 14) was added, mixed and placed on ice for another 5 min. Few drops of chloroform were added, mixed and the cell solution centrifuged for additional 5 min (13.000 rpm). An aliquot of 0.4 ml of the supernatant was transferred to a new 1.5 mL tube containing 0.8 mL 100 % isopropanol and vortexed vigorously. Afterwards, the tube was centrifuged for 10 min., the supernatant discarded, the pellet washed with 1 mL 70% ethanol and dried at 37 °C. The DNA pellet was then resuspended in 50 µL H_2O and the DNA concentration quantified using a NanoDrop spectrophotometer prior to storage at -20 °C. The plasmids were prepared following the company's instructions and sequenced at either MWG (Ebersberg, Germany), Source BioScience (Berlin, Germany) or GATC Biotech (Konstanz, Germany).

Table 14. Composition of plasmid isolation buffers by alkaline lysis and ethanol precipitation

Buffer	Component	Concentration
Buffer 1 pH 8.0 (Resuspension Buffer)	Tris-HCl	50 mM
	EDTA	10 mM
	RNase A (10 mg/mL)	100 µg/mL
Buffer 2 (Lysis Buffer)	SDS	1% w/v
	NaOH	0.2 M
Buffer 3 pH 5.5 (Neutralization Buffer)	Potassium Acetate	3 M
	Glacial acetic acid is used for pH adjustment	

2.7.7. Plasmid construction for genome integration of DNA fragments into *S. cerevisiae* using Easyclone

The development of efficient production strains to produce chemicals and APIs requires efficient methods of genetic engineering. One major aspect is the stable integration of the required enzyme cascade into the genome. The plasmid-based expression is firstly limited to the number of genes, which can be functionally expressed, and secondly to the number of antibiotics which can be used for the selection of positive transformants. Detailed background explanation can be found in the discussion part of this thesis (section 4.5., page 90). A number of different cloning methods, e.g. Infusion cloning, Gateway cloning, Gibbson assembly, Ligase Cycling Reaction, and Golden Gate cloning have been developed during the last decades [23,97–102].

For the stable integration of the enzymes used in this thesis, the EasyClone USER method for iterative chromosomal integration of multiple genes in *S. cerevisiae* was used (personal communication Dr. Irina Borodina from the University of Technical University of Denmark) [103].

The principle behind this method will be described in more detail in this section. USER cloning is the abbreviation for uracil-specific excision reaction. The basic principle behind this cloning technique is to generate compatible overhangs of vector and GOI independent of any restriction enzyme. This enables to ligate every GOI with a vector without considering any misdigestion of the vector backbone or the target gene by using the restriction enzyme-based cloning techniques. This can be achieved by using the so-called “USER cassette” and USER primer. The USER cassette has to be available in the plasmid backbone of interest and the gene-specific primer, containing compatible ends of the vector and target gene created without commonly used restriction enzymes. The primers used for the amplification of the GOI contain one uracil base, which enables later the generation of the overhangs compatible with each other. For the amplification of the GOI, a special Phusion polymerase is required, which is called Phusion U polymerase. This Phusion polymerase is able to read over the uracil base, due to a mutation without losing the proofreading activity. With a “normal” Phusion polymerase, the amplification would not be possible, because the enzyme would stall (´fall down´) from the template. The obtained PCR product is treated with a uracil DNA glycosylase and DNA glycosylase-lyase Endo VIII. These enzymes remove

the two uracil bases and generate the 8nt long compatible ends of the PCR product and of the USER cassette of the plasmid backbone. The length of 8 nt enables a very efficient ligation reaction with the USER enzyme in the subsequent steps [103]. In the following Figure 10, the detailed cloning procedure is shown.

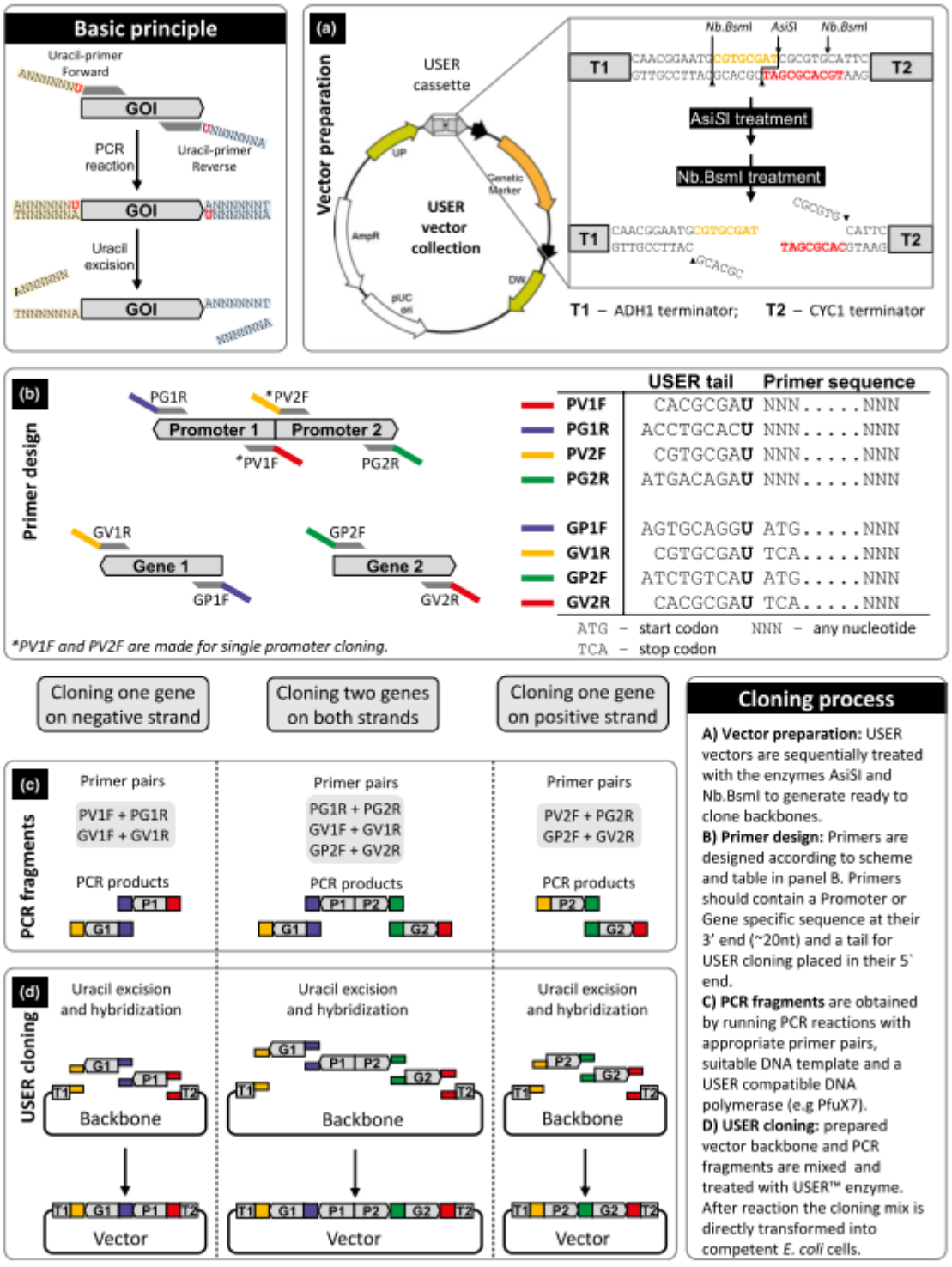

Figure 10. Overview of the gene cloning procedure into EasyClone vectors [103].

2.7.7.1. PCR amplification of integration parts for USER cloning

The Phusion U DNA Polymerase was exclusively used for the amplification of fragments required for the genome integration and recombinant protein expression in *S. cerevisiae*. The standard reaction volume was 50 µL, which was prepared as described in Table 15.

Table 15. PCR setup using Phusion U Polymerase for USER cloning

Composition	Quantity
5x Phusion HF Buffer	10.0 µL
dNTPs (2 mM)	5.0 µL
pESC_URA_rv gene+USER	5.0 µL
pESC_URA_fw gene+USER	5.0 µL
Template	1 pg – 10 ng
Phusion U Polymerase	0.5 µL
ddH_2O ad.	50 µL

Table 16. Thermocycler program using Phusion U polymerase for USER cloning

Step	Temperature (°C)	Time (min:sec)
1. Initial Denaturation	98	00:30
2. Denaturation	98	00:10
3. Annealing	55 - 65	00:30
4. Extension*	72	00:15 – 00:30 /kb
5. Final Extension	72	04:00
6. Hold	4	-

* 25 - 30 cycles from step 1 - 4.

After the PCR reaction, the sample was treated in the same way as described in the section 2.7.3.1., page 21.

2.7.7.2. Preparation of integration vector for USER cloning

USER cloning vector backbones isolated from *E. coli* (DH5α), must be treated with two different enzymes to generate compatible overhangs, enabling the ligation with the PCR product. The treatment must be carried out in two subsequent steps due to the different incubation temperature and buffer requirements. In the following two tables (Table 17 and Table 18) the standard reaction conditions are shown.

Table 17. Preparation of USER vector backbone step 1

Component	Quantity
10x Fast Digest Buffer	5.0 µL
pCfB389	20 µg
*AsiS*I	2.0 µL
ddH_2O ad.	50 µL
Incubation time and temp.	4 h at 37 °C

After *AsiS*I digestion, the innuPREP DOUBLEpure kit was used for the purification of the PCR DNA. The purification was done according to the manual, except that the elution was done twice with 20 µL elution buffer.

After the *AsiS*I enzyme treatment, the purified DNA fragment was treated with *Nb.Bsm*I enzyme (Table 18).

Table 18. Preparation of USER vector backbone step 2

Component	Quantity
purified *AsiS*I treated DNA	40 µL (>1 µg)
10x Buffer 3.1	5.0 µL
*Nb.Bsm*I	2.0 µL
10x Buffer 3.1	5.0 µL
ddH_2O ad.	50 µl
Incubation time and temp.	2 h at 65 °C

Following *Nb.Bsm*I digestion, the innuPREP DOUBLEpure kit was used for the purification of the PCR DNA. The purification was done according to the manual, except that the elution was done twice with 20 µL elution buffer.

2.7.7.3. USER reaction

After the preparation of the USER vector and the amplification of the target gene, the ligation using the USER enzyme was performed. A molar ratio of vector:GOI = 1:3 was chosen. A typical ligation reaction composition can be reviewed in Table 19.

Table 19. USER reaction

Component	Quantity
USER plasmid*	x µL
GOI*	x µL
USER Enzyme	1 µL
Buffer 3.1	4 µL
ddH_2O ad.	50 µL
1. Incubation time and temp.	15 min. at 37 °C
2. Incubation time and temp.	15 min. at 25 °C

*Plasmid:GOI ratio = 1:3

After the USER reaction, the plasmid was directly transformed into *E. coli* DH5α (section 2.8.1.2., page 34), positive transformants tested by colony PCR (section 2.7.8., page 32) and one positive plasmid isolated (section 2.7.6., page 25). For successful genome integration, the plasmid must be linearized which was achieved by *Not*I digestion as described in Table 20.

Table 20. USER plasmid *Not*I digestion

Component	Quantity
Plasmid	100 µg
10x Buffer O	1.0 µL

*Not*I	2.0 µL
ddH_2O ad.	10.0 µL
Incubation time and temp.	4 h at 37 °C

After *Not*I digestion, the GOI fragment was separated and isolated from the remaining plasmid backbone by agarose gel electrophoresis (section 2.7.5, page 24). The obtained eluent was concentrated up by lyophilization overnight. About 300 – 700 µg linearized genome integration fragment was finally transformed into *S. cerevisiae* (section 2.8.2.2., page 36) and the cells plated out on selection plates (depending on the USER backbone used). Successful DNA fragment integration was verified by yeast genomic DNA extraction (section 2.7.9., page 33) and the subsequent amplification of the target insert and/or promoter by PCR (section 2.7.2., page 32).

2.7.8. Colony PCR of *E. coli*

Verification of successful cloning, as described previously, was carried out by colony PCR. A single colony was picked from a LB-agar plate, replica plated on a master plate containing the appropriate antibiotic and finally resuspended in the *Taq*-polymerase master mix (Table 21). The *Taq*-polymerase requires 60 s/kb for amplification, so the elongation time has to be adjusted according to the gene length. A standard PCR program is shown in Table 22, page 33.

Table 21. Components for colony PCR

Component	Quantity
10x *Taq* Reaction Buffer	1.25 µL
dNTPs (2 mM)	1.25 µL
Forward Primer (5 µM)	1.25 µL
Reverse Primer (5 µM)	1.25 µL
Taq Polymerase	0.125 µL
ddH_2O ad.	7.375 µL

Table 22. Colony PCR program

Step	Temperature (°C)	Time (min:sec)
1. Initial Denaturation	98	04:00
2. Denaturation	98	00:30
3. Annealing	55 – 65	00:30
4. Extension*	72	01:00 /kb
5. Final Extension	72	04:00
6. Hold	4	-

* 25 cycles from step 1 - 4.

2.7.9. Colony PCR of *S. cerevisiae* for isolation of plasmid- and genomic DNA

Genomic DNA was extracted after the integration was carried out [104].

One colony was picked or 100 – 200 µL liquid yeast culture was centrifuged down for 5 min at 14.000 rpm. The supernatant was discarded and the obtained cell pellet used for the next step. The cell pellet or colony was resuspended in 50 - 100 µL of 200 mM lithium acetate, 1 % w/v SDS solution. The cell suspension was then incubated for 15 min. at 70 °C. About 150 – 300 µL of 96 - 100 % ethanol was added and the tube shortly vortexed. Genomic DNA and cell debris were centrifuged down at 14.000 rpm for 5 min. The pellets were washed with 150 – 300 µL 70 % ethanol with a subsequent centrifugation step as described in the prior step. The obtained cell pellet was resuspended in 50 - 100 µL sterile ddH_2O or TE-buffer. The suspension was finally centrifuged for 15 – 30 sec. at 10.000 rpm. Use 1 - 2 µL of supernatant for PCR.

Alternatively, the Yeast DNA Extraction Kit (Thermo Scientific) was used and the procedure followed according to the manual.

2.8. Microbial Methods

2.8.1. Microbial methods for *E. coli*

2.8.1.1. Preparation of competent *E. coli* cells

Competent *E. coli* cells were prepared chemically according to [105] by the technician Ms. Ines Rahaus. A single colony of *E. coli* strain was transferred to 10 mL LB medium and incubated at 37 °C and 220 rpm overnight. One mL of the overnight culture was transferred to new 50 mL LB-medium (with an appropriate antibiotic) and further incubated until OD_{600} reached 0.5 - 0.8. The cell suspension was centrifuged at 8000 rpm for 10 min. at 4 °C and the obtained cell pellets were resuspended in 10 mL ice-cold 50 mM $CaCl_2$ solution and centrifugedt under the same conditions. After discarding the supernatant, pellets were washed by re-suspending in 20 mL 50 mM $CaCl_2$ followed by incubation on ice for 30 min. The last step was repeated using 2 mL $CaCl_2$ to resuspend the pellets followed by incubation on ice for 15 min. For long-term storage, 140 µL ice-cold sterile glycerin solution (86%) was added per 960 µL cell suspension. Aliquots of 50 - 100 µL competent cells were transferred into 1.5 mL tubes and directly frozen at -80 °C.

2.8.1.2. Transformation of plasmid DNA into *E. coli*

For the transformation of plasmid DNA, 50 or 100 µL of frozen competent *E. coli* DH5α or BL21 cells were thawed on ice for about 10 - 15 min. Up to 5 µL (10 – 100 ng), plasmid DNA was mixed with 100 µL competent cells and incubated for additional 30 min on ice. Afterwards, the heat shock was performed by placing the tube containing cells and plasmid DNA into a water bath at 42 °C for 45 – 60 seconds. After the heat shock, tubes were directly placed on ice for 2 min. Subsequently, 500 µL sterile LB-medium (Table 5, page 19) was added and the cells were recovered for 60 min by shaking at 37 °C and 250 rpm. The recovered cells (20 – 100 µL) were plated out on LB-agar plates containing the appropriate antibiotics and incubated overnight at 37 °C.

2.8.1.3. Protein expression in *E. coli*

E. coli BL21 was grown in LB-medium at 37 °C and 200 rpm. Ampicillin was supplemented at a final concentration of 100 µg/mL, while chloramphenicol was at a final concentration of 35 µg/mL.

The starter culture consisted of 5 mL LB-medium and was inoculated with a single colony. After 12-16 h of incubation, 2 mL of the starter cultures were transferred to 50 mL LB-medium (supplemented with ampicillin and chloramphenicol) and incubated until OD_{600} reached 0.6 - 0.8. The protein expression was induced by the addition of IPTG to a final concentration of 0.25 mM and the incubation was for 4 h at 25 °C.

2.8.1.4. Cell disruption using sonicator

The pellet, which was received after centrifugation of the 50 mL culture at 5000 rpm for 5 min., was resuspended in 3 mL lysis buffer. The cells were then sonicated for 2-3 min on ice. A centrifugation at 14000 rpm and 4 °C for 15 min resulted in the supernatant, i.e. the crude extract.

2.8.1.5. Preparation of *E. coli* cryo-stock

E. coli cryo-stocks were prepared by picking a single positively transformed colony from a LB-agar plate (Table 5, page 19) and inoculating it into 5 mL LB-medium containing appropriate antibiotics. The cells were grown overnight at 37 °C and 230 rpm. *E. coli* cell suspension (0.5 mL) was mixed within a cryo-stock tube with 0.5 mL sterile 50 % glycerol (v/v) solution. The tubes were vortexed vigorously prior to long-term storage at -80 °C.

2.8.2. Microbial methods for *S. cerevisiae* expression system

2.8.2.1. Preparation of competent *S. cerevisiae* cells

Preparation and transformation of competent *S. cerevisiae* cells were carried out according to [106].

For the preparation of plasmid-free *S. cerevisiae* competent cells, either 25 mL pre-warmed (30 °C) 2x YPD-medium (Table 5, page 19) was inoculated with a single colony picked from a YPD-plate (Table 5, page 19) or a sterile 100 mL flask was inoculated with a swab taken from a cryo-stock (section 2.8.2.6., page 38). For *S. cerevisiae* cells containing URA-plasmid-DNA, either 25 mL pre-warmed SGI-medium (Table 5, page 19) (30 °C) was inoculated with a single colony picked from an SGI-plate (Table 5, page 19) or a sterile 100 mL flask was inoculated with a swab taken from a cryo-stock. The pre-cultures were incubated overnight at 30 °C and 220 rpm. A main culture with OD_{600nm} = 0.1 – 0.2 was prepared in pre-warmed 2x YPD-medium from the pre-culture. The main culture was further grown as mentioned previously for 4 – 6 h until an OD_{600nm} = 1.0 – 1.5 was reached. The cells were harvested by centrifugation at 3.000 rpm for 5 min at RT, washed once with 50 mL and a second time with 10 mL sterile water. The obtained cell pellets were resuspended in 1 mL sterile “frozen competent cell” (FCC) solution (5% v/v glycerol and 10% v/v DMSO). Aliquots of 50 µL competent cells were wrapped into paper towels and directly frozen at -80 °C. The paper towels are required to guarantee slow freezing of the competent cells. Next day, the paper towels were removed and the competent cells were further stored at – 80 °C until use.

2.8.2.2. Transformation of plasmid DNA into *S. cerevisiae*

A 50 µL aliquot of frozen competent cells was thawn for 15 – 30 sec. in a water bath at 37 °C. The tube was subsequently centrifuged at 13.000 rpm for 2 min and the supernatant removed. Meanwhile, a 50 µL aliquot of salmon sperm (carrier ssDNA; 2.0 mg/mL) was boiled at 95 °C for 5 min and directly chilled on ice until use. The transformation mix, prepared as described in Table 23, page 37, was used to resuspend the cell pellet with subsequent incubation in a 42 °C water bath for approximately 60 min. Afterwards, the cell suspension was centrifuged at 13.000 rpm for 30 seconds and the cell pellet was resuspended in 500 µL sterile water. 100 µL

were plated out on SGI-plates (Table 5, page 19) with a following incubation at 30 °C for 3 – 5 days.

Table 23. *S. cerevisiae* transformation mix

Composition	Quantitiy
PEG 3350 (50% (w/v)) (autoclaved)	260 µL
LiAc 1.0 M (sterile filtrated)	36 µL
carrier ssDNA (2.0 mg/mL)	50 µL
Plasmid DNA (>1 µg) plus sterile water	14 µL
Total volume	360 µL

2.8.2.3. Carbon source variation of the cultivation media

To test which carbon source is the most efficient for recombinant protein expression in *S. cerevisiae*, glucose and sucrose as carbon sources were tested. To do so, a pESC_URA_GFP plasmid was transformed in *S. cerevisiae* cells (section 2.8.2.2., page 36) and a pre-culture was grown for 24 h at 30 °C and 220 rpm in SGI-medium. (Table 5, page 19). After 24 h, 1 mL of the pre-culture was transferred into a new flask containing again either SGI or SSI medium (sucrose). Following 24 h of growth, the GFP expression was induced by adding sterile-filtrated galactose (2 % final concentration). The GFP fluorescence was investigated under a confocal fluorescence microscope in collaboration with Dr. David Kaufholdt (Prof. Dr. Robert Hänsch group, Institut of Plant Biology, TU-Braunschweig).

2.8.2.4. Protein expression in *S. cerevisiae* using Gal1/10 promoter

S. cerevisiae cells were grown at 30 °C and 220 rpm. For cells grown on plates as well as for the starter cultures of *S. cerevisiae*, either SGI medium or SGI plates were used. The main culture was grown in YPSE-medium.

The starter culture consisted of 10 mL SGI-medium in a 100 mL flask and was inoculated with a colony or cryo-stock (section 2.8.2.6., page 38). After 24 - 48 h of incubation, the main-culture was initiated by inoculating a 1L flask containing 100 mL YPSE-medium with about 5 mL of the starter culture. After incubation for 24 h, protein expression was induced by adding 10 mL sterile 20 % galactose solution and finally incubated for another 24 h. Afterwards, the culture was centrifuged using a 50 mL Falcon tube, the supernatant discarded and the pellet directly used for cell disruption (section 2.8.2.7., page 38) or stored at – 80 °C until use.

2.8.2.5. Protein expression in *S. cerevisiae* using pTEF1/pPKG1 promoter

A pre-culture was prepared as described in the previous section (section 2.8.2.4., page 37). After 24 - 48 h in the incubator, the main-culture was prepared by inoculating sterile 100 mL YPSE-medium in a 1 L flask with about 5 mL of the pre-culture. The main-culture was incubated for 24 h. After 24 h, new sterile sucrose solution was added to the culture and cultivated for another 24 h. Afterwards, the culture was centrifuged using a 50 mL Falcon tube, the supernatant discarded and the pellet directly used for cell disruption (section 2.8.2.7., page 38) or stored at – 80 °C until use.

2.8.2.6. Preparation of *S. cerevisiae* cryo-stocks

S. cerevisiae cryo-stocks were prepared by inoculating 10 mL SGI-medium with a single colony from a SGI-plate (Table 5, page 19). The cultures were grown overnight at 30 °C and 220 rpm. 0.5 mL *S. cerevisiae* cell suspension was mixed with 0.5 mL sterile 50 % glycerol (w/w) solution in a cryo-tube. The tubes were vortexed vigorously prior to long time storage at -80 °C.

2.8.2.7. Preparation of *S. cerevisiae* microsomal fraction

Yeast microsomal fractions were obtained as described with some minor modifications [107]. The obtained yeast cell pellet (section 2.8.2.4., page 37) was mixed with an equal amount (w/v) of TES-buffer (Table 24, page 39). About 3 mL was added to a 15 mL

Falcon tube containing 2 – 3 spatula of acid-washed glass beads (425 - 600 µm, Sigma). The cell suspension was then vortexed for about 30 min at 4 °C. To remove cells, cell debris, nuclei and glass beads, the cell suspension was centrifuged at 5000 rpm for 5 min at 4 °C. The supernatant (crude protein) was then transferred into a new 15 mL Falcon tube and kept on ice until further usage. The whole procedure was repeated once more. To obtain a microsomal pellet, ultracentrifugation was carried out at 100.000 g for 1 h at 4 °C using the supernatant obtained from the previous step. The obtained yeast microsomal pellet was diluted in TEG buffer (Table 24, page 39) to give a protein content of either 25 µg/µL (*Hp*PT2) or 50 µg/µL (*Hp*PT6). Protein concentrations were determined either by the method of Bradford (1976) calibrated with bovine serum albumin as a standard or by the Nanodrop (setting: BSA as standard).

Table 24. Yeast cell disruption and storage buffer

Buffer	Composition
TES buffer: pH 7.4	Tris-HCl 50 mM
	EDTA 1 mM
	Sorbitol 0.6 mM
TEG buffer: pH 7.4	Tris-HCl 50 mM
	EDTA 1 mM
	Glycerol 20%

2.8.2.8. Bradford protein assay

All protein concentrations were measured either according to Bradford [108] or using the SimpliNano (protein setting: BSA). Firstly, 900 µL Bradford solution was pipetted into a plastic cuvette with subsequent addition of 98 µL buffer, in which the protein is dissolved. Afterwards, 2 µL protein was added, mixed and further incubated for 5 min. The absorbance was measured at 595 nm against a blank containing Bradford solution (900 µL) and 100 µL buffer. The protein concentration was then calculated based on a BSA calibration curve.

Table 25. Composition of Bradford solution

Component	Quantity
Coomassie-Brilliant blue G250	100 mg/L
Ethanol abs. (96 %)	50 mL
Phosphoric acid (85 %)	100 mL
ddH_2O ad.	1 L

2.8.2.9. DASGIP® bioreactor cultivation

The yeast strains containing the genes *Hp*IBCL and *Hp*IBS were cultivated in the DASGIP® bioreactor systems to compare the productivity between the genes expressed either episomally or genome-integrated. In total, four different strains were cultivated: 1. pESC_URA_IBCLepi_IBS, 2. pESC_URA_IBCLgint_IBS, 3. pESC_URA_BZCLepi_IBS, 4. pESC_URA_BZCLgint_IBS. All genes used were under the control of the constitutive promoters pTEF1/pPGK1. A pre-culture was prepared in SGI-medium by picking single colonies and cultivating them in 50 mL SGI-medium at 30 °C and 180 rpm for about 24 h.

The reactor setup consisted of the following components: DASGIP® cultivation system (Bioblock CWD 4), temperature control module (TC4 SC4), gas regulation module (MX4/4), pH and DO control module (PH4 PO4), pump module (MP8) (DASGIP® Information and Process Technology, Jülich, Germany); three bioreactors (Dasgip® - Sr0400ss Advanced Stirrer 150 – 300 mL, Magnetic Drive) equipped with a pH sensor (Mettler Toledo® MTI D12 mm, L225 mm), a DO sensor (Hamilton, VisiFerm DO 225) and an exhaust condenser (DASGIP®, AD 12 mm, filter: Sartorius stedim Midisart® 2000, 0.2 µm PTFE). The bioreactors were filled with 250 mL SGI-medium and initiated with a pre-culture to reach an OD_{600} between 0.1 – 0.2. The reactors were operated at 30 °C, flushed with 15 sL/h air at 40 rpm (stirrer setting: BMXD) for about 48 – 60 h.

2.9. Biochemical Methods

2.9.1. Isobutyrophenone synthase (*Hp*IBS) assay

This work was performed in cooperation with Dr. Benye Liu and the Bachelor students David Quast and Henning Ummethum [109,110]. The general activity screening of full-length and truncated versions of *Hp*IBS was performed in a total volume of 250 µL containing 100 mM Tris buffer (pH 7.5), 7.62 µM isobutyryl-CoA, 18.76 µM malonyl-CoA and 100 µg yeast crude protein, determined by Bradford (section 2.8.2.8, page 39). The mixture was incubated for 1 h at 37 °C. The reaction mixture was extracted and analyzed by HPLC (section 2.11.2, page 53).

Table 26. Composition of the *Hp*IBS assay

Component	Concentration
Tris-HCl (250 mM) pH 7.5	100 mM
Protein	100 - 200 µg
Isobutyryl-CoA	7.62 µM
Malonyl-CoA	18.76 µM

2.9.2. Aromatic prenyltransferases investigated in this study

Templates used in the current study were kindly provided by Dr. Fiesel and Dr. Gaid (HcPT1–3 and HpPT1 – 9/pFastBac1 plasmids) [34,111,112]. All PTs were cloned into the yeast expression vector pESC-URA or pESC-HIS and transformed into the yeast strain INVSC.1.

2.9.2.1. Prenyltransferase screening experiments

The general PT activity screening of full-length and truncated versions was performed in a total volume of 250 µL containing 100 mM PBS buffer (pH 7), 100 mM $MgCl_2$, 10 mM NaF, 200 µM substrates, 200 µM DMAPP or GPP and 100 µg yeast crude protein. The mixture was incubated for 2 h at 30 °C under continuous shaking at 200 rpm. The products were extracted and analyzed by HPLC (section 2.11.2, page 53). After stopping the reaction with 50 µL 2 N HCl, the assay mixture was extracted twice with

ethyl acetate using double the reaction volume each time. The ethyl acetate extracts were collected and air-dried. The obtained residue was resuspended in 100 µL of either DMSO or methanol (HPLC grade), of which a 25 µL aliquot was analyzed by HPLC (section 2.11.2., page 53).

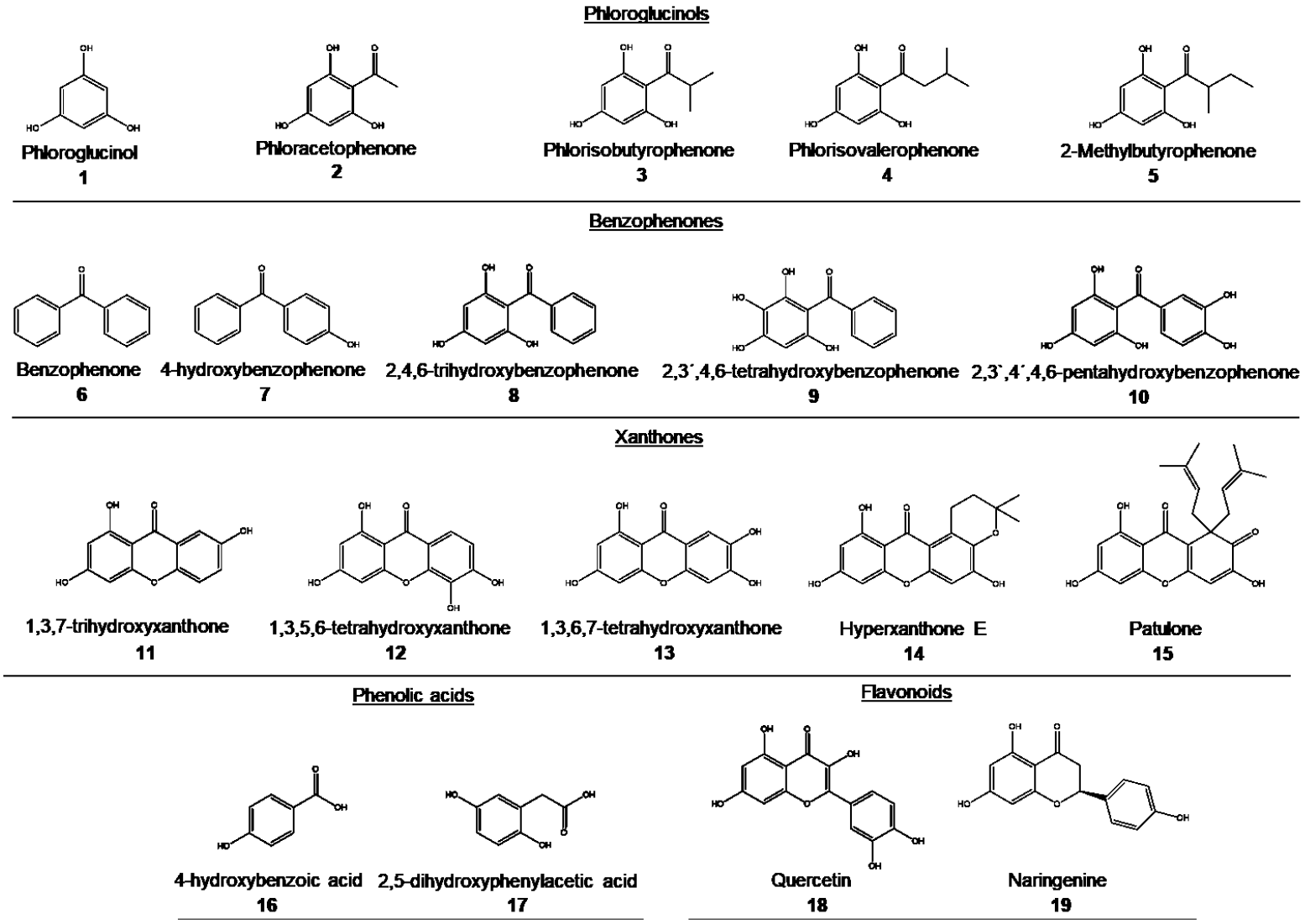

Figure 11. PT substrates used for incubations in this study.

2.9.2.2. Kinetic characterization of *Hp*PT2

The standard enzyme assays were carried out in a total volume of 125 µL containing 100 mM Tris buffer (pH 8), 10 mM $MgCl_2$, 400 µM Substrate, 600 µM GPP and 100 µg yeast microsomal protein. The mixture was incubated for 10 min at 40 °C and 700 rpm. All substrates were dissolved in methanol or DMSO.

2.9.2.3. Kinetic characterization of *Hp*PT6

The standard enzyme assays were carried out in a total volume of 125 µL containing 100 mM Tris-buffer (pH 9), 10 mM $CaCl_2$, 250 µM substrate, 400 µM DMAPP, 2.5 µL DMSO to solubilize the substrate and 400 µg yeast microsomal protein. The mixture was incubated for 10 min at 50 °C and 700 rpm. All substrates were mainly dissolved in methanol and/or DMSO.

2.9.2.4. Determination of K_M and V_{max}

The Michaelis-Menten equation (Figure 12, page 45) describes the velocity (V_{max}) and affinity of an enzyme, which depend on the substrate concentration. The enzymatic affinity towards a substrate is expressed by the term Michaelis constant (K_M). The maximum enzymatic reaction velocity is expressed by the term V_{max}.

The apparent K_M values for the most preferred substrates of *Hp*PT2 and *Hp*PT6 were determined by using varying concentrations of acceptor substrate and co-substrate (DMAPP, GPP). The acceptor substrate ranged from 5 – 400 µM while keeping the GPP (600 µM) and DMAPP (400 µM) concentrations constant. The apparent K_M values for GPP and DMAPP were quantified by using concentrations ranging from 5 – 1500 µM with constant acceptor concentrations (400 µM and 250 µM for *Hp*PT2 and *Hp*PT6, respectively). All measurements were done in three technical triplicates. Extraction and quantification of the enzymatic products were done as mentioned above (section 2.9.2.1., page 41). All K_M and V_{max} values were estimated using either OriginPro (Version 2016G) or Hyper32 (Version 1.0.0, Hyper) employing the “Michaelis-Menten” equation (Figure 12).

$$V_0 = \frac{V\max * [S]}{K_M + [S]}$$

V_0 = Enzymatic reaction velocity
V_{max} = Maximum enzymatic reaction velocity
K_M = Michaelis–Menten constant [mM]
S = Substrate concentration [mM]

Figure 12: Michaelis-Menten equation.

2.9.2.5. Large-scale incubation and purification for NMR structure elucidation

To obtain enough amount of a product for verifying the structure by NMR, large-scale incubation was performed. The standard assay volume was increased at least 200 – 250 times. After incubation, the reaction was stopped by the addition of 2 mL 1N HCl. The product was extracted 3 times with an amount of ethyl acetate equal to the incubation mixture. The ethyl acetate phase was dried under nitrogen gas, dissolved in 100 µL MeOH (HPLC grade) and purified via HPLC. The collected fractions were again dried under nitrogen until the organic phase (methanol) was removed. The aqueous phase was then finally dried by lyophilization. After freeze-drying, the obtained enzymatic product was dissolved in deuterated solvents ($CDCL_3$ or CD_3OD; Deutero, Kastellaun, Germany).

2.10. Chemical Methods

2.10.1. Synthesis and purification of dimethylallypyrophosphate (DMAPP)

The synthesis of DMAPP was carried out according to the following literature [113]. The synthesis was done in collaboration with Dr. Mariam Gaid, Dr. Eline Biedermann, and Mohamed Nagia, whereas MS spectrometry was carried out together with Dr. Till Beuerle.

2.10.1.1. Synthesis of DMAPP

A 100 mL round-flask was heat-dried overnight at 150 °C for residual water removal before starting the synthesis. Tris(tetrabutylammonium)hydrogen pyrophosphate 97 % (5.64 mmol, Sigma) was resuspended in 20 mL water-free acetonitrile (dried over anhydrous Na_2SO_4, Zentrales Lager für Chemikalien [ZLChem], TU Braunschweig) by stirring at room temperature. Dimethylallylchloride (345 µl, Sigma) 97 % (2.91 mmol) was added, the flask closed (rubber) to avoid the entrance of water and further mixed for additional 2 h at room temperature. The acetonitrile was subsequently removed using a rotary evaporator and a water bath at 40 °C and the remaining pale-yellow viscous residue was stored at -20 °C.

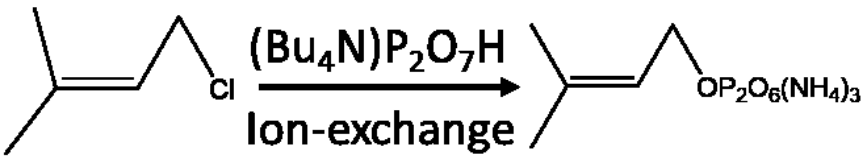

Figure 13. Synthesis of DMAPP according to Woodside et al. (1993).

2.10.1.2. Purification of DMAPP

Preparation of the cation-exchange column

For the conversion of the acidified material Dowex AG 50W-X8 (100–200-mesh, H^+ form) into the ammonium counterpart, 188 mL was washed four times with concentrated ammonium hydroxide solution. The material was washed with 200 mL ddH_2O until pH 7 was reached. Finally, the material was packed into a column and equilibrated with 2 x 200 mL cation-exchange buffer (Table 27).

Preparation of Whatman CF11 fibrous cellulose column

For the preparation of a Whatman CF11 fibrous cellulose column, 1 L cellulose powder was mixed with 700 mL ddH_2O water and stirred with a glass rod for few minutes. The suspension was allowed to settle for about 30 min with subsequent decanting of the water phase. The previous steps were repeated with 2 x 700 mL portions of 0.1 N hydrochloric acid, 2 x 700 mL portions of deionized water, 2 x 700 mL portions of 0.1 N sodium hydroxide, 2 x 700 mL portions of deionized water, and 2 x 700 mL portions of 1:1 (v/v) isopropyl alcohol : water (overnight storage at 4 °C). After packaging the column, the cellulose material was first washed with 1.3 L acetonitrile and then with 1.3 L of a 1:1 (v/v) isopropyl alcohol: water mixture. Finally, the cellulose column was equilibrated with 1.3 L chromatography buffer (Table 27).

Table 27. Ion-exchange buffer for DMAPP purification

Buffer	Composition	Quantity
Cation-exchange buffer (25 mM)	Ammonium carbonate	2 g
	Isopropanol	20 mL
	ddH_2O	980 mL
Chromatography – buffer (50 mM)	Ammonium carbonate	4 g
	Isopropanol	500 mL
	Acetonitrile	250 mL
	ddH_2O	250 mL

2.10.1.3. Purification of DMAPP after the synthesis

The remaining pale-yellow residue from the previous step was dissolved in 3 mL cation-exchange buffer (Table 27, page 47) and the obtained clear solution was loaded onto the previously prepared cation-exchange column. The flask was washed 2 x with 5 mL cation-exchange buffer to collect the remaining synthetic DMAPP and then loaded onto the column. The elution was carried out with 360 mL cation-exchange buffer (Table 27, page 47) and the eluent was collected in a 500 mL flask. The collected fractions were frozen in liquid N_2 and further lyophilized for 18 – 24 h until a white solid powder remained. The remaining material was dissolved in 5 mL of 50 mM ammonium bicarbonate and the clear solution was transferred to a 50 mL Falcon tube. Afterwards, 20 mL of a 1:1 (v/v) acetonitrile: isopropyl alcohol mixture was added and the tube was vigorously vortexed until a white precipitate was formed. The suspension was centrifuged for 5 min at 2000 rpm until a clear solution occurred. The supernatant was discarded and the white residue washed twice with 5 mL of 50 mM ammonium bicarbonate. Three further extractions were carried out by the addition of 2 mL 50 mM ammonium bicarbonate and 8 mL 1:1 (v/v) acetonitrile: isopropyl alcohol. The supernatants were combined and concentrated up to about 5 mL using a rotary evaporator and a water bath at 40 °C. The obtained concentrated solution was dissolved in an equal amount of chromatography buffer (Table 27, page 47) and loaded onto the Whatman CF11 fibrous cellulose column. The flask was washed three times with 5 mL chromatography buffer and loaded on the column. The product was eluted using 900 – 1500 mL chromatography buffer, fractions of about 20 mL being collected. Every second fraction was analyzed by thin-layer chromatography (DC-plates cellulose, 20 x 20 cm, layer thickness 0.1 mm; Merck Darmstadt, Germany) using the chromatography buffer as mobile phase. After the thin layer chromatography, the plate was sprayed with a freshly prepared sulfosalicylic acid solution (Table 28, page 49), air-dried, followed by spraying with freshly prepared iron(III)-chloride solution (Table 28, page 49). Phosphate-containing compounds appear as white dots on a pink background (section 3.1.1., page 57). All fractions containing the target product were pooled, concentrated up to about 120 mL (rotary evaporator at 40 °C), frozen in liquid N_2 and further lyophilized for 18 – 24 h until a white flocculent solid remained. Aliquots containing 1 mL of 50 mM DMAPP were prepared by dissolving the previously obtained material in methanol:ammonia 10 mM (7:3) and stored at -80 °C until use. The

formation of DMAPP and its purity were further verified via MS-spectrometry (2.11.5., page 55).

Table 28. Spray solution for the detection of DMAPP after chromatography

Solution	Composition	Quantity
Sulfosalicylacid solution	5 - Sulfosalicacid	1 g
	Ethanol	60 mL
	ddH_2O	40 mL
Iron(III)- chlorid solution	Iron(III)- chloride	0.2 g
	Ethanol	80 mL
	ddH_2O	20 mL

2.10.2. Synthesis of PIBP and PIVP

The synthesis of phlorisobutyrophenone (PIBP) was done according to [114] with minor modifications:

Anhydrous phloroglucinol (10.0 g, 79.3 mmol, Merck, Germany) was dissolved by stirring in 80 mL nitrobenzene (Merck, Germany). $AlCl_3$ (42.3 g, 317 mmol, Merck, Germany) was added in three portions until the solution turned into a pale brown solution. The complete reaction mixture was stirred for at least additional 30 min at RT until a clear solution was obtained. Afterwards, 9.14 mL (87.2 mmol) of the alkyl-halide isobutyryl-chloride solution (Sigma, Germany) was added stepwise and the reaction mixture heated up to 65 °C using an oil bath for about 21 h. The reaction was stopped by pouring it into ~200 mL ice-water. The product was then extracted from the reaction mixture using 3 x 500 mL EtOAc. The organic phase was concentrated up until a thick oily residue was formed. To remove the $AlCl_3$ from the reaction mixture, the oily residue was loaded and purified over a celite column using EtOAc as an eluent. The effluent was concentrated up again and further purified by column chromatography using SiO_2 (250 g) and petrol ether/EtOAc (4:1 → 2:1) as eluent. For structure elucidation or enzymatic incubations, PIBP was further purified by semi-preparative HPLC (section 2.11.4., page 55). The structure was validated by MS spectrometry (section 2.11.5., page 55) and ^{1}H-NMR and ^{13}C-NMR (section 2.11.6., page 56).

PIVP was synthesized according to the procedure described in this section, except that only 1/5 of this amount was synthesized and isovaleryl-chloride was used as alkyl-halide.

2.10.3. Synthesis of 2-methylbutanoyl-phloroglucinol (2-MBP)

The synthesis of 1-(2,4,6-trihydroxyphenyl)-2S-methylbutanone was adapted from the procedure described elsewhere [115].

2.10.3.1. Synthesis of (S)-2-methylbutanoic chloride

(S)-(+)-2-methylbutanoic acid (4.9 mmol in 0.5 mL; Alfa Aesar, Germany) was added to a 50 mL round bottom flask and stirred at room temperature at 150 rpm. Afterwards, 0.5 mL oxalyl-chloride (5.9 mmol; Sigma, Germany) was added, the bottom flask closed and the mixture stirred at room temperature for about 30 min. After 30 min, 2 ml dichloromethane was added and the whole mixture proceeded to the second step as described below in section 2. The synthesized (S)-2-methylbutanoic chloride was used without purification.

2.10.3.2. Synthesis of 1-(2,4,6-trihydroxyphenyl)-2S-methylbutanone

For the final synthesis, 0.5 g phloroglucinol (3.9 mmol) was dissolved in a mixture of 3 mL dichloromethane and 5 mL nitromethane. Aluminum-trichloride (2.1 g ~ 15.6 mmol) was added in three portions and the mixture was stirred at room temperature for 30 min. After 30 min, the freshly prepared (S)-2-methylbutanoic-chloride solution (from step 1) was added slowly and stirred for another 5 min at room temperature. The mixture was refluxed for 16 h at 40 °C in an oil bath. The mixture was cooled down to room temperature and the reaction stopped with 100 mL ice-cold water. The mixture was acidified using HCl until pH 1 - 2 was reached. Volatile organic solvents were evaporated under N_2. The reaction mixture was extracted three times with 150 mL EtOAc with subsequent evaporation under N_2. The remaining solution was dissolved in methanol (HPLC grade) and purified via semi-preparative HPLC. The structure was confirmed via MS-spectrometry and NMR-spectroscopy.

2.10.4. Synthesis of 3-prenyl-PIBP

The synthesis of 3-prenyl-PIBP was carried out according to Li Xiao et al. (1998). In a round bottom flask, PIBP 0.5 g (0.25 M) was dissolved in 10 mL 4.9 mmol KOH (2.8 mg), stirred and cooled on ice. Prenyl-bromide 450 µL (0.3 M; Sigma, Germany) was added dropwise over 5 min while warming up to room temperature. After stirring for about 3 – 4 h, the reaction was stopped by adding 10 ml ice-cold HCl-acidified (pH 2) water. Finally, the 3-prenyl-PIBP product was extracted three times with ethyl acetate (30 mL). The combined organic phases were evaporated under N_2 and purified by HPLC (section 2.11.4., page 53).

2.10.5. Synthesis of 3-geranylated PIBP, PAP, PBP, PIVP, and 2-MBP

The synthesis were carried out according to the following publication [116], here exemplified by the synthesis of 3-geranyl-PIBP.

A mixture of 1 molar equivalent of PIBP (synthesized as described in section 2.10.2., page 49) (100 mM), 1 molar equivalent of geranyl-bromide (100 mM, Sigma, Germany) and 2 M equivalents of K_2CO_3 (0,27 g) in 10 mL water-free acetone (dried over sodium sulfate) was stirred at RT for 24 h under reflux. Firstly, PIBP was dissolved in acetone and cooled down in an ice bath prior to addition of geranyl-bromide (exothermic reaction!). Geranyl-bromide was then added dropwise within about 5 min and the reaction was carried out under reflux for 24 h. After 24 h, the acetone was evaporated under N_2 and the reaction stopped by the addition of about 2 mL 2 N HCl (pH should be about 3 – 4). Chemically synthesized 3-geranyl-PIBP was extracted 3 times with about 5 mL EtOAc. Following extraction, EtOAc was evaporated under N_2 and the remaining oily residue dissolved in MeOH (HPLC grade) and purified via semi-preparative HPLC (section 2.11.4., page 55). Structure verification was carried out by MS–spectrometry. The enzymatic product of *Hp*PT2, which was NMR verified and identified as 3-geranyl-PIBP, was used as an authentic reference compound for chromatography.

2.10.6. Synthesis of 1,3,6,7-tetrahydroxyxanthone

The synthesis of 1,3,6,7-tetrahydroxyxanthone was performed according to [117]. Mangiferin (30 mg; Avachem, San Antonio, USA) was dissolved in 150 µL HBr and 120 µL phenol, heated up at 150 °C for 6 h under reflux. Then, 3 mL of saturated sodium bicarbonate solution was added to the mixture to obtain 1,3,6,7-tetrahydroxyxanthone. The product was extracted 3 times with about 20 mL EtOAc. Following extraction, EtOAc was evaporated under N_2 and the remaining oily residue dissolved in MeOH (HPLC grade) and purified via semi-preparative HPLC (section 2.11.4., page 55). Structure verification was carried out by MS spectrometry.

2.11. Analytical Methods

2.11.1. HPLC theoretical background

High-performance liquid chromatography is one of the most commonly used methods for the separation and quantification of compounds in natural science. For the reversed phase separation principle, the separation is based on the interaction of the analyte dissolved in the polar mobile phase and the non-polar stationary phase. Common mobile phases are water, methanol and acetonitrile and columns containing modified silica (SiO_2) microparticles (typically a size 1.5 – 5 µm) are the stationary phase. For the separation of a mixture of hydrophilic and hydrophobic analytes, C_{18} modified reversed phase (RP) columns are the most widely spread columns. For the detection of the analytes, DAD is the most common UV/VIS detectors due to the ability to record the UV (ultraviolet) spectra ranging from 190 to 390 nm and the VIS spectra ranging from 390 nm to 700 nm. These types of detectors guarantee the detection of aromatic and unsaturated conjugated compounds.

2.11.2. HPLC Measurements

In the current study, three different types of HPLC machines were used for analytical purposes; the Agilent 1260 Infinity Quaternary LC System (Agilent Technologies; Santa Clara, CA, USA) with a diode array detector (G4212A); the Waters 2795 Separations Module with a Waters 2996 PDA Detector (Waters, Germany). They were equipped with either a Symmetry® C_{18} column (4.6 x 75 mm, 3.5 µm; Waters, Germany) or a ZORBAX SB-C18 (3.5 µm, 4.6 × 150 mm; Agilent) column.

Bidest water containing 0.1 % formic acid (solvent A) and methanol (solvent B) were used as solvents. The flow rate was set to 1 mL/min (Waters column) or 0.5 mL/min (ZORBAX column) with the following linear gradient (v/v) for solvent B: 0 to 6 min., 40% to 60%; 6 to 10 min., 60% to 85 %; 10 to 11 min., 85% to 95%; 11 to 16 min., 95 to 100%. The column was washed with 100% solvent B for 3 min and then equilibrated with 40% solvent B for 5 min. The third HPLC was used for semi-preparative purposes (section 2.11.4., page 55).

2.11.3. Calibration curve:

Three PIBP (Stock 100 mg/mL) calibration curves have been prepared according to the following dilution series as described in Table 29. Each dilution (20 µL) series was analyzed by HPLC and the detection wavelength was set at 286 nm.

Table 29. Composition of the calibration curve for PIBP, PIVP, and 2-MBP

No.	Final in HPLC (µg)	Vial Stock (µg/mL)	dilution series
1	0.1	5	1/10 of 50
2	0.2	10	1/10 of 100
3	0.5	25	1/10 of 250
4	1.0	50	1/10 of 500
5	2.0	100	1/10 of 1mg
6	5.0	250	1/1 of 500
7	10.0	500	1/2 of 1mg
		1000	1/100 of 100 mg/mL

Additional calibration curves have been prepared for the other chemically synthesized compounds with a concentration of 50 mg/mL: 3-geranyl-PIBP, 3-geranyl-PIVP, 3-geranyl-PAP, 3-geranyl-2-MBP, 3-geranyl-PBP. Due to the low availability of the compounds, only three dilution series have been prepared and injected with different injection volumes. Dilution series were analyzed by HPLC and the detection was performed at the compound-specific wavelengths (nm).

Table 30: Composition of calibration curves for 3-g-PIBP, 3-g-PIVP, 3-g-PAP, 3-g-PBP, 3-g-2-MBP

No.	Final in HPLC (µg)	Vial Stock (µg/mL)	injection Volume
1	0.025	2.5	10 µL
2	0.050	2.5	20 µL
3	0.100	2.5	40 µL
4	0.250	25	10 µL
5	0.500	25	20 µL

6	1.000	25	40 µL
7	2.500	250	10 µL

2.11.4. Semi-preparative HPLC

For a large-scale purification of enzymatically or chemically synthesized products, semi-preparative HPLC was used. VWR Hitachi HPLC L-2130 (VWR) with a diode array detector (L-2455) equipped with either a Hyperclone 5µ ODS (C_{18}) 120A column or a Phenomenex column (10 x 250 mm, 5 µm; Phenomenex, Germany).

Bidest water containing 0.1 % formic acid (solvent A) and methanol (solvent B) was used as a solvent. The flow rate was set to 5 mL/min with a linear gradient (v/v), which was as follows for solvent B: 0 to 4 min, 40% to 75%; 4 to 39 min, 75% to 86 %; 39 to 40 min, 86% to 100%; 40 to 41 min, 100% isocratic elution for 5 min. The column was washed with 100% solvent B for 5 min and then equilibrated with 40% solvent B for 3 min. Depending on the compound, some modifications had to be adjusted based on the previously described method.

2.11.5. Mass spectrometry

All MS measurements of the current Ph.D. project were carried out in cooperation with Dr. Till Beuerle. Each analysis was performed using the QTrap 3200 System (Applied Biosystems/MDS SCIEX, Darmstadt; II6). The Analyst software (version 1.6.2; Applied Biosystems/MDS Sciex, Waltham, MA, USA) served for data acquisition and processing. The samples were HPLC-purified and prepared in concentrations of about 5 - 10 µg/mL. If required, they were dried and finally dissolved in 500 µL methanol (MS-Grade) before injection. All samples were injected into the electrospray-ionization source (ESI, Turbo V) using a Hamilton syringe pump with 5 µL/min.

The target molecular-ion peaks $[M + H]^+$ or $[M - H]^-$ were further analyzed by MS^2 experiments in the enhanced product ion (EPI) mode of the instrument using nitrogen gas for collision-induced dissociation at the high-level setting.

2.11.6. NMR spectroscopy

All NMR samples were analyzed and evaluated in cooperation with Prof. Dr. Ludger Ernst (Zentrales NMR-Labor, Technische Universität Braunschweig). ^{13}C-NMR and ^{1}H-NMR analyses were carried out on a Bruker Avance II 600 spectrometer using $CDCl_3$ or CD_3SOCD_3 (Deutero, Kastellaun, Germany) as solvents. Purified samples (2 mg) were stored at -20 °C in the dark until analysis. Enzymatic products for NMR-spectroscopy were prepared as described under section (section 2.11.2., page 45). Detailed information is described in the following sections as prepared by. Prof. Dr. Ludger Ernst.

^{1}H and ^{13}C NMR spectra of **grr133194**–**grr133197 (Appendix)** were recorded at 500.3 and 125.8 MHz, respectively, on an Avance III HD 500 spectrometer with a Prodigy probehead (nitrogen-cooled) from Bruker BioSpin (Rheinstetten, Germany). The spectra of **grr132394**, **grr133479**, **grr133480** and **gam129944 (Appendix)** were recorded on an Avance II 600 spectrometer with a TCI cryo probehead (helium-cooled) at 600.1 and 150.9 MHz, respectively. The solvents were dimethylsulfoxide-d_6 or chloroform-*d* at concentrations < 5 mg/0.45 mL in 5 mm o. d. NMR tubes. Chemical shifts are reported in δ units (ppm). They were measured relative to tetramethylsilane (TMS, δ_H = 0.00 ppm) and to the solvent $CDCl_3$ (δ_C = 77.01 ppm) and DMSO-d_6 (δ_C = 39.50 ppm), respectively. Assignment techniques used throughout were DEPT-135 (distortionless enhancement by polarization transfer), H,C-HSQC (heteronuclear single quantum correlation) and H,C-HMBC (heteronuclear multiple-bond correlation). To facilitate assignments in difficult cases, H,H-COSY (correlation spectroscopy) or H,H-NOESY (nuclear Overhauser effect spectroscopy) spectra were also recorded. Digital resolutions in the two-dimensional NMR spectra were chosen small enough to permit the distinction of cross-peaks with similar chemical shifts (if possible). The mixing time in the NOESY experiment was 1.0 s. The HSQC and HMBC experiments were optimized for C,H-coupling constants of 145 and 8 Hz, respectively.

3. Results

3.1. Chemical synthesis of potential substrates

3.1.1. Synthesis of DMAPP

Plant-derived aromatic prenyltransferase (PT) enzymes transfer prenyl moieties, such as C_5 (dimethylallyl), C_{10} (geranyl), C_{15} (farnesyl) or C_{20} (geranylgeranyl), to their acceptors, while forming C-C, C-N or C-O bonds [74,76]. In this work, DMAPP and GPP (provided by Mohamed Nagia) were required as isoprenoid donors to perform *in vitro* enzymatic assays. The synthesis was carried out according to Woodside et al. (1993). Dimethylallylchlorid was phosphorylated by tris(tetrabutylammonium)hydrogen pyrophosphate, followed by purification *via* a Whatman CF11 fibrous cellulose column. In total, 80 fractions (10-15 mL) were collected and every second fraction was analyzed by thin-layer chromatography (TLC; cellulose plates). The phosphate group of DMAPP was visualized by spraying the plates with a sulfosalicylic acid solution and then iron(III)-chlorid solution. Fractions containing DMAPP appeared white on a pink background (Figure 14).

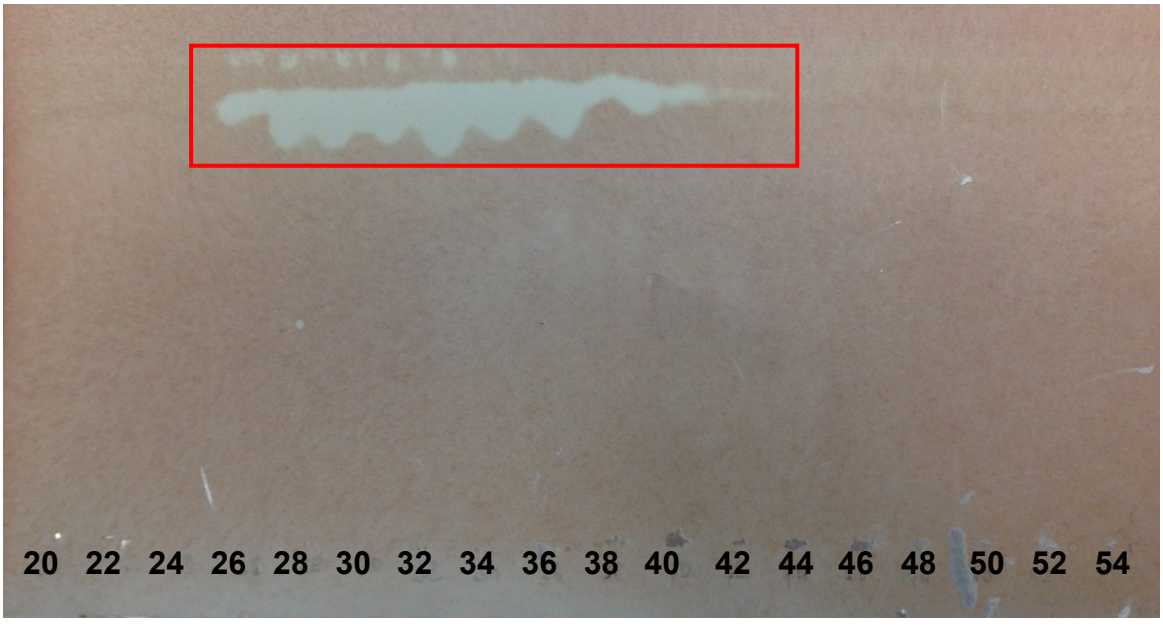

Figure 14. A TLC plate after visualization of chemically synthesized prenyl donors in fractions of cellulose column chromatography.

All fractions containing DMAPP (26-42) were collected, concentrated up and lyophilized for 18–24 h until a white flocculent solid remained. In total, 640 mg DMAPP was obtained and dissolved in methanol:10 mM ammonia = 7:3, giving a solution of a final concentration of 50 mM DMAPP, which was stored at -80 °C until use. Structure validation was carried out by mass-spectrometry using a 10 µg/mL DMAPP methanolic solution. Upon applying an ESI - MS^2 analysis (collision energy of -50 V), the molecular ion $[M - H]^-$ was detected at *m/z* = 245.0, which corresponded to the MW of DMAPP. Additional characteristic fragment ions at *m/z* = 159.0 $[M - H]^-$ and *m/z* = 79.0 $[M - H]^-$ were confirmed. The MS^2-fragmentation pattern (Figure 15) agrees with the previously reported data [111,112].

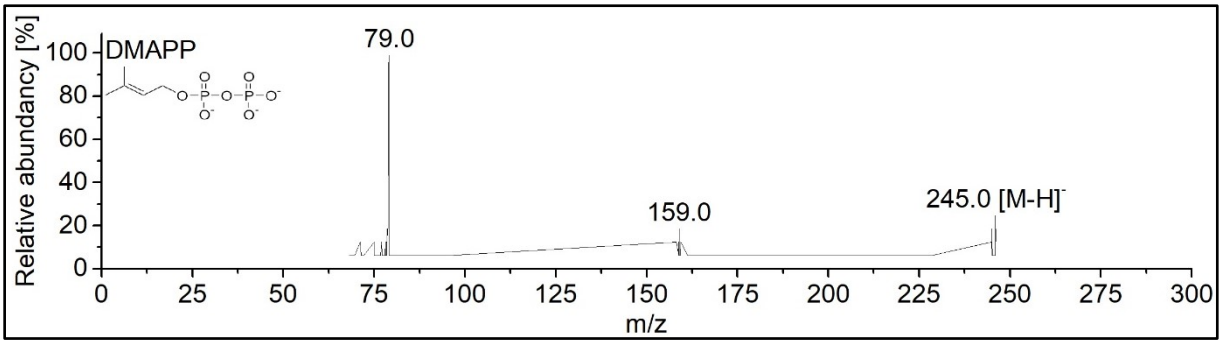

Figure 15. Mass spectrometry of DMAPP. EPI-MS^2 of m/z 245.0.

3.1.2. Synthesis of PIBP, PIVP, and 2-MBP

Plant-derived aromatic PTs are reported to accept a number of aromatic derivatives, such as phloroglucinols, xanthones, benzophenones, flavonoids and phenolic acids (Figure 11, page 43) [28,118]. Since the biosynthesis of hyperforin and congeners (e.g. adhyperforin) in *Hypericum* was the focus of the current study, cores of these molecules were targeted for chemical synthesis. Due to the lack of cost-effective commercial sources, chemical synthesis was required to provide reliable prenyl acceptors for the activity screening of potential PTs.

Phlorisobutyrophenone (PIBP) and 2-methylbutyrophenone (2-MBP) are the biosynthetic precursors of hyperforin and adhyperforin, respectively. Recently, auxin-induced root cultures of *H. peforatum* were reported to accumulate colupulone, whose precursor is PIBP. Colupulone and lupulone are known as β-acids, which are characteristic of the hop female flower (*Humulus lupulus*). To cover the latter aspect, phlorisovalerophenone (PIVP) was chemically synthesized and included in the activity

assays, speculating on a side activity for a PIVP-accepting PT. Except for 2-MBP, which was synthesized according to Forbofou et al. (2016), PIBP and PIVP were synthesized as described by George et al. (2010). A Friedel-Craft reaction using phloroglucinol and either isobutyryl-chloride or isovaleryl-chloride was used for the synthesis of PIBP and PIVP, respectively. The synthesis of 2-MBP was done in two steps. Firstly, the synthesis of the alkyl-halide (*S*)-2-methylbutanoic chloride and secondly the Friedel-Craft reaction as described above for the formation of 2-MBP. Worthy to say that a racemic mixture of 2-MBP did not end in an enzymatically accepted product. Purification *via* semi-preparative HPLC was performed for all prenyl acceptors, which was preceded by column chromatography only in the case of PIBP (section 2.10.2., page 49).

The molecular ion peaks $[M + H]^+$ of all three products were further analyzed by MS^2-spectrometry (section 2.11.5., page 55). The molecular ions $[M + H]^+$ of PIBP (*m/z* = 197), PIVP (*m/z* = 211) and 2-MBP (*m/z* = 211) are shown in Figure 16 (A-C). They correspond to the MW of PIBP (196 g/mol), PIVP (210 g/mol) and 2-MBP (210 g/mol), as described in the literature (Li et al., 2015). All samples were additionally analyzed *via* ^{1}H-NMR and ^{13}C-NMR (Appendix 6.7. NMR Data**,** page 143).

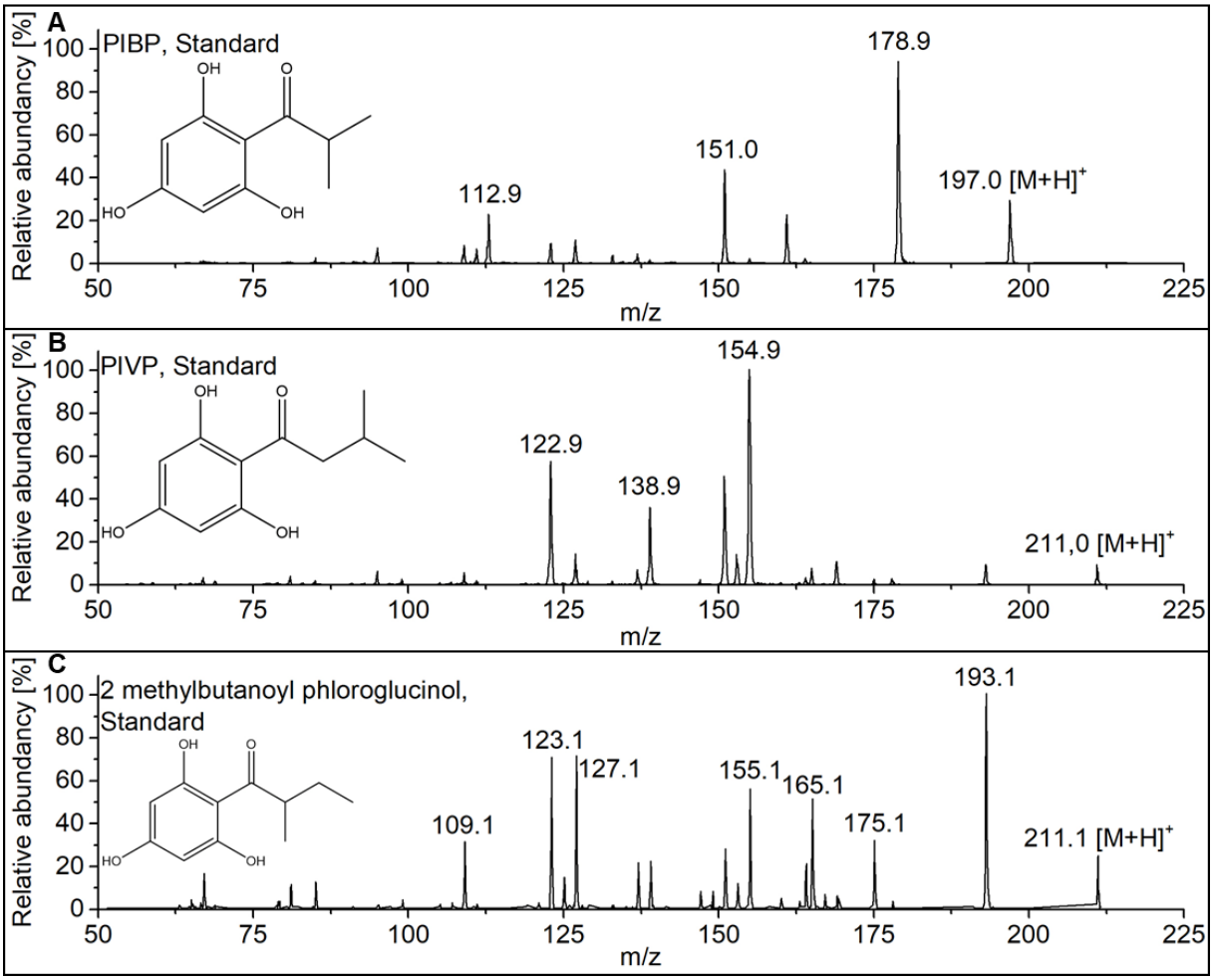

Figure 16. MS^2 Fragmentation pattern of (A) PIBP (m/z = 197.0), (B) PIVP (m/z = 211.0) and (C) 2-MBP (m/z = 211.1). The analysis was carried out in the positive ion mode (EPI+).

3.1.3. Synthesis of 3-geranyl acylphloroglucinols

In section 2.10.2, page 49, the chemical synthesis of the hyperforin skeleton, PIBP, was described. A cascade of 4–5 enzymes are required for the total hyperforin biosynthesis [28]. Each enzymatic intermediate related to the hyperforin biosynthesis must therefore be considered as a potential PT substrate. Based on the results obtained in section 3.3.4., page 79, *Hp*PT6 has been identified to accept exclusively 3-geranyl-acylphloroglucinol derivates as substrates. All major substrates accepted by *Hp*PT2, namely PIBP, PIVP, PAP, PBP and 2-MBP (section 3.3.4.4., page 82) have been chosen to synthesize as its 3-geranylated derivatives, as described previously [116]. Briefly, a mixture consisting of 1 molar equivalent acylphloroglucinol derivative (PIBP, PAP, PBP, 2-MBP or PIVP), 1 molar equivalent of geranyl bromide and 2 molar equivalents of K_2CO_3 were stirred at RT for 24 h under reflux. The products were

extracted and purified *via* semi-preparative HPLC (section 2.11.2., page 55). Structure verification was carried out by mass spectrometry and NMR spectroscopy.

All five molecular-ion peaks $[M + H]^+$ were further analyzed by MS^2 spectrometry (section 2.11.5., page 55). The molecular ion $[M + H]^+$ of 3-geranyl-PIBP (*m/z* = 333.2), 3-geranyl-PAP (*m/z* = 305.0), 3-geranyl-PIVP (*m/z* = 347.5), 3-geranyl-PBP (*m/z* = 367.1) and 3-geranyl-2-MBP (*m/z* = 345.4) are shown in Figure 17 (A-E) and correspond to the MW of 3-geranyl-PIBP (332 g/mol), 3-geranyl-PAP (304 g/mol), 3-geranyl-PIVP (347 g/mol), 3-geranyl-PBP (366 g/mol) and 3-geranyl-2-MBP (344 g/mol), respectively. Structure elucidation was additionally confirmed *via* ^{13}C-NMR and ^{1}H-NMR analyses (section 6.7. NMR Data**,** page 143).

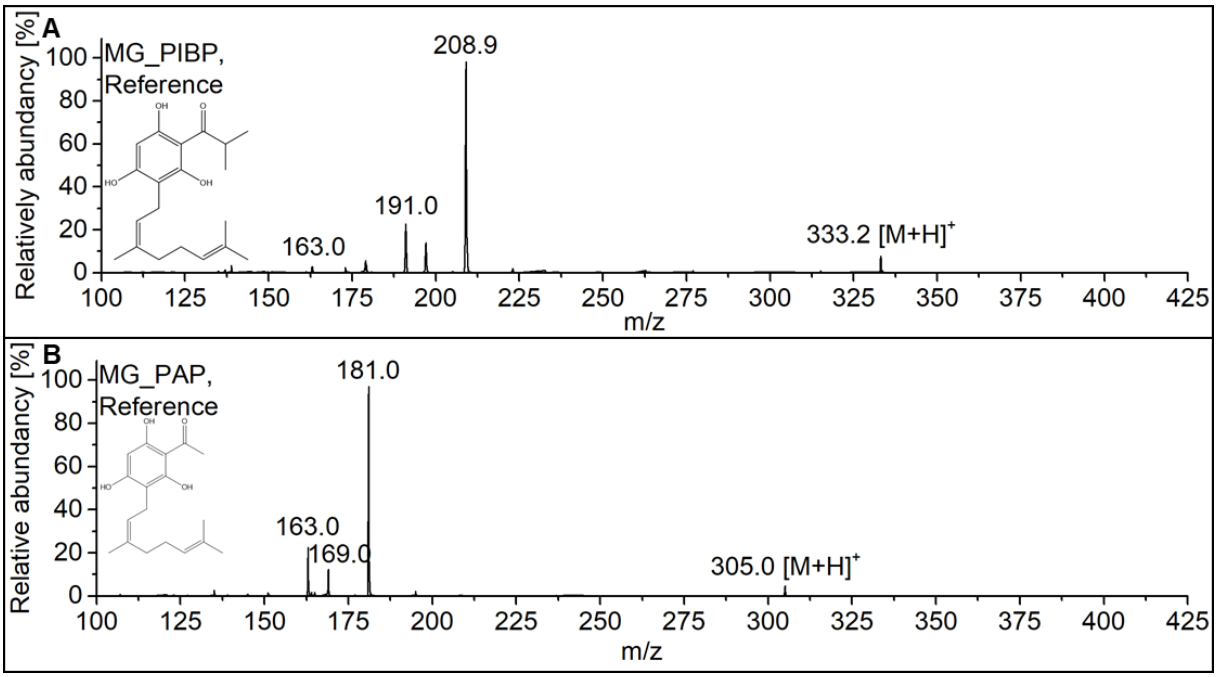

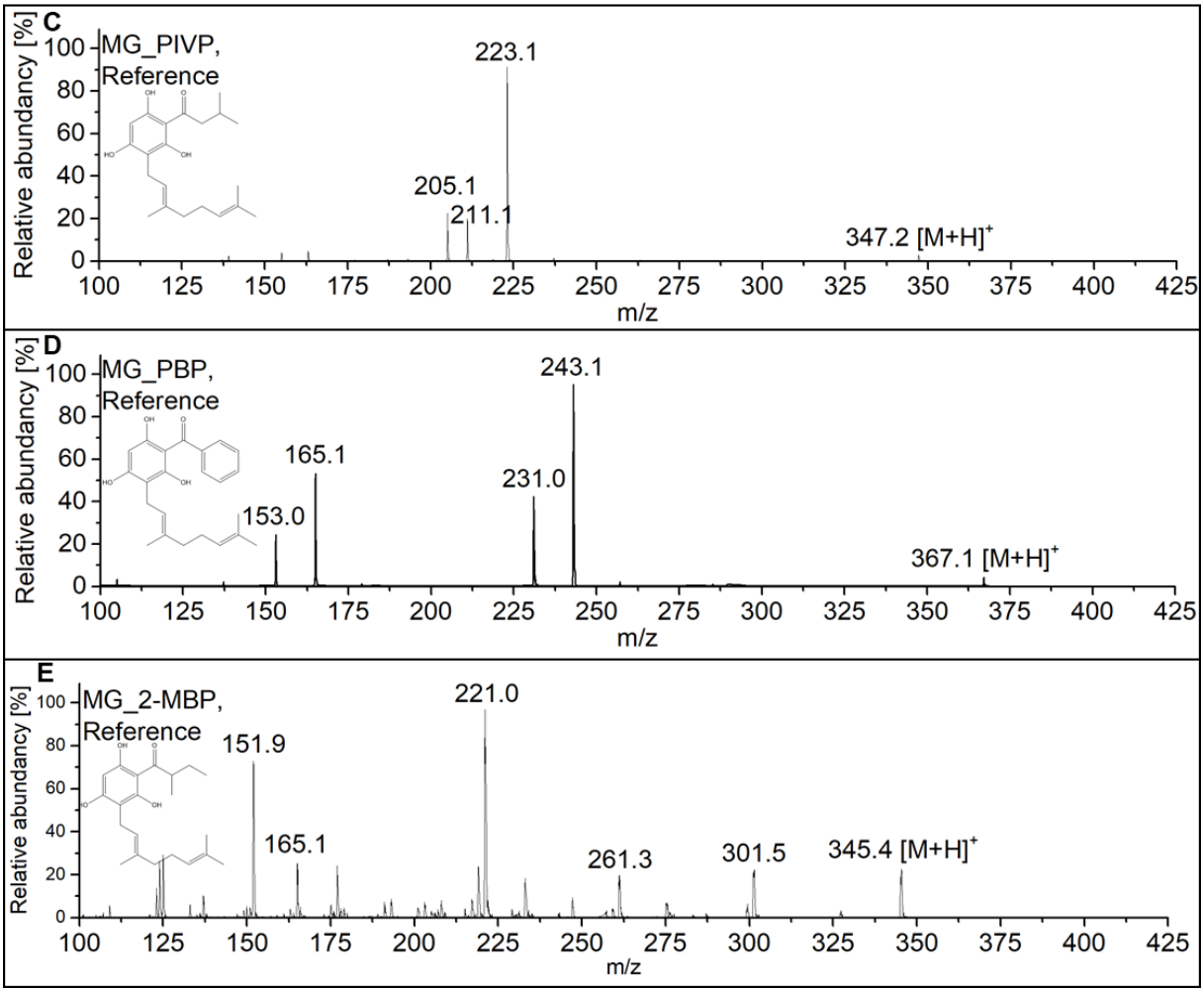

Figure 17. MS^2-Fragmentation patterns of chemically synthesized monogeranylated (MG) acylphloroglucinols, namely 3-geranyl-PIBP (A), 3-geranyl-PAP (B), 3-geranyl-PBP (C), 3-geranyl-PIVP (D) and 3-geranyl-2-MBP (E). Analyses were carried out in positive ion mode (EPI+).

3.2. Biosynthesis of the hyperforin skeleton PIBP

3.2.1. Activity assay of episomally expressed *Hp*IBCL

The results in this paragraph were produced in collaboration with Dr. Benye Liu who performed the enzymatic assay. The collaboration on product purification and analysis also involved Dr. Till Beuerle.

The formation of the hyperforin core structure, PIBP, starts by the condensation of three molecules of malonyl-CoA and one molecule of isobutyryl-CoA [24]. Consequently, the occurrence of isobutyryl-CoA in proper amounts is a prerequisite for *in vivo* production systems. Due to low availability of intracellular isobutyryl-CoA in yeast, an alternative approach was focused. Dr. Benye Liu cloned a cDNA for isobutyrate-CoA

ligase from *H. perforatum*, which forms isobutyryl-CoA from isobutyric acid and CoA in the presence of ATP. The cDNA was expressed in *E. coli* and the resulting protein was tested for *in vitro* activity. The product formed was purified and analyzed by mass spectrometry. The molecular ion peak $[M - H]^-$ with the *m/z* ratio of 836.6 (Figure 18, A) has been further analyzed by MS^2 spectrometry and additionally compared with commercially available isobutyryl-CoA (Figure 18, B). The MW of the enzymatic product corresponded to the MW of isobutyryl-CoA (836.3 g/mol). The same fragmentation patterns were observed by comparing the enzymatic product with the reference compound (Figure 18, A and B).

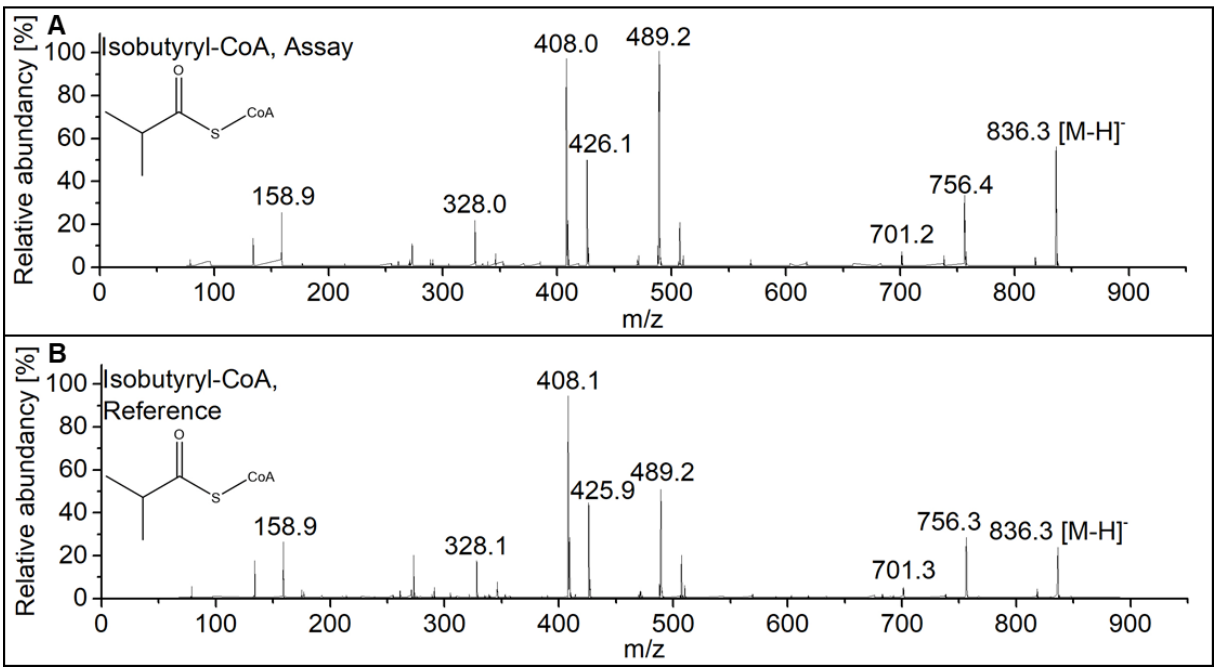

Figure 18. MS^2 Fragmentation patterns of (A) the *Hp*IBCL product isobutyryl-CoA (m/z = 836.3) and (B) the isobutyryl-CoA reference (m/z = 836.3.0). Analyses were carried out in negative ion mode (EPI^-).

3.2.2. Expression of *Hp*IBS in *S. cerevisiae*

Based on the positive findings described in the previous paragraph, the subsequent step was the *in vivo* formation of PIBP. This was carried out by a type III polyketide synthase (isobutyrophenone synthase, IBS) performing the condensation of malonyl-CoA and isobutyryl-CoA. Since a large number of PKSs were already omnipresent in our lab, Dr. Benye Liu provided an *Hp*IBS with its known function as described above. The coding sequence was first heterologously expressed in *E. coli* and purified *via* Ni-NTA agarose in collaboration with the Bachelor student David Quast [109]. After successful activity evidence, the *Hp*IBS (plus HIS_6-tag) was cloned into the pESC-URA vector for the expression in *S. cerevisiae*. However, all trials failed to detect any enzymatic activity (Figure 19, A and B). Different variations have been investigated to overcome the bottleneck, such as varying incubation time, temperature, medium, and inducer concentration (galactose). Surprisingly, heterologous expression of a non-tagged protein finally showed the expected activity. Enzymatic assay optimization was carried out in collaboration with the Bachelor student Henning Ummethum (Figure 19, C and D) [110]. UV spectrum of the enzymatic product (Figure 19, C) corresponded to that of the PIBP reference compound (Figure 19, E). All trials to produce an active 6xHis-tagged protein were unsuccessful, even when the optimized assay conditions of the untagged protein was applied.

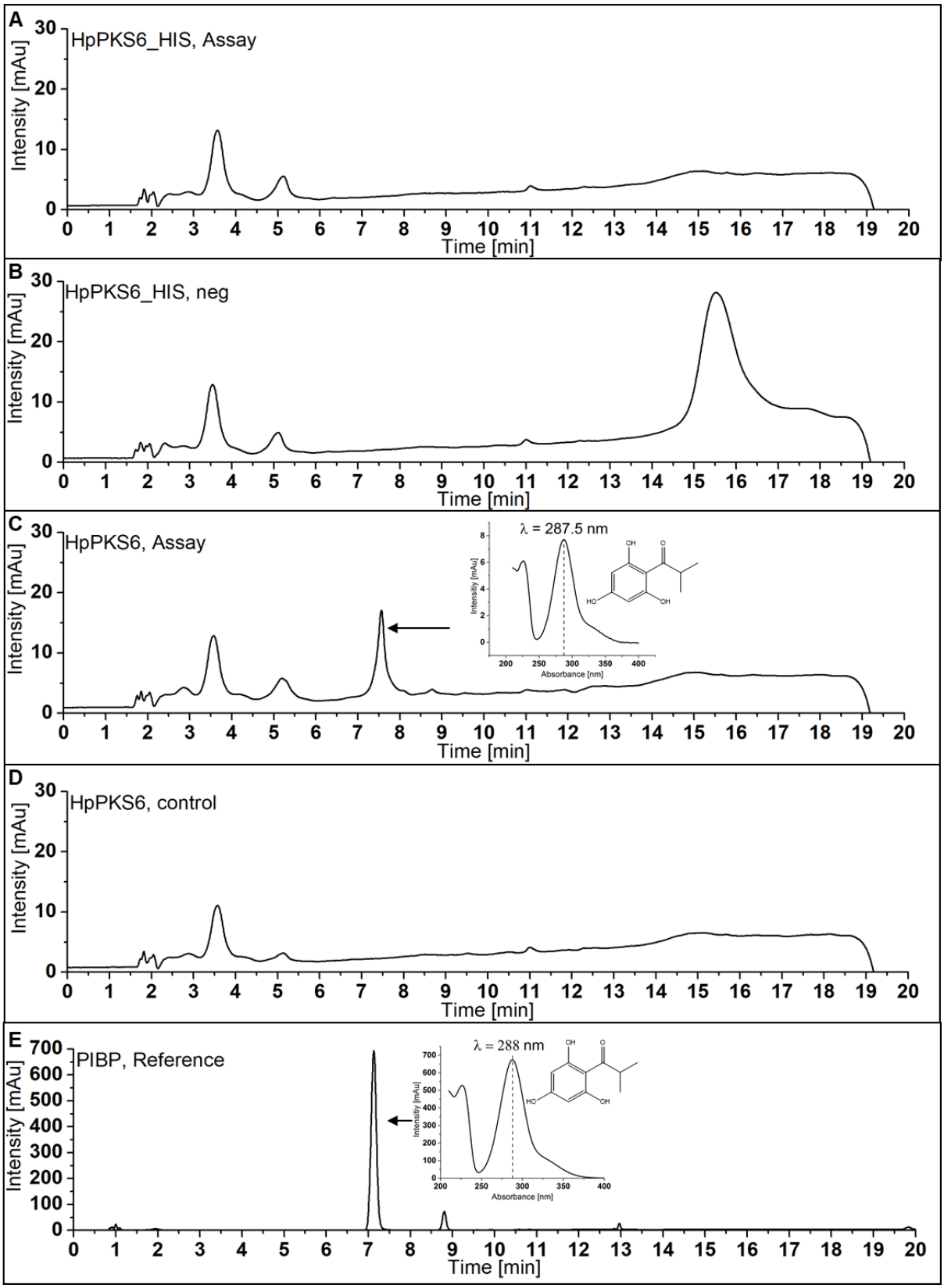

Figure 19. Activity assays of episomally expressed *Hp*IBS in *S. cerevisiae*. (A) Activity assay of His_6 tagged *Hp*IBS; (B) Corresponding negative control; (C) Activity assay of untagged *Hp*IBS; (D) Corresponding negative control; (E) PIBP reference compound.

3.2.3. Isobutyric acid toxicity test

Yeast cells co-expressing *Hp*IBCL and *Hp*IBS were able to produce PIBP when isobutyric acid was supplied. To enable proper cultivation experiments, an isobutyric acid toxicity screening was performed. A yeast strain harboring the plasmid pESC-URA_*Hp*IBCL_*Hp*IBS has been cultivated under different isobutyric acid concentrations. The Gal1/10 promoter was replaced by the two constitutive promoters pTEF1/pPGK1. This enables cultivation using sucrose as a carbon source for future experiments. A pre-culture was prepared in SGI-medium (Table 5, page 19) and the main culture was made in 10 mL YPSE-medium (Table 5, page 19) containing 0, 10, 50 and 100 mM isobutyric acid. After 24 h of cultivation, new sterile sucrose (2 % final concentration) was added and growth continued for another 12 h. Finally, the yeast culture was harvested and the weight of the cell pellet was estimated (Table 31). The yeast cells were disrupted with glass beads and the enzymatic product was extracted twice with 10 mL ethyl acetate from both the cell pellet and the medium (10 mL).

The following wet masses of the cell pellets were obtained as summarized in Table 31. For 0 mM (control), 0.2168 g were obtained, followed by 0.1557 g for 10 mM (72 %), 0.1225 g for 50 mM (57 %) and finally 0.0107 g for 100 mM (5 %, i.e. ~ no growth).

Table 31. Isobutyric acid toxicity effect on the yeast cultures*

Isobutyric acid [mM]	Pellet amount [g]	Toxicity effect/growth inhibition [%]
0	0.2168	0
10	0.1557	28
50	0.1225	43
100	0.0107	95

* Data from a single experiment

Control extract prepared from isobutyric acid-free cultures showed traces of the PIBP product (Figure 20, A and B). The medium extracted with ethyl acetate contained many impurities, which overlapped with the PIBP product peak (Figure 20, B).

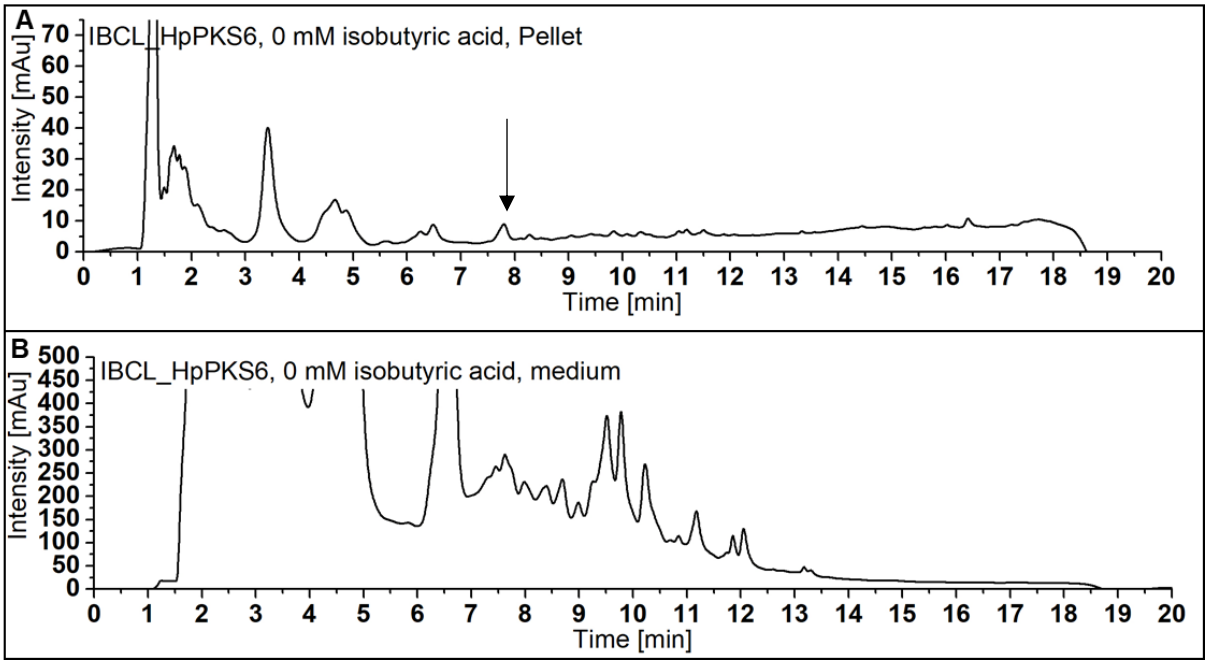

Figure 20. HPLC-DAD chromatograms of ethyl acetate extracts prepared from (A) cell pellet and (B) medium of a yeast culture episomally expressing *Hp*IBCL and *Hp*IBS. These cultures were grown on isobutyric acid-free medium. Arrow indicates the PIBP product peak.

In contrast, the PIBP product was readily detected in the pellet and medium extracts from a culture that was supplemented with 10 mM isobutyric acid (Figure 21). The amount of cell mass decreased by about 28 % (Table 12, page 24) compared to the control culture. The PIBP yield obtained was 1.15 µg/g fresh weight of the cell pellet and 0.059 µg/ml culture medium. Practically, it was impossible to calculate the absolute PIBP product amount due to the large extent of impurities, especially in the medium.

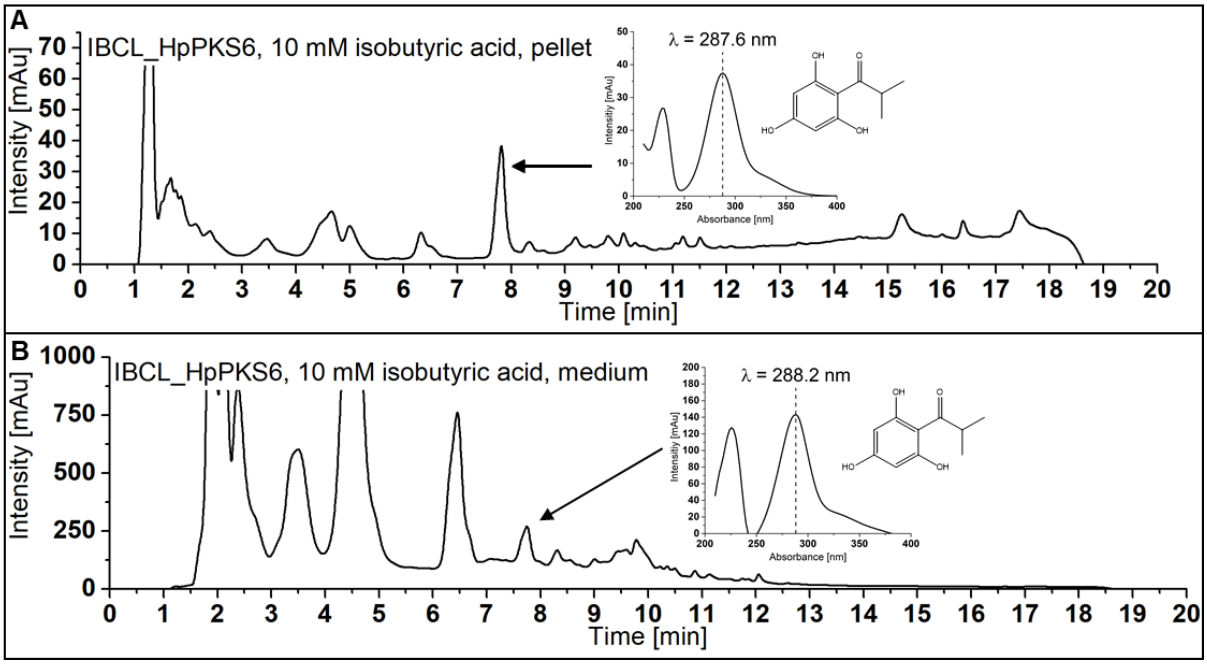

Figure 21. HPLC-DAD chromatograms of ethyl acetate extracts prepared from (A) cell pellet and (B) medium of a yeast culture episomally expressing *Hp*IBCL and *Hp*IBS. The cultures were supplemented with 10 mM isobutyric acid.

The cell mass of the culture fed with 50 mM isobutyric acid was about 43 % less than the control culture, indicating an increasing toxicity level. The PIBP yield was 0.15 µg/g fresh weight of the cell pellet and 0.013 µg/ml culture medium.

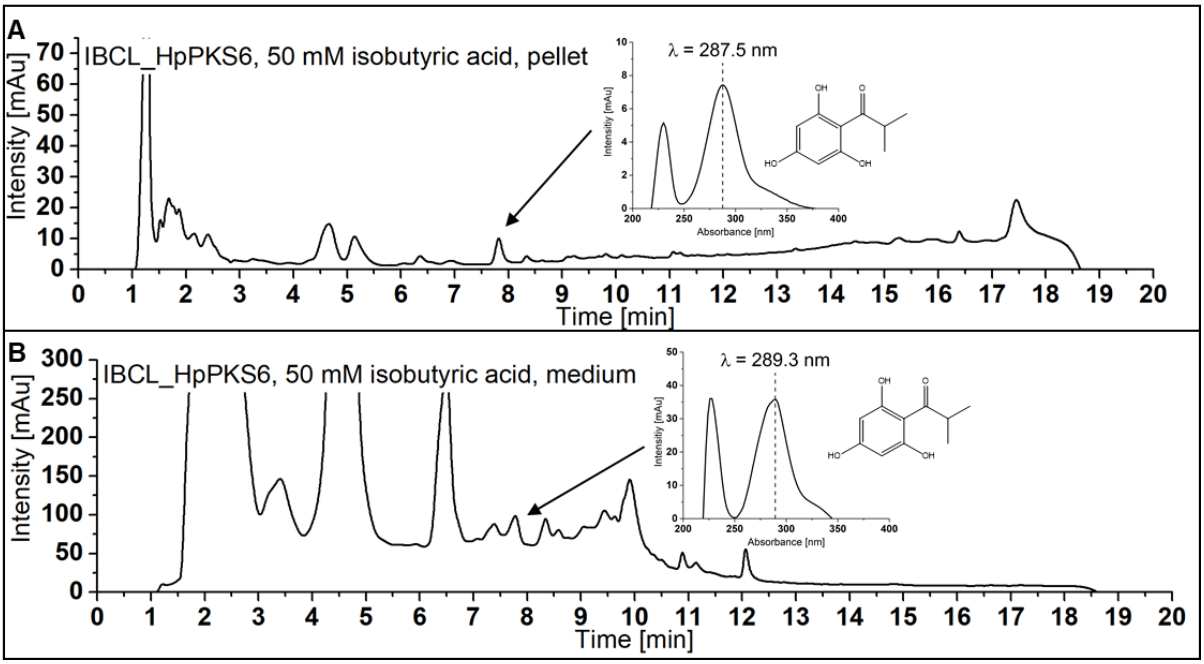

Figure 22. HPLC-DAD chromatograms of ethyl acetate extracts prepared from (A) cell pellet and (B) medium of a yeast culture episomally expressing *Hp*IBCL and *Hp*IBS. The cultures were supplemented with 50 mM isobutyric acid.

The ethyl acetate extract from the culture medium supplied with 100 mM isobutyric acid contained no PIBP peak at all (Figure 23). Only 5 % of the cell mass compared to the control was reached, which can be considered as no growth. This clearly indicates a toxicity potential, leading to cell death using isobutyric acid at 100 mM. Since the yeast cells did not grow anymore, the medium was not tested for product formation.

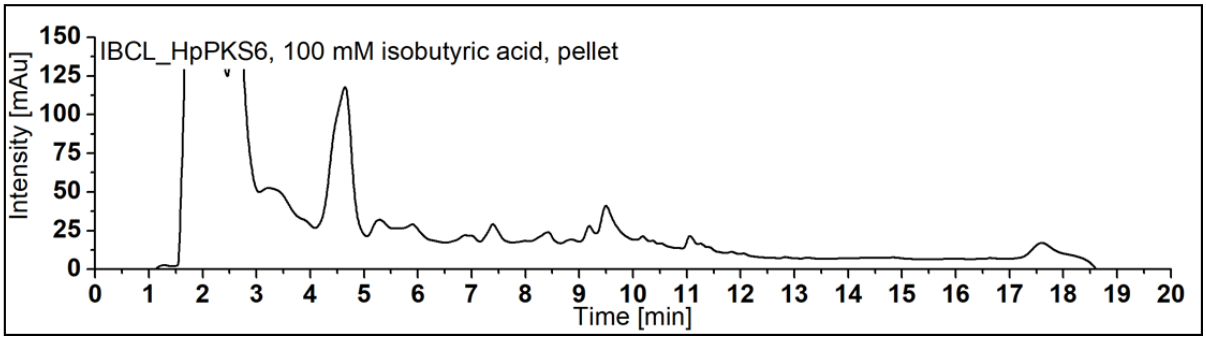

Figure 23. HPLC-DAD chromatogram of an ethyl acetate extract prepared from the cell pellet of a yeast culture episomally expressing *Hp*IBCL and *Hp*IBS. The culture was supplemented with 100 mM isobutyric acid.

The PIBP product from the culture supplemented with 10 mM isobutyric acid (pellet and medium) was HPLC purified and further analyzed by MS^2 spectrometry (section 2.11.5, page 55). The molecular ion peaks $[M - H]^-$ of pellet (Figure 24, A) and medium (Figure 24, B) show *m/z* = 195, which corresponds to the *m/z* of the reference PIBP (Figure 24, C). The same fragmentation patterns were observed for the PIBP products from the cell pellet (Figure 24, A) and the medium (Figure 24, B), compared to that of the reference PIBP (Figure 24, C).

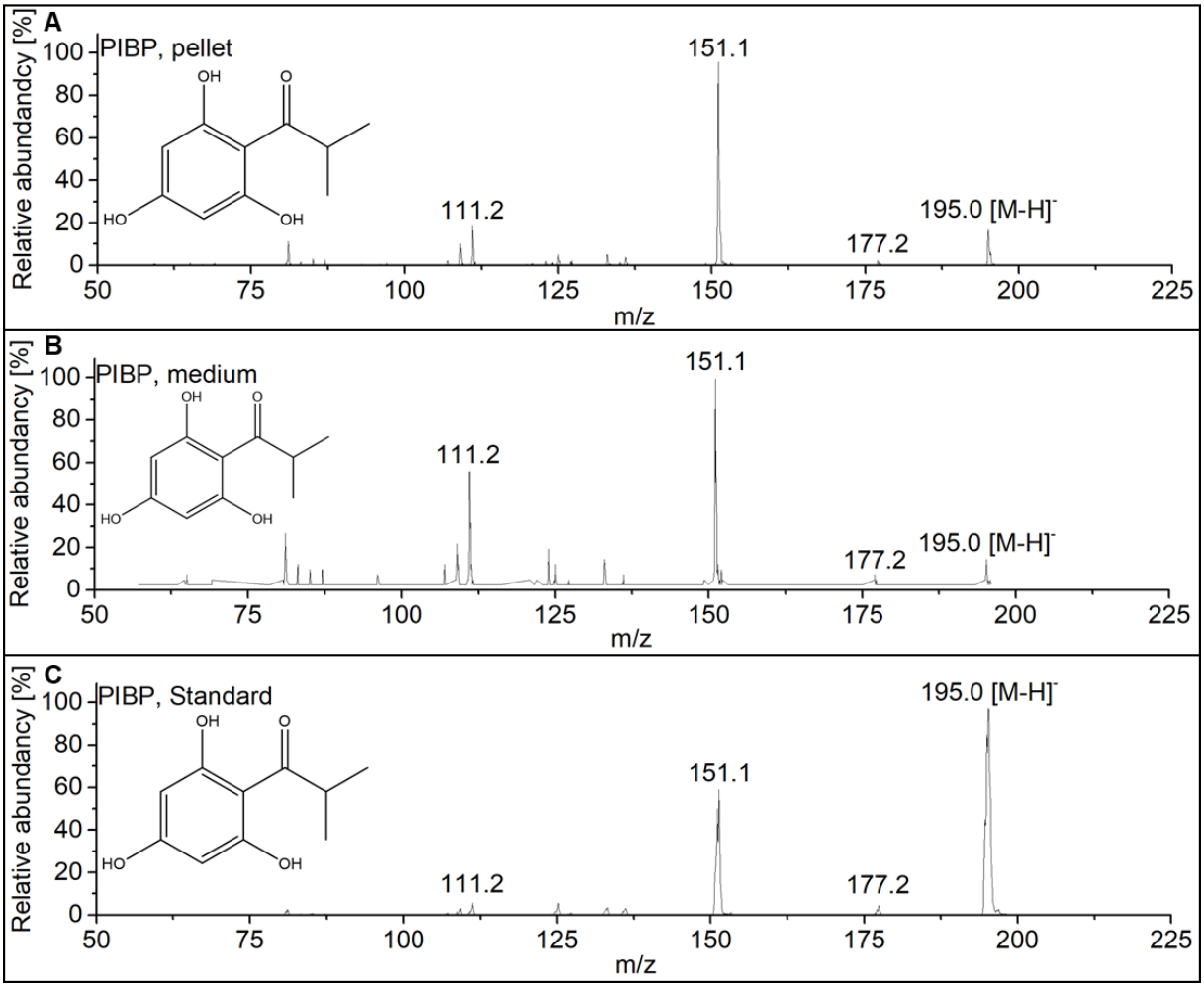

Figure 24. ESI-MS^2 of PIBP purified from yeast cultures episomally co-expressing *Hp*IBCL and *Hp*IBS after feeding with 10 mM isobutyric acid. Analyses were carried out in negative ion mode (EPI^-).

Another control was conducted by using the enzymatically formed PIBP as a substrate for *Hp*PT2 in the presence of GPP. As shown in Figure 25 the enzymatic PIBP product was accepted by *Hp*PT2 forming 3-geranyl-PIBP. PIBP was co-eluted with impurities in the purification step, as shown at a retention time between 7–8 min.

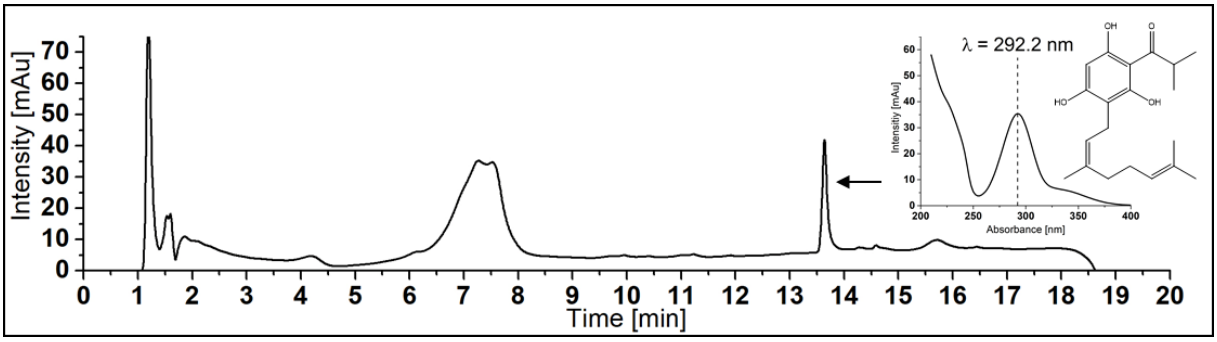

Figure 25. HPLC-DAD analysis of an *Hp*PT2 assay, in which the *Hp*IBCL_*Hp*IBS enzymatic product served as the substrate.

3.2.4. Large scale cultivation of *Hp*IBCL_*Hp*IBS yeast (DASGIP®)

The yeast strain containing *Hp*IBCL and *Hp*IBS sequences either episomally or genome integrated was cultivated at 250 mL scale using the DASGIP® bioreactors. The yeast strains used during this study did not contain any antibiotic-based selection markers. Therefore, the SGI-selection medium was used to maintain a selection pressure during the cultivation experiments to reduce a potential contamination risk. However, no PIBP product was detected in all experiments. This is most probably due to the selection of the wrong medium (SGI), because the PIBP product was detectable in YPGE and YPD media, respectively.

3.3. Activity screening of *Hypericum perforatum* prenyltransferases

In total, 12 different PT sequences were cloned in our group and provided for this project [111,112]. The obtained PTs were cloned as both full-length and truncated versions into the pESC-URA expression vector. All 24 PT sequences were expressed in *S. cerevisiae* (section 2.8.2.4., page 37). The cells were disrupted and investigated for PT activity. The screening experiments were carried out using yeast crude protein extract (section 2.9.2.1., page 41) and a number of potential aromatic substrates

(Figure 11, page 43) as well as DMAPP and GPP as isoprenoid donors. The results obtained are summarized in Table 32. In this current study, only the yeast expression system was used for activity screening. No activities were found for *Hc*PT1-3, *Hp*PT3, *Hp*PT4, *Hp*PT7, and *Hp*PT9. However, *Hp*PT1, *Hp*PT2, *Hp*PT5, *Hp*PT6, and *Hp*PT8 were active (Table 32, page 73). No dramatic differences were observed in the activities detected after heterologous expression of full-length or truncated proteins. Previously, an insect expression system was able to confirm additionally the activities for *Hc*PT1 to *Hc*PT3 [112]. The active PTs identified in this study can be divided into xanthone- and acylphloroglucinol-specific PTs. The enzymes *Hp*PT1, *Hp*PT5, and *Hp*PT8 were found to be xanthone-specific (section 3.3.1., page 74 and section 3.3.2., page 76), whereas *Hp*PT2 and *Hp*PT6 were acylphloroglucinol-specific. The latter two enzymes offer potential candidates for assembling the hyperforin biosynthesis in yeast. Thus, they were subjected to experiments to explore the optimum incubation conditions and enzyme kinetics (section 2.9.2.1. page 41 and section 2.9.2.4., page 44).

Table 32. PT activities detected

Enzyme	Active	Accepted substrates	Co-substrate
*Hc*PT1	no	-	-
*Hc*TP2	no	-	-
*Hc*PT3	no	-	-
*Hp*PT1	yes	1,3,6,7-tetrahydroxyxanthone	DMAPP
*Hp*PT2	yes	PIBP, PAP, PBP, PIVP, 2MBP	GPP
*Hp*PT3	no	-	-
*Hp*PT4	no	-	-
*Hp*PT5	yes	1,3,7-trihydroxyxanthone	DMAPP/GPP
*Hp*PT6	yes	3-G-PIBP*, 3-G-PAP*, 3-G-PBP*, 3-G-PIVP*, 3-G-2MBP*	DMAPP
*Hp*PT7	no	-	-
*Hp*PT8	yes	1,3,6,7-tetrahydroxyxanthone	DMAPP
*Hp*PT9	no	-	-

* 3-G = 3-Geranyl

3.3.1. Enzymatic activity of *Hp*PT5

The xanthone-specific PT *Hp*PT5 was cloned in collaboration with the Master student Svenja Patz[119]. The assay conditions were optimized using a “Design of Experiments” approach (Software: Modde), undertaken in collaboration with the internship students Sandra Grünhoff and Karna Meyer.

The *Hp*PT5 assay was carried out under the conditions described above (section 2.9.2.1., page 41). The enzyme was found to accept 1,3,7-trihydroxyxanthone as the major acceptor substrate (synthesized by Dr. Gaid) and DMAPP and GPP as prenyl-donors (Figure 26, C and E). The *Hp*PT5 products, i.e. monoprenylated and monogeranylated 1,3,7-trihydroxyxanthones, were HPLC-purified and further analyzed by MS^2-spectrometry (section 2.11.5., page 55). No product was detected in the control incubations containing either denatured protein or EDTA (100 mM) (Figure 26, A and B).

The molecular-ion peak $[M - H]^-$ with *m/z* = 242.9 (Figure 26, A and B) corresponded to the *Hp*PT5 substrate 1,3,7-trihydroxyxanthone (MW = 244 g/mol). A molecular ion peak at m/z = 311.4 confirmed the monoprenylation by the transfer of one isoprene unit (m/z = 68 g/mol) (Figure 26, C and D).

Using GPP instead of DMAPP as a co-substrate, a molecular ion peak at *m/z* = 379.0 confirmed the monogeranylation by the transfer of one geranyl unit (m/z = 136 g/mol) (Figure 26, E and F). Due to time limitation, it was not possible to produce a proper amount of the enzymatic products for further NMR spectroscopy analyses.

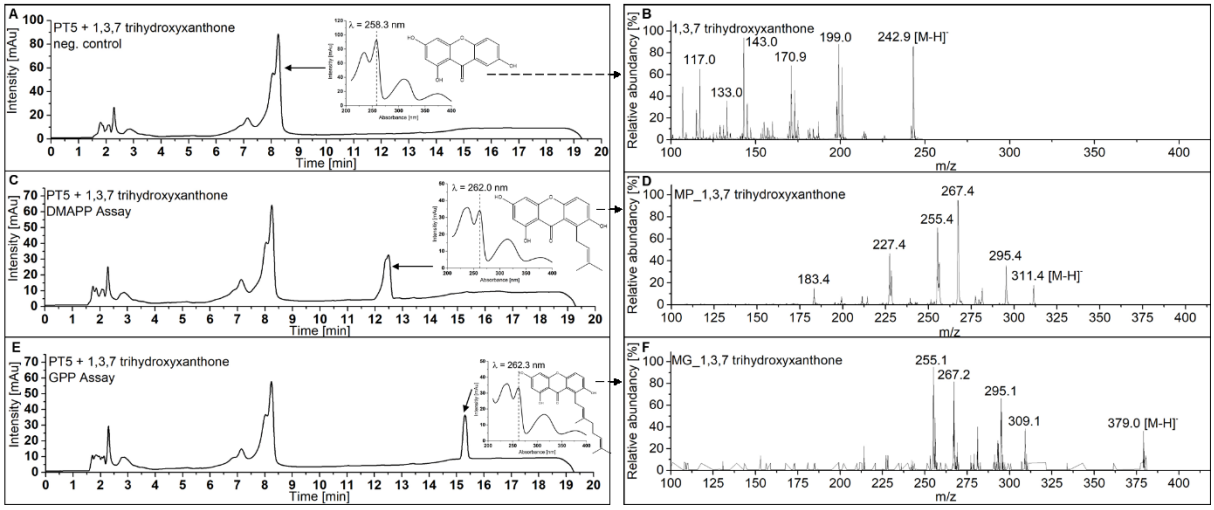

Figure 26. HPLC-DAD and ESI-MS^2 of *Hp*PT5 activity assays. (A) HPLC-DAD chromatogram of *Hp*PT5 control incubation (EDTA) and (B) ESI-MS^2 of the substrate 1,3,7-trihydroxyxanthone. (C) HPLC-DAD chromatogram of *Hp*PT5 incubated with DMAPP and (D) ESI-MS^2 of the product monoprenyl-1,3,7-trihydroxyxanthone. (E) HPLC-DAD chromatogram of *Hp*PT5 incubated with GPP and (F) ESI-MS^2 of the product monogeranyl-1,3,7-trihydroxyxanthone. MP and MG stand for monoprenylated and monogeranylated, respectively.

3.3.1.1. Localization of *Hp*PT5 in *S. cerevisiae*

Membrane-bound aromatic PTs are known to be localized in plants within the outer membranes of the chloroplast [88,120]. However, yeast cells do not possess chloroplasts, therefore it was unknown to which membrane the PTs are finally targeted. *Hp*PT5 was the first PT with an identified activity expressed in yeast during this study. Therefore, it was chosen for the localization experiment as an example PT. *Hp*PT5 was cloned in frame with a C-terminal translational GFP fusion protein. The stop codon of *Hp*PT5 was removed by using a mutation primer to guarantee a continuous transcription of the cDNA. The obtained PCR fragment was cloned into a pESC-URA vector containing a GFP protein at the C-terminal end. Yeast cells containing the *Hp*PT5_GFP fusion protein were cultivated under standard conditions (section 2.8.2.4., page 2.9.2.1.) and used for confocal microscopic screenings in collaboration with Dr. David Kaufholdt (Prof. Dr. Robert Hänsch group, Institute of Plant Biology, TU-Braunschweig).

The intracellular fluorescence was evenly distributed over the cytoplasm of the cells but absent from the nucleus (Figure 27, A and C). This localization differed from the expression of the GFP protein only, which was also present in the nucleus due to its small size and solubility (section 3.3.3., page 78). These results agreed with the GFP

fluorescence detection in the insect expression system [112]. In conclusion, the fusion protein in yeast cells may be localized to any organelle containing membranes, such as endoplasmatic reticulum, Golgi, and mitochondria. Another possibility might be the formation of evenly distributed inclusion bodies within the cytoplasm due to incorrect folding of the protein.

Regarding the activity of the enzyme, no activity was detected when the *Hp*PT5_GFP protein was incubated with 1,3,7-trihydroxyxanthone, which was opposite to the GFP-free protein.

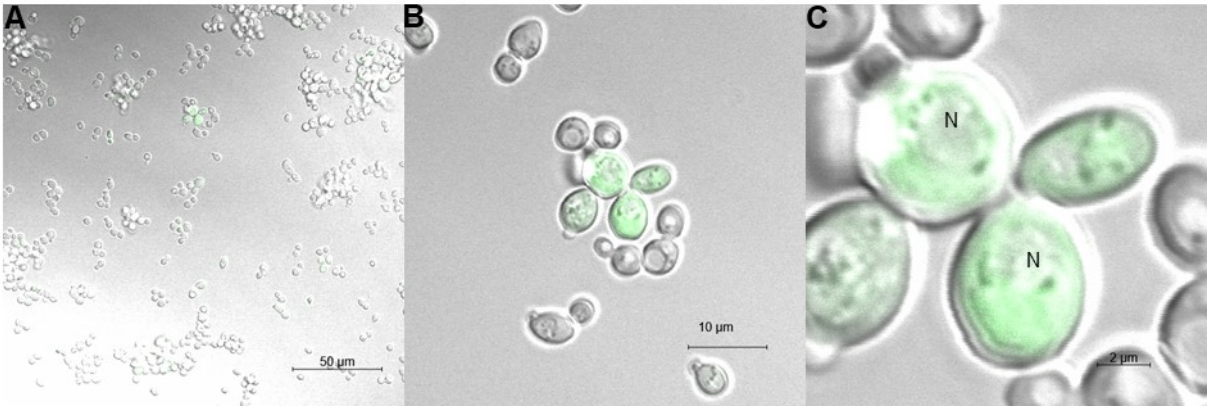

Figure 27. Confocal laser scanning microscopy of *S. cerevisiae* expressing the *Hp*PT5_GFP fusion protein at different magnification scales. N = nucleus.

3.3.2. Enzymatic activity of *Hp*PT8

*Hp*PT8 assays were carried out as described above (section 2.9.2.1, page 41). *Hp*PT8 was found to accept 1,3,6,7-tetrahydroxyxanthone as the major acceptor molecule and only DMAPP as prenyl donor (Figure 28, C and E). The *Hp*PT8 product was HPLC purified and further analyzed by MS^2-spectrometry (section 2.11.5., page 55). No product was detected in the control incubation containing either denatured protein or EDTA (100 mM) (Figure 28, A and B).

The molecular ion peak $[M - H]^-$ of the *Hp*PT8 substrate 1,3,6,7-tetrahydroxyxanthone (MW = 260 g/mol) appears at *m/z* = 259.3 (Figure 28, B). The *Hp*PT8 product peak resulting from incubation with DMAPP (Figure 28, C) showed *m/z* = 327.3 (Figure 28, D), which corresponded to the addition of one prenyl group (MW = 68 g/mol) to the substrate.

No further product formation was observed using GPP instead of DMAPP as a co-substrate (Figure 28, E). Due to time limitation, it was not possible to produce enough enzymatic product for further NMR spectroscopy analysis.

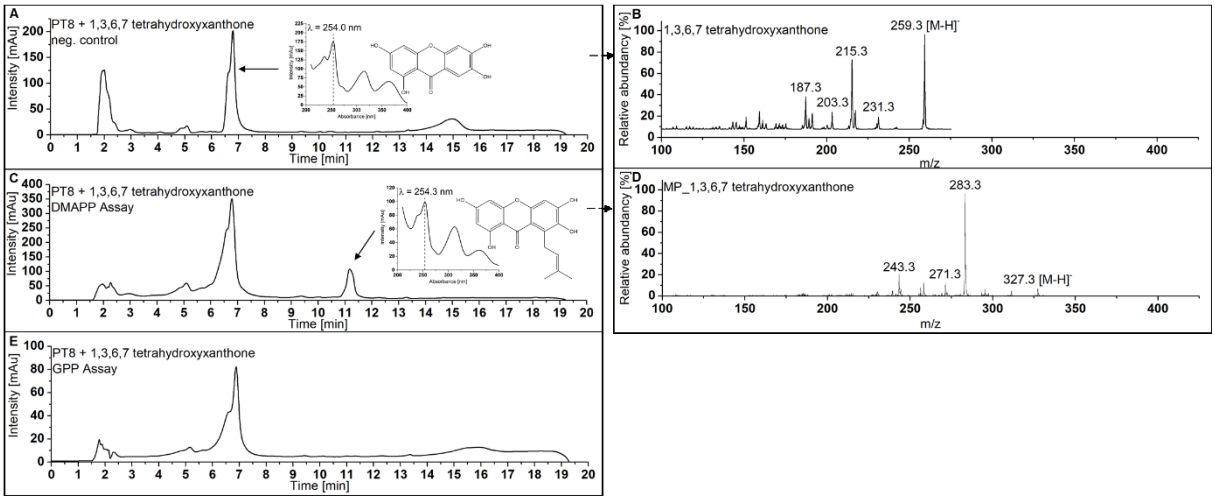

Figure 28. HPLC-DAD and ESI-MS^2 of *Hp*PT8 activity assays. (A) HPLC-DAD chromatogram of *Hp*PT8 control incubation (EDTA) and (B) ESI-MS^2 of the substrate 1,3,6,7-tetrahydroxyxanthone. (C) HPLC-DAD chromatogram of *Hp*PT8 incubated with DMAPP and (D) ESI-MS^2 of the product monoprenyl-1,3,6,7-tetrahydroxyxanthone. (E) HPLC-DAD chromatogram of *Hp*PT8 incubated with GPP. MP_1,3,6,7-tetrahydroxyxanthone stands for monoprenylated 1,3,7-trihydroxyxanthone.

3.3.3. Carbon source improvement for the pESC-URA expression system

To investigate the effect of different carbon sources on the protein expression level, four different carbon sources (glucose, sucrose, raffinose, and glycerol) were tested. The Gal1/10 promoter present in the pESC-URA expression vector is repressed in the presence of glucose. Therefore, the GFP coding sequence was cloned into the pESC-URA vector and expressed under standard conditions (section 2.8.2.4., page 37). Glucose, glycerol, raffinose and sucrose were used at a final concentration of 2 % for the main culture. Galactose was used as protein expression inducer after 24 h of cultivation. The GFP protein expression level with glucose was markedly lower (Figure 29, A), compared to that in the culture supplemented with sucrose (Figure 29, B and C). The fluorescence was evenly spread over cytoplasm and nucleus. The growth rates using glycerol and raffinose were lower compared to glucose and sucrose. Notably, raffinose is more expensive (>1 € / 1 g) and was therefore not furthermore considered as a cost-effective carbon source.

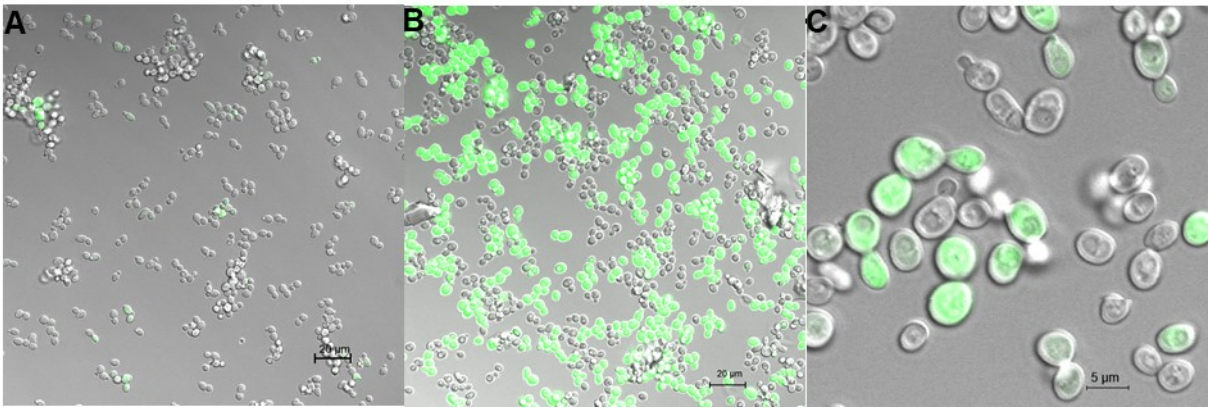

Figure 29. Confocal laser scanning microscopy of *S. cerevisiae* expressing GFP protein under use of different carbon sources (A) glucose; (B, C) sucrose at different magnification scales.

3.3.4. Biochemical investigation of acylphloroglucinol-specific *Hp*PT2

3.3.4.1. Incubation time and protein dependency

The linearity of the enzyme activity with respect to incubation time and protein amount is an important aspect for the further kinetic study. For kinetic characterization, appropriate enzyme concentrations and incubation times must be selected to achieve linear reaction velocity during the assay period. Extended incubation times will lead to false measurements due to the gradual slowing in the reaction velocity and potential instability of the end product. High protein amounts might have inhibitory effects leading to inaccurate measurements. These experiments were carried out under standard conditions (section 2.9.2.2., page 44), except for varying the incubation time and protein amount from 2 -120 min and 10 - 1200 µg, respectively.

The *Hp*PT2 activity was linear up to 15 min reaching a plateau from 20 min to 40 min. After 60 min of incubation, the 3-geranyl-PIBP product amount started to decrease due to degradation effects (Figure 30, A).

The incubation time of 10 min was selected to investigate the protein dependency. A linear enzyme activity was analyzed up to 400 µg protein whereas the maximum product formation was observed at 1000 µg of microsomal fraction (Figure 30, B).

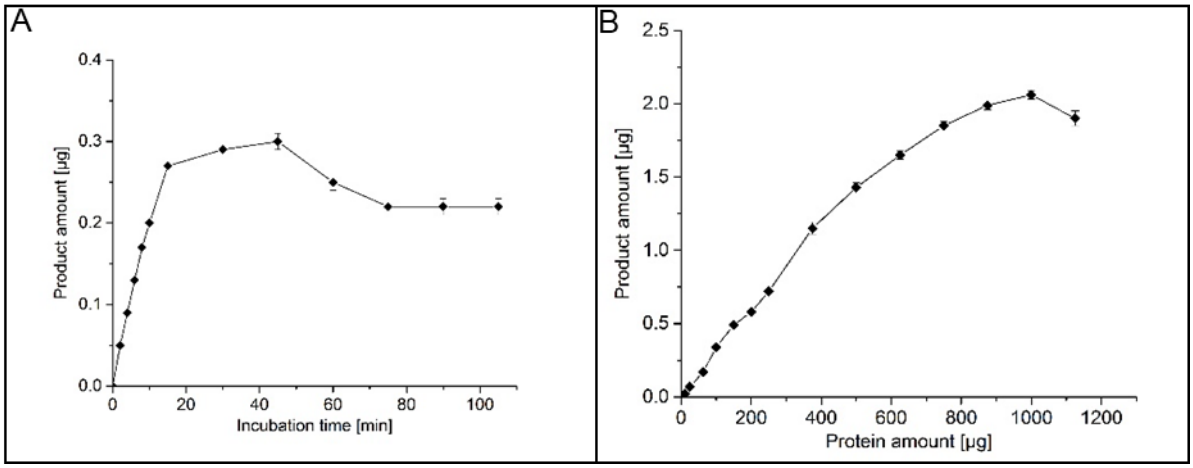

Figure 30. The linearity of *Hp*PT2 activity with (A) incubation time and (B) protein amount. The results are means ± SD from three independent experiments.

3.3.4.2. Effect of divalent cations

Different classes of enzymes are dependent on co-factors such as divalent cations. Aromatic PTs are divalent cation dependent and require mainly Mg^{2+}, Ca^{2+}, Fe^{2+} or Mn^{2+} to perform the biochemical reactions [75]. The effect of divalent cations was investigated under standard assay conditions (section 2.9.2.2., page 44), except for varying the type of the divalent cation. The concentration of each divalent cation was constant at 10 mM for all incubation reactions.

The most preferred cation was found to be Mg^{2+} for *Hp*PT2. Comparing the relative activity of other cations tested, the following activities were detected: Ca^{2+} = 16 %, Fe^{2+} = 15 %, Zn^{2+} = 13 %, Co^{2+} = 8 %, Mn^{2+} = 3 %, and Cu^{2+} = no activity. No activity was observed when metal ions were chelated using EDTA, indicating the absolute dependency on divalent cations (Figure 31).

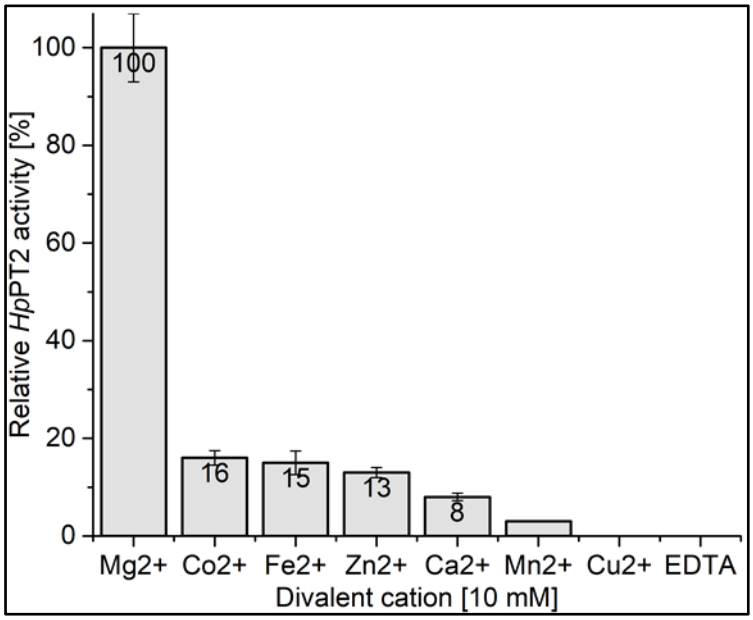

Figure 31. Effect of divalent cations on *Hp*PT2 enzymatic activity. The results are means ± SD from three independent experiments.

3.3.4.3. Effect of incubation temperature and pH

The temperature and pH are critical parameters influencing the activity of enzymes. The pH has a large influence on the overall protein charge and therefore on the tertiary structure. The temperature has an influence on the reaction velocity of the enzyme itself. Temperature and pH values far away from the natural environment can cause improper folding and/or inactivation of the enzyme.

The experiments were carried out under standard conditions (section 2.9.2.2., page 44), except for varying the temperature and pH from 20 - 80 °C and the pH from 5 – 10. The temperature and pH optima were identified to be 40 °C and 7–8, respectively (Figure 32, A and B). The enzymatic activity started to decrease when the temperature was higher or lower than 40 °C. In addition, pH ranges below or above 7 – 8 negatively affected the enzymatic activity by about 50 % (Figure 32, B).

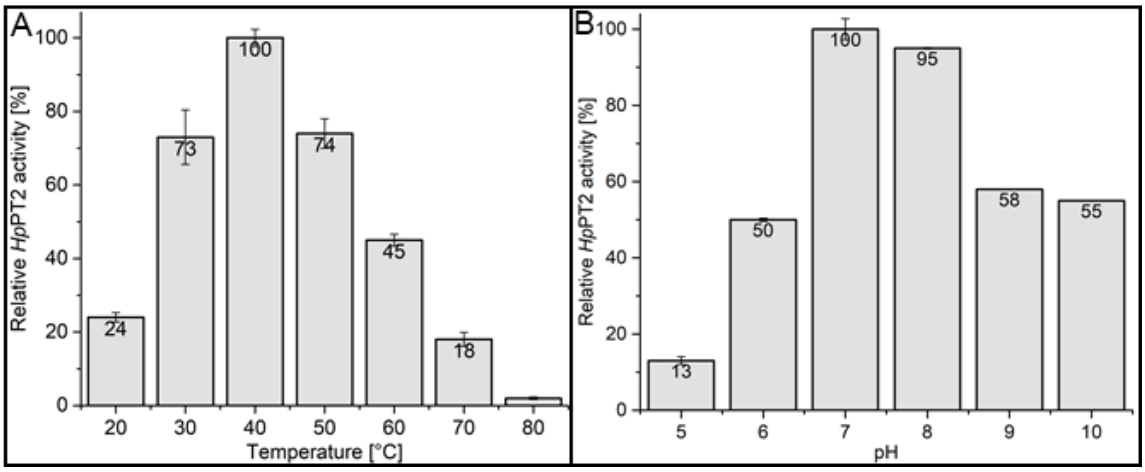

Figure 32. The dependency of *Hp*PT2 activity on incubation conditions. (A) Effect of incubation temperature. (B) Effect of incubation pH. The results are means ± SD from three independent experiments.

3.3.4.4. Substrate specificity of *Hp*PT2

Most enzymes accept a series of closely related substrates with varying preference. To determine which substrates are accepted and which are preferred, *Hp*PT2 was incubated with a series of different aromatic substrates (Figure 11, page 43) under standard conditions (section 2.9.2.2., page 44).

*Hp*PT2 was identified to be highly specific for acylphloroglucinol derivates. No activity was observed with other aromatic compounds, e.g. xanthones. The acylphloroglucinol derivative PIBP was the preferred substrate (100 %). PIBP, 2-MBP, 2,3',4,6-tetrahydroxybenzophone, PAP, PIVP, and PBP were also accepted but at lower relative activities of 70.6, 31.7, 16.9, 16.3, and 5 %, respectively (Figure 33, page 82).

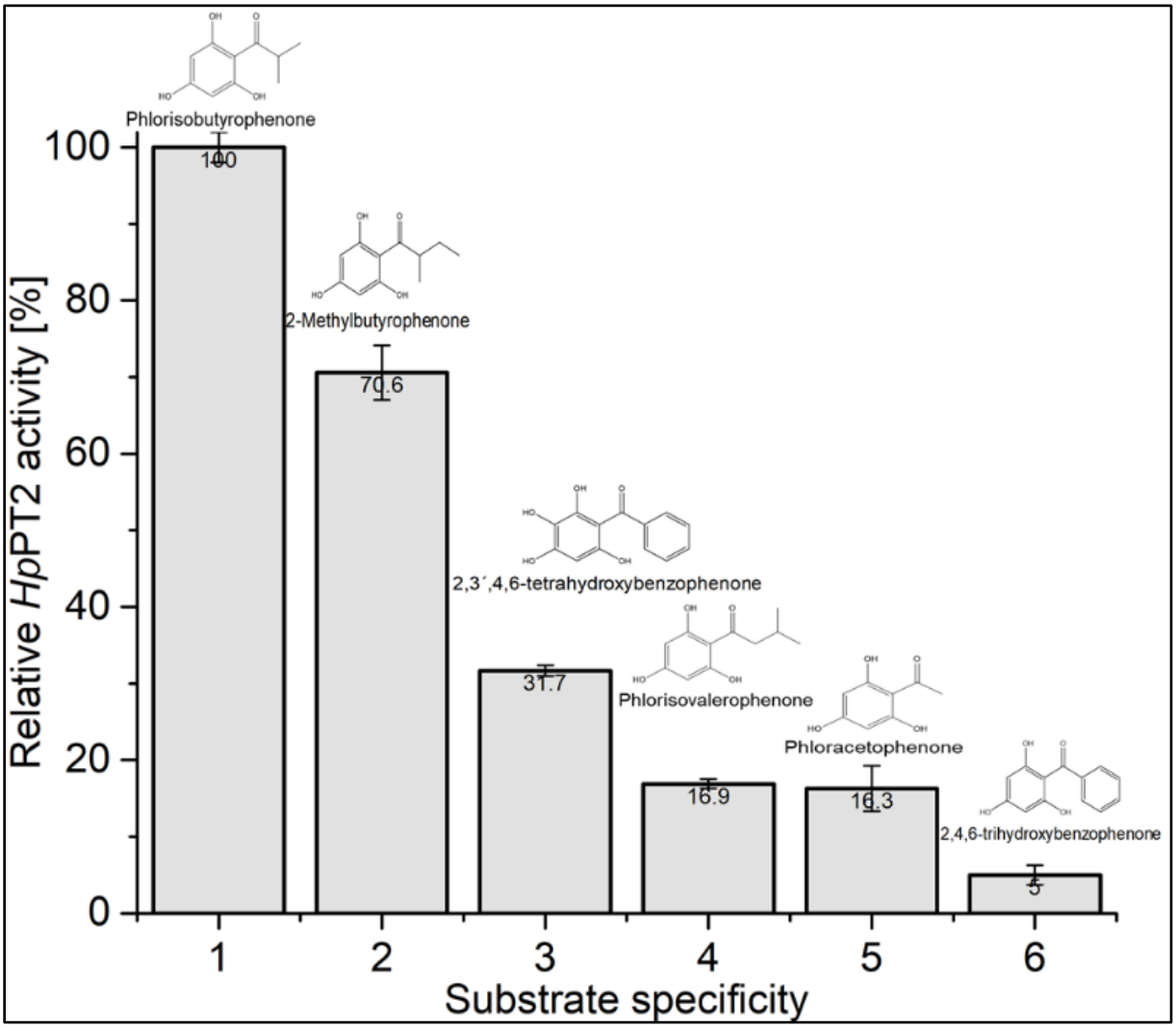

Figure 33. Substrate specificity of *Hp*PT2. The results are means ± SD from three independent experiments.

3.3.4.5. Determination of kinetic parameters for *Hp*PT2

The determination of the kinetic parameters for *Hp*PT2 was carried out for the two preferred substrates, i.e. PIBP and 2-MBP (section 3.3.4.4., page 82).

The apparent K_M values were determined by varying the PIBP or 2-MBP concentrations, while keeping the GPP concentration saturating and constant. The apparent K_M value for GPP was determined by using varying GPP concentrations while keeping PIBP and 2-MBP at saturating constant concentration. All measurements were done by three technical replicates (section 2.9.2.2., page 44).

The best substrate affinity was observed for 2-MBP with K_M = 85 ± 15 µM (V_{max} = 5.1^{-3} ± 5^{-4} nmol/mg microsomal protein/min), followed by PIBP with K_M = 124 ± 19 µM (V_{max} = 8.0^{-3} ± 9^{-5} nmol/mg microsomal protein/min). The apparent K_M value for $GPP_{2\text{-}MBP}$ was 60 ± 11 µM (V_{max} = 4.6^{-3} ± 3^{-4} nmol/mg microsomal protein/min) and that for GPP_{PIBP} was 89 µM ± 35 (V_{max} = 7.1^{-3} ± 9^{-4} nmol/mg microsomal protein/min), as summarized in Table 33. Data presented are the means of three technical replicates.

Table 33. Kinetic parameters of *Hp*PT2

Substrate	**K_M [µM]***	**V_{max} [nmol/mg microsomal protein/min]***
2-MBP	85 ± 15	5.1^{-3} ± 5^{-4}
PIBP	124 ± 19	8.0^{-3} ± 9^{-5}
$GPP_{2\text{-}MBP}$	60 ± 11	4.6^{-3} ± 3^{-4}
GPP_{PIBP}	89 ± 35	7.1^{-3} ± 9^{-4}

*The results are means ± SD from three independent experiments.

3.3.4.6. Structure elucidation of *Hp*PT2-formed 3-geranyl-PIBP

*Hp*PT2 was found to prefer PIBP as acceptor substrate and GPP as geranyl donor (Figure 34 (C, D), page 84). No product was detected in the control incubation containing either denatured protein or EDTA (Figure 34, A and B). The molecular-ion peak $[M + H]^+$ of the *Hp*PT2 substrate PIBP (MW = 196 g/mol) is at *m/z* = 197.0 (Figure 34, B). The *Hp*PT2 product peak (Figure 34, C) is at *m/z* = 333.2 (Figure 34, D), which corresponds to the addition of one geranyl group (MW = 136 g/mol) to the substrate. Chemically synthesized 3-geranyl-PIBP was structurally confirmed by MS^2

spectrometry (section 2.11.5., page 51). The retention time, UV-spectrum and fragmentation pattern of the *Hp*PT2 product using PIBP as substrate matched the data obtained for the authentic reference 3-geranyl-PIBP (Figure 34, C-F). Authentic 3-geranyl-PIBP was then used as a substrate for *Hp*PT6 (section 2.9.2.4., page 44).

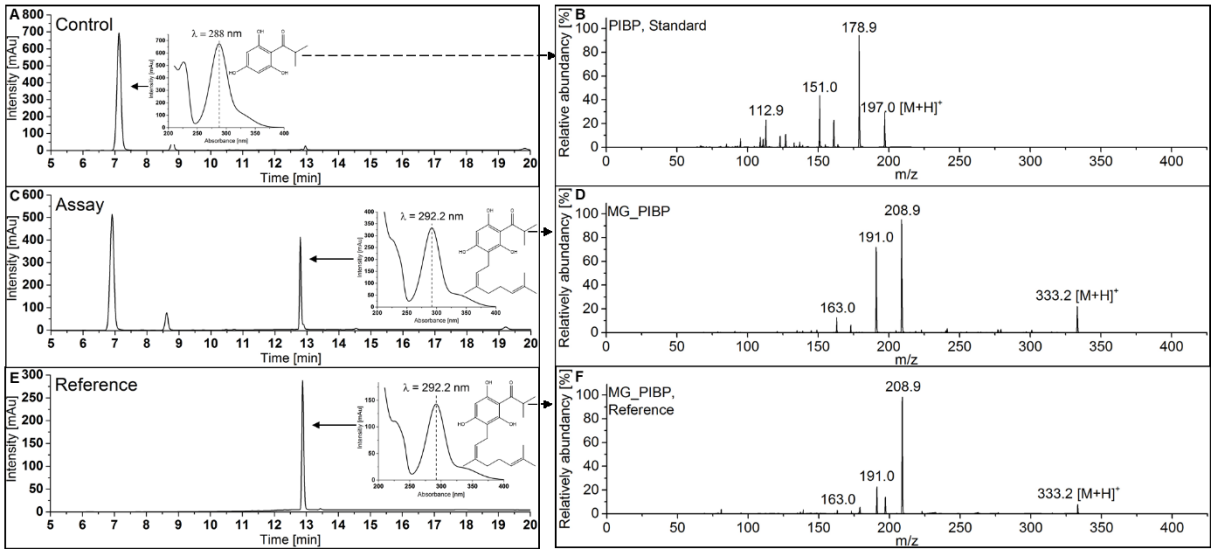

Figure 34. HPLC-DAD and ESI-MS^2 of *Hp*PT2 activity assays. (A) HPLC-DAD chromatogram of *Hp*PT2 control incubation (EDTA) and (B) ESI-MS^2 of the substrate PIBP. (C) HPLC-DAD chromatogram of *Hp*PT2 incubated with GPP and (D) ESI-MS^2 of the product 3-geranyl-PIBP. (E) HPLC-DAD chromatogram of 3-geranyl-PIBP as a reference and (F) ESI-MS^2 of 3-geranyl-PIBP.

3.3.5. Biochemical investigation of acylphloroglucinol-specific *Hp*PT6

3.3.5.1. Incubation time and protein dependency

These experiments were carried out under standard conditions (section 2.9.2.3., page 44), except for varying the incubation time and protein amount from 2-120 min and 10 - 1600 µg, respectively. Product detection and quantification were performed by HPLC-DAD analysis using a calibration curve (section 2.11.2., page 53).

A linear dependency of the incubation time was detected up to 15 min. After 15 min, the rate of product formation became lower reaching a plateau from 30 to 60 min. A severe degradation of the 5-prenyl-3-geranyl-PIBP product started after 60 min of incubation time (Figure 35, A). A linear dependency was detected up to 800 µg microsomal protein with subsequently reaching a plateau at around 1500 µg (Figure 35, B).

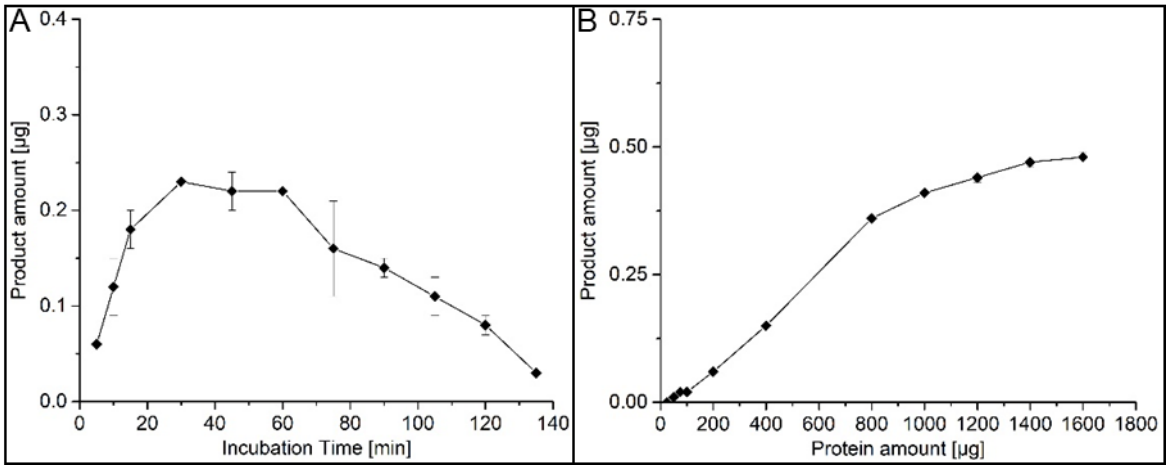

Figure 35. The dependency of *Hp*PT6 on A) incubation time and B) protein amount. The results are means ± SD from three independent experiments.

3.3.5.2. Effect of divalent cations

These experiments were carried out under standard conditions as described (section 2.9.2.3., page 44), except for varying the divalent cations. The concentration of each divalent cation was constant at 10 mM in all incubation reactions.

For *Hp*PT6, the divalent cation Ca^{2+} was identified to be the most preferred metal cation. Comparing the relative activities of other cations tested, the second preferred cation was Mn^{2+}, followed by Mg^{2+}, and Fe^{2+} with 64, 37 and 19% activities relative to that detected in the presence of Ca^{+2}. No activities were detected with Co^{2+}, Mn^{2+} and Cu^{2+}. EDTA (10 mM) abolished the enzymatic activity, indicating a clear dependency on a divalent cation (Figure 36).

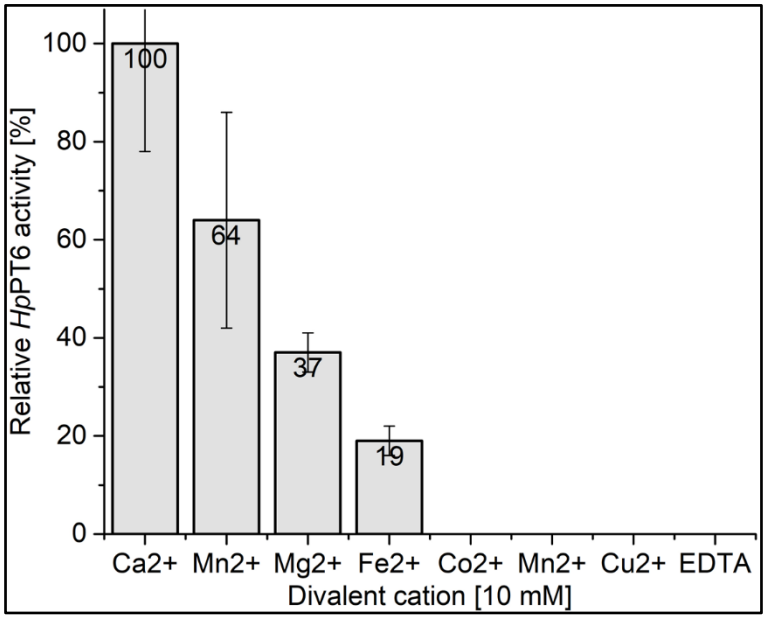

Figure 36. The dependency of *Hp*PT6 activity on divalent cations. The results are means ± SD from three independent experiments.

3.3.5.3. Effect of incubation temperature and pH

The experiments were carried out under standard conditions (section 2.9.2.3., page 44), except for varying the temperature from 20-80 °C and the pH from 5-10. The temperature and pH optima were identified to be at 50 °C and pH 8–9, respectively (Figure 37, A). The enzymatic activity started to decrease when the temperature was higher or lower than 50 °C. Furthermore, pH ranges below or above 7–9 decreased the activity by about 40 % (pH 7) and 20 % (pH 10) (Figure 37, B).

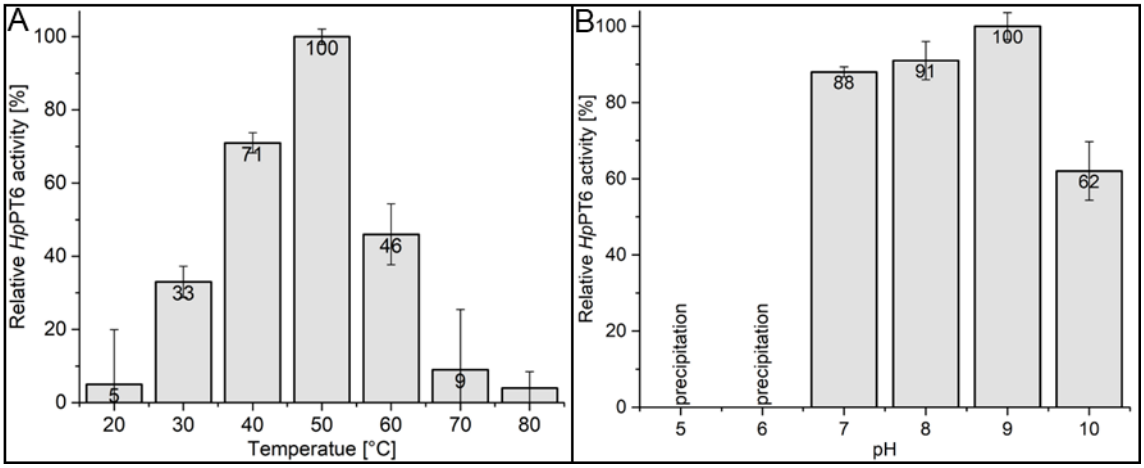

Figure 37. The dependency of *Hp*PT6 on incubation temperature (A) and pH (B). The results are means ± SD from three independent experiments.

3.3.5.4. Substrate specificity of *Hp*PT6

*Hp*PT6 was identified as highly specific for 3-geranyl-acylphloroglucinol derivates. The substrate 3-geranyl-PIVP was the preferred one (100 %), followed by 3-G-2-MBP, 3-G-PIBP, 3-G-PBP and 3-G-PAP (Figure 38), which were accepted with relative activities of 91, 90, 32 and 28 %, respectively.

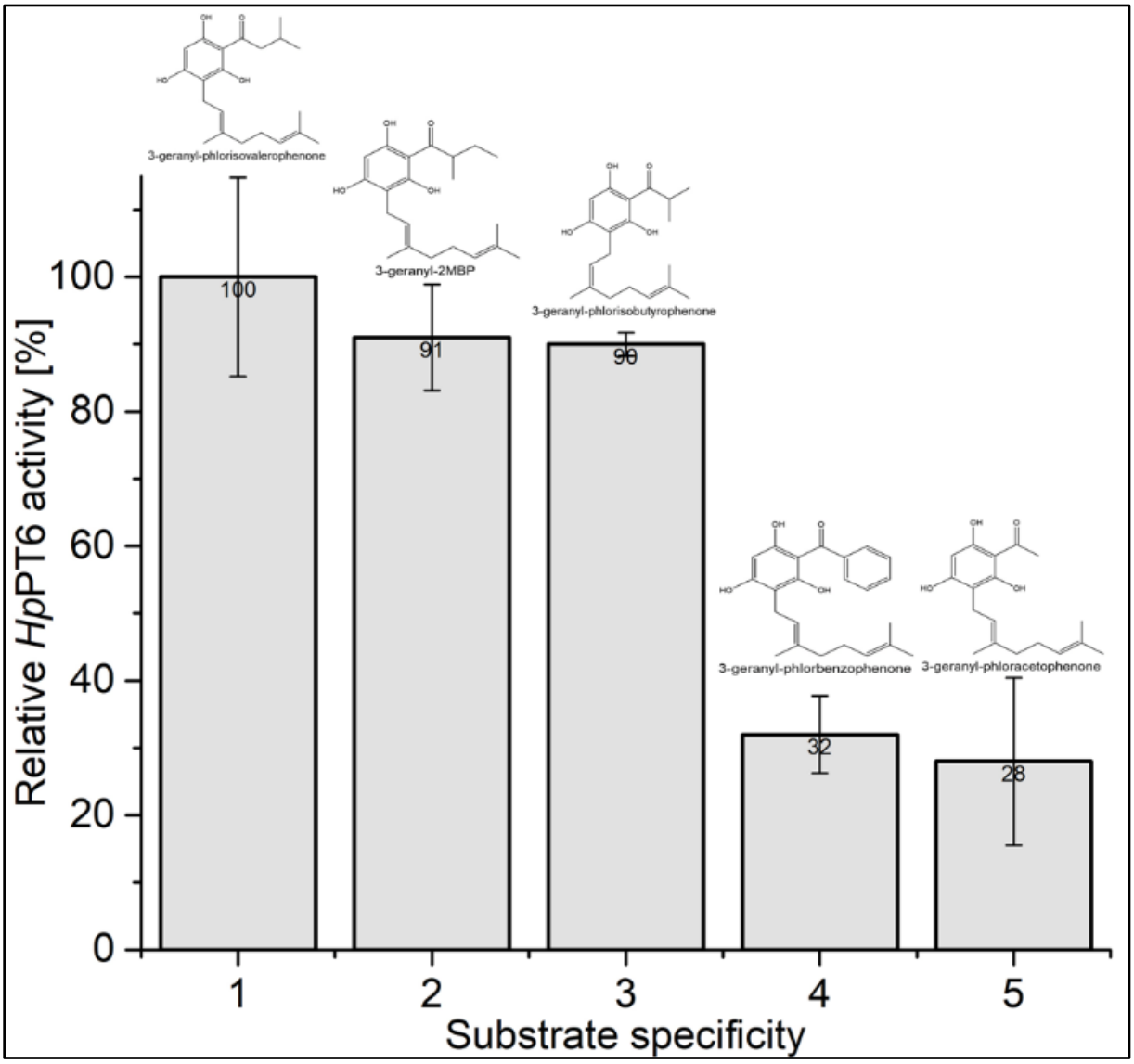

Figure 38. Substrate specificity of *Hp*PT6. The results are means ± SD from three independent experiments.

3.3.5.5. Determination of kinetic parameters for *Hp*PT6

The determination of the kinetic parameters for *Hp*PT6 was carried out for the three best accepted substrates, namely 3-G-PIVP, 3-G-2MBP and 3-G-PIBP (section 3.3.5.4., page 88).

The apparent K_M values were determined by using varying acceptor concentrations while keeping the DMAPP concentration constant at saturation. The apparent K_M value for DMAPP was determined by using varying DMAPP concentrations while keeping the acceptor substrate at a constant saturating concentration. All measurements were done as three technical replicates (section 2.9.2.3., page 44).

The apparent K_M value for 3-G-PIVP was 78 ± 8.6 µM (V_{max} = 1.1^{-3} ± 4^{-4} nmol/mg microsomal protein/min), that for 3-G-2MBP was 73 ± 10 µM (V_{max} = 8.2^{-4} ± 8^{-4} nmol/mg microsomal protein/min) and that for 3-G-PIBP was 181 ± 218* µM (V_{max} = 5.8^{-4} ± 3^{-4} nmol/mg microsomal protein/min). The apparent K_M value for $GPP_{3\text{-}G\text{-}PIVP}$ was 185 ± 12 µM (V_{max} = 1.3^{-3} ± 6^{-5} nmol/mg microsomal protein/min), that for $GPP_{3\text{-}G\text{-}2\text{-}MBP}$ was 100 ± 18 µM (V_{max} = 9.1^{-4} ± 9^{-5} nmol/mg microsomal protein/min), and that for $GPP_{3\text{-}G\text{-}PIBP}$ was 141 ± 17 µM (V_{max} = 8.7^{-4} ± 7^{-5} nmol/mg microsomal protein/min). Data presented are the means of three technical replicates.

Table 34. Kinetic parameters determined for *Hp*PT6

Substrate	**K_M [µM]***	**V_{max} [nmol/mg microsomal protein/min]***
3-G-PIVP	78 ± 8.6	1.10^{-3} ± 4^{-4}
3-G-2-MBP	73 ± 10**	0.80^{-3} ± 8^{-4}
3-G-PIBP	181 ± 218	5.8^{-4} ± 3^{-4}
$DMAPP_{3\text{-}G\text{-}PIVP}$	185 ± 12	1.30^{-3} ± 6^{-5}
$DMAPP_{3\text{-}G\text{-}2\text{-}MBP}$	100 ± 18	0.91^{-3} ± 9^{-5}
$DMAPP_{3\text{-}G\text{-}PIBP}$	141 ± 17	0.87^{-3} ± 7^{-5}

*The results are means ± SD from three independent experiments. **Value is a mean of two replicates.

3.3.5.6. Structure elucidation the *Hp*PT6 product

*Hp*PT6 was found to accept the *Hp*PT2 product 3-G-PIBP as prenyl acceptor substrate and DMAPP as prenyl donor substrate (Figure 39, C and D). No product was detected in the control incubation containing either denatured protein or EDTA (Figure 39, A and B). The molecular-ion peak $[M + H]^+$ of the *Hp*PT6 substrate 3-G-PIBP (MW= 332 g/mol) was at *m/z* = 333.2 (Figure 39, B). The *Hp*PT6 product peak (Figure 39, C) appeared at *m/z* = 401.2 (Figure 39, D), which corresponded to the addition of one prenyl-group (MW = 68 g/mol) to the substrate. Due to the instability of 3-geranyl-5-prenyl-PIBP, it was not possible to synthesize a reference compound. Chemically synthesized polyprenylated phloroglucinol derivatives were spontaneously degraded, hindering further structural elucidation. Only the non-prenylated and mono-geranylated compounds were stable for long time periods.

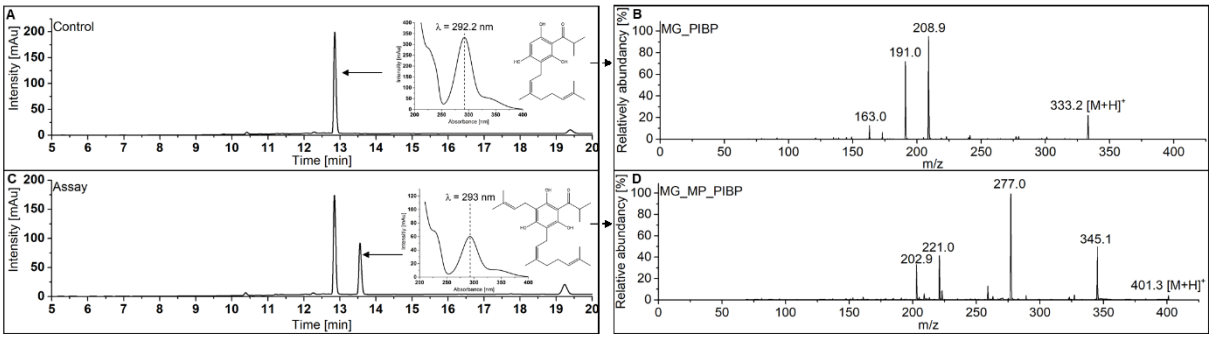

Figure 39. The activity of *Hp*PT6 using 3-G-PIBP as a substrate. (A, C) HPLC-DAD analysis of assays done with heat-denatured protein (A) and crude microsomal fraction (C). (B, D) ESI-MS^2 of the substrate (B) and the enzymatic product 3-geranyl-5-prenyl-PIBP (D).

3.3.6. Genome integration of *Hp*IBCL_*Hp*IBS, *Hp*PT2, and *Hp*PT6

For the heterologous production of plant secondary metabolites in microbial hosts, a number of genes must be expressed to yield an enzyme cascade. Many laboratory organisms such as *S. cerevisiae* are limited to few antibiotics, which can be used for selection purposes. Therefore, the integration of heterologous genes into the genome with subsequent marker removal is a commonly used strategy [121]. *Hp*IBS and *Hp*IBCL sequences were integrated into the genome and expressed (Figure 41, section 2.7.7., page 27). The product of the enzymes was extracted from 100 mL culture, purified by HPLC and further analyzed by MS^2 spectrometry (Figure 40). Comparing its UV

spectrum upon HPLC-DAD analysis and its fragmentation pattern (Figure 40) with those of the PIBP reference (Figure 21, page 68) confirmed the formation of the correct product. Feeding 10 mM isobutyric acid after episomal expression of *Hp*IBCL and *Hp*IBS led to production of PIBP at levels of 1.15 ng/mg fresh weight cell pellet and 59.2 ng/ml culture medium. However, the product amount obtained after integrating *Hp*IBCL and *Hp*IBS into the yeast genome was much lower than the corresponding episomal production and could not be calculated exactly.

The PTs *Hp*PT2 and *Hp*PT6 were additionally integrated into the same yeast strain containing *Hp*IBCL and *Hp*IBS (Figure 41, section 2.7.7., page 27). The activity was tested by feeding the substrates isobutyric-acid or PIBP. Only traces of the *Hp*PT2 product could be detected by HPLC analysis (data not shown).

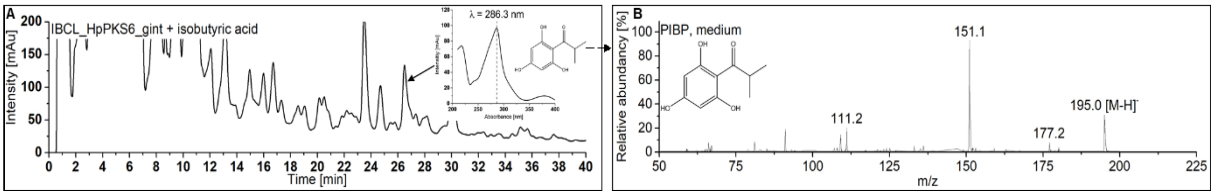

Figure 40. HPLC-DAD (A) and ESI-MS^2 (B) of PIBP (m/z = 195) purified from yeast cultures co-expressing *Hp*IBCL and *Hp*IBS (genome integrated). The cultures were supplemented with 10 mM isobutyric acid.

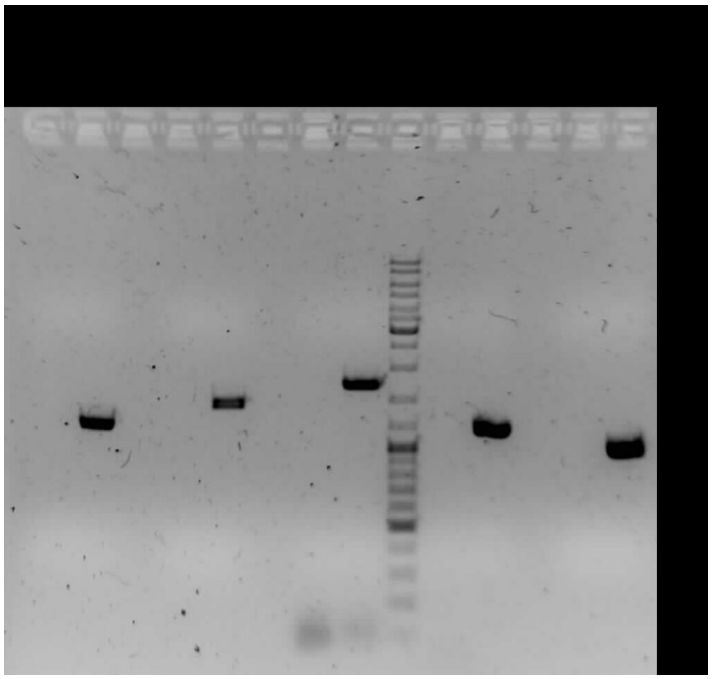

Figure 41. Integration of *Hp*IBCL, *Hp*IBS, *Hp*PT2, and *Hp*PT6 into the yeast genome, as indicated by PCR amplification of target sequences from genomic DNA and gel electrophoretic detection.

4. Discussion

Basic research leads to an increasing fundamental knowledge, which is usable for human beings. One major research part is focused on medical progress enabling to cure or alleviate many diseases. Since thousands of years, our ancestors knew about the healing effects of plants without understanding the underlying mechanisms. Nowadays, human beings constantly recognize the advantages of using plant secondary metabolites as food additives (e.g. Golden Rice) or medicinal applications (e.g. antidepressants). The isolation of plant secondary metabolites is still very costly due to the downstream processing to remove chlorophyll and other undesired constituents. Multistep reactions, e.g. the synthesis of highly complex secondary metabolites such as hyperforin, are very time-consuming and costly due to low productivity. Therefore, the recombinant production of secondary metabolites is an alternative approach to provide larger amounts of plant secondary metabolites for clinical research and subsequent medical applications. To date, the full biosynthetic sequences of many valuable natural secondary metabolites are not well understood, which demands further basic research into this field. One of the most famous medicinal plants is *H. perforatum*. It contains the secondary metabolite hyperforin, which is responsible for the use of *Hypericum* extracts to treat mild to moderate depression. The chemical synthesis of hyperforin requires at least 10 steps, which is very laborious and expensive. Additionally, the yield of this chemical synthesis is very low [44–46]. Thus, the focus of the present research was the investigation of enzymes involved in the biosynthesis of hyperforin.

4.1. Carbon source optimization

Engineering metabolic pathways requires, besides the coding sequence of target genes, the correct control of the protein expression. This should be optimized regarding the induction time, gene copy number and expression level. There are a number of inducible and constitutive promoters available for yeast expression systems [122–125]. The most commonly used promoters are pGal1 and pGal10 for inducible expression and pTEF1 and pPGK1 for constitutive expression with varying expression strengths [124]. While pTEF1/pPGK1 work under glucose, the Gal1/10 promoters are activated by galactose and repressed in the presence of glucose [126]. The latter expression system

was used for the recombinant expression of *H. perforatum*-derived PTs. To improve the PT expression level, different carbon sources were tested and compared with glucose as the standard carbon source. To have a test gene, the GFP cDNA was cloned into the pESC-URA expression vector. The yeast strain containing the GFP cDNA was cultivated using glycerol, sucrose, raffinose, and glucose. Utilizing glycerol has several advantages like it does not exert the Crabtree effect; it is a cheap waste product from fuel production and therefore does not interfere with the food industry [127–129]. However, the growth rate and biomass formation are lower compared to the other carbon sources used, which agreed with our findings [130]. A possibility to overcome this bottleneck would be genetic engineering or evolutional engineering approaches [130–132]. The advantage of using raffinose is that there is no repression or induction at all of the Gal1/10 promoter systems [133]. The major disadvantage of using raffinose is the high cost (1 €/ 1 g). Therefore, glycerol and raffinose have been omitted as a useful carbon source from further experiments.

S. cerevisiae itself possesses the enzyme invertase which converts sucrose into glucose and fructose, encoded by the SUC gene cluster [134]. The monosaccharides (glucose and fructose) enter the cells and become available for glycolysis (Embden-Meyerhof-Parnas glycolytic pathway), which guarantees proper growth [134]. By comparing the GFP fluorescence using either glucose or sucrose, a much higher fluorescence was found with sucrose (Figure 29, page 78). This can be explained by the strong inhibition effects of glucose on the Gal1/10 promotors [135]. Furthermore, sucrose was identified as a usable carbon source because of its higher cell mass formation and higher functional expression rate compared to glucose [122].

During this study, we decided to use sucrose because it is very cost effective and the growth rate and biomass formation are higher than with glucose. Additionally, it can be used for gene expression using constitutive promoters, as done with *Hp*IBCL and *Hp*IBS.

4.2. Chemical synthesis of PT substrates

Most enzymes require, besides the substrates, additional co-factors and co-substrates to perform the biosynthesis. Aromatic PTs catalyze the transfer of isoprenoid moieties, e.g. DMAPP, GPP, and FPP, to a variety of aromatic acceptors. Most aromatic and co-substrates used in this study were either commercially unavailable and/or too expensive. Therefore, a number of substrates were chemically synthesized by our working group.

Chemical synthesis of DMAPP

Isoprenyl moieties, such as DMAPP (C_5), GPP (C_{10}) and FPP (C_{15}), are the major co-substrates utilized by the aromatic PTs. DMAPP for hyperforin biosynthesis is derived from the non-mevalonate pathway by isomerization of IPP catalyzed by isopentenyl diphosphate isomerase (IPPI). Subsequent geranyl diphosphate (GPP) synthase or farnesyl diphosphate (FPP) synthase condense DMAPP and IPP or GPP and IPP to form GPP and FPP, respectively [136]. The aromatic PT cDNAs used in this study were cloned by Dr. Tobias Fiesel, Dr. Andreas Müller, and Dr. Mariam Gaid [111,112]. To determine the active PTs and their substrate scope, DMAPP was synthesized in collaboration with Dr. Mariam Gaid, Dr. Eline Biedermann, and Mohamed Nagia. The synthesized DMAPP was validated by MS^2 spectrometry and its properties were compared with the data of Dr. Andreas Müller and Dr. Tobias Fiesel [111,112]. The molecular ion $[M - H]^-$ was at m/z = 245.0, which corresponded to the molecular mass of 246 g/mol. The fragmentation pattern of DMAPP compared to that of DMAPP synthesized by Dr. Andreas Müller and Dr. Tobias Fiesel [111,112].

Chemical synthesis of acylphloroglucinol derivatives

Acylphloroglucinols are secondary metabolites occurring in various plant families such as Hypericaceae (e.g. *H. perforatum*) and Cannabinaceae (e.g. *Humulus lupulus*). These constituents are naturally derived from the polyketide pathway and their biosynthesis is catalyzed by type III polyketide synthases. Several acylphloroglucinol derivatives were required as PT substrates in this study. Since they are not commercially available, they were chemically synthesized. PIBP, 2-MBP, and PIVP represent the core skeletons of hyperforin, adhyperforin, and lupulone (hop *β*-bitter

acid), respectively. These compounds were used as substrates for *Hp*PT2. All synthesized substrates were analyzed by MS^2 spectrometry and NMR spectroscopy. Besides these synthesized compounds, further commercially available substrates were employed for enzymatic incubations with *Hp*PT2. The major difference between the substrates is the residue (R-), i.e. the acyl moiety attached to the aromatic ring (Figure 42). The conformation and length of the acyl-side chain can influence the substrate specificity of the enzyme. Therefore, it was necessary to synthesize and test a large variety of potential substrates.

In this study, *Hp*PT2 was identified to transfer one geranyl side chain to substrates tested as described above. A second enzyme named *Hp*PT6 was found to accept the enzymatic product of *Hp*PT2 as a substrate. Therefore, it was also necessary to chemically synthesize the 3-geranyl-derivatives of the major *Hp*PT2 substrates, namely PIBP, PAP, PBP, PIVP, and 2-MBP (Figure 42). The monogeranylated analogs served to characterize *Hp*PT6.

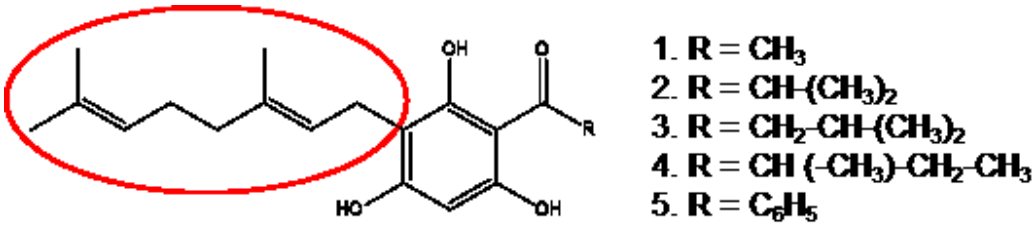

Figure 42. Chemically synthesized substrates for *Hp*PT2 (without the 3-geranyl side chain) and *Hp*PT6 (with the 3-geranyl-side chain, red oval).

4.3. Biosynthesis of the hyperforin core structure PIBP

The recombinant production of plant secondary metabolites like hyperforin or precursor molecules such as PIBP requires the expression of enzymes involved in their biosynthesis. The hyperforin biosynthesis starts with the formation of the core structure PIBP. This is achieved in two major enzymatic reactions, involving a short chain fatty acyl-CoA ligase and a type III polyketide synthase [24].

During this Ph.D. project, the first aim was to increase the intracellular isobutyryl-CoA concentration because of its low intracellular availability. Isobutyryl-CoA is present in *S. cerevisiae* as intermediate for the biosynthesis of isopropanol [137]. For this, valine is

degraded by the branched-chain *α*-ketoacid dehydrogenase complex forming isobutyryl-CoA as intermediate [28,48,49,54,137,138]. Based on transcriptomic data, a short chain fatty acyl-CoA ligase (isobutyryl-CoA ligase) from *H. perforatum* was cloned by Dr. Benye Liu using a previously cloned CoA ligase from *H. lupulus* as a blast template [48]. The *Hp*IBCL cDNA was first expressed in *E. coli* to verify the activity and substrate specificity. The enzymatic product was isolated and analyzed by MS^2 spectrometry, confirming the identity as isobutyryl-CoA in comparison to the commercially available reference.

For yeast, to avoid ester purification and development of an enzymatic assay, which is difficult and time-consuming, we decided to perform an indirect activity test. This approach was carried out by cloning together the *Hp*IBCL and *Hp*IBS sequences with their known functions to form PIBP. Both genes were expressed under the constitutive promoters pTEF1/pPGK1, which enable the use of sucrose instead of glucose as carbon source. For the toxicity of isobutyric acid, a toxicity test was simultaneously performed once by testing different concentrations (10, 50, 100 mM).

In the control culture without isobutyric acid supplementation, only traces of PIBP could be detected. This result confirmed the presence of intracellular isobutyric acid and isobutyryl-CoA derived from the degradation of valine by the branched-chain alpha-keto complex, enabling the formation of PIBP just in the presence of *Hp*IBS and *Hp*IBCL [48]. The amount of cell mass decreased (~ 28 %) at 10 mM isobutyric acid, whereas nearly no growth was detectable using 100 mM. These results clearly confirm the toxicity of isobutyric acid for cell growth when used as a substrate. This finding raises the question how to overcome the bottleneck for future large-scale or long-time cultivation experiments. There are two potential approaches, which may be useful to pave the way. One approach may be fed-batch cultivation experiments, enabling the continuous feeding of the substrate below the toxicity level. Another approach may be the adaptation of the yeast cells to grow on higher isobutyric acid concentrations, achievable by applying a microbial adaptive laboratory evolution (ALE) approach [7,131,132,139].

An approach similar to ours for the recombinant production of PIBP or PIVP in *S. cerevisiae* was achieved by the co-expression of *Humulus lupulus* (hop)-derived isobutyryl-CoA ligase or isovaleryl-CoA ligase together with a valerophenone synthase [34]. That is because acylphloroglucinols PIBP and PIVP are also precursors of cohumulone and humulone (hop bitter tast), respectively. By the co-expression of

isobutyryl-CoA ligase and valerophenone synthase, about 2.3 µM PIBP (0.4 µg/mL) was detected after 96 h of galactose induction without any precursor feeding. This indicates a clear evidence of the presence of isobutyric acid, which can be further converted to the starter acyl-CoA [34]. This also agreed with our findings obtained in this study, as described previously. The PIBP product amount was increased by supplementing 2 mM valine to about 2.83 µM PIBP, pointing to the direct connection of valine degradation to isobutyryl-CoA [48,137].

However, the recently published results [34] cannot be directly compared with the results obtained in this study. Both genes used here were expressed under a constitutive promoter to enable the cultivation on sucrose as carbon source. Furthermore, the PIBP product was isolated and quantified from the cell pellet due to fewer impurities compared to the medium. Additionally, the focus of this study was to increase the PIBP product yield by feeding isobutyric acid, circumventing the need of further intermediate degradation steps of valine.

Additional experiments must be carried out to finally prove the involvement of these enzymes in the biosynthesis of hyperforin. These include the determination of kinetic parameters of *Hp*IBCL and *Hp*IBS compared to other IBLs and IBSs found in *H. perforatum*. Furthermore, the transcript levels for *Hp*IBCL and *Hp*IBS within the plant organs containing PIBP, hyperforin and closely related derivates should be investigated. This experiment includes fruits, flowers, and leaves and there should be a high abundance of highly similar sequences in all the transcriptomes. Additionally, all enzymes should show the same or comparable activity regarding their substrate specificity. In this study, no detailed information about the transcripts and enzymes was obtained.

To summarize, the experiments described in this section must be considered as a proof of principle for the functional expression in yeast of *Hp*IBCL and *Hp*IBS derived from *H. perforatum*. It was possible in this study to express two consecutive enzymes to form the hyperforin precursor molecule PIBP (Figure 43).

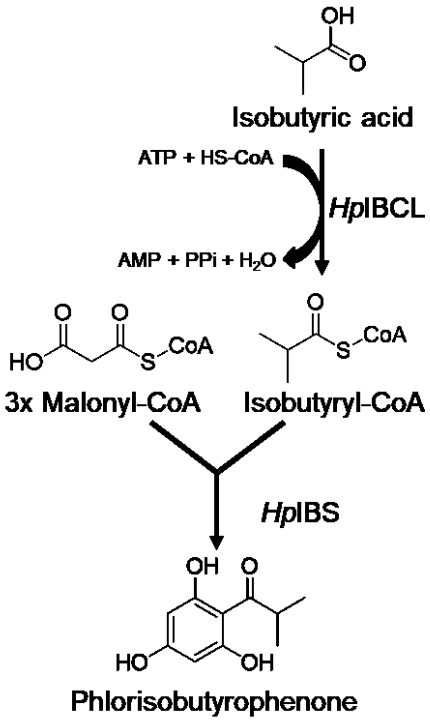

Figure 43. Biosynthesis of the hyperforin core structure PIBP.

4.4. Aromatic Prenyltransferases

Aromatic PTs have already been isolated and biochemically characterized from species throughout different kingdoms of life such as fungi, bacteria and plants [12,74,75]. They are involved in the biosynthesis of primary and secondary metabolites such as terpenoids and pigments, hormones etc. Plant-derived aromatic PTs are located in the envelope of plastids and transfer isoprenoid moieties to different aromatic compounds including xanthones, benzoic acid derivatives, (iso)flavonoids, coumarins, and phloroglucinol derivatives [34,77–95]. The most abundant compounds carry dimethylallyl and geranyl side chains rather than farnesyl and geranylgeranyl residues [77]. Prenylated compounds demonstrate a large variety of biological activities and are therefore promising high-potential candidates for future drug development [77].

The PTs used in this study were isolated based on available transcriptomes of *H. perforatum* and a subtracted cDNA library of *H. calycinum*, prepared in our working group [51]. In total, three full-length cDNAs from *H. calycinum* and nine from *H. perforatum* were obtained based on the aspartate-rich motifs “NDxxDxxxD” and “KDxxDxxGD” [12,25,74,75]. Both aspartate-rich motives are typically known for plant-derived PTs, discovered and published by Prof. Kazufumi Yazaki [12]. These motifs are

made responsible for substrate binding as well as chelating divalent cations such as Mg^{2+}, Mn^{2+} etc, required to perform the catalytic reaction [75]. Bacterial and fungi aromatic PTs lack the aspartate-rich motifs [75]. Here, positively charged amino acids take over the function of the divalent cations to perform the catalytic reaction [140]. Besides the mentioned different characters, there are two more major differences compared to bacterial and fungi-related PTs. The first divergence is the solubility of bacterial and fungal PTs. Second, they belong to the ABBA superfamily, members of which form an antiparallel β-sheet structure (αββα motif) and perform their catalytic reaction within the β-barrel. This structure also leads to a wider substrate specificity compared to plant-derived prenyltransferases [75]. Plant PTs are located within the outer membranes of the plastids and possess typically several transmembrane domains. Therefore, these PTs are not soluble and proposed to perform their catalytic reaction on the exterior of the protein domains [75,141].

The PTs tested in this study possess the usual plant-PT characteristics as described above. The PTs isolated by Dr. Tobias Fiesel have been bioinformatically defined to have between 5–9 transmembrane domains [112]. Furthermore, all functionally expressed PTs were dependent on divalent cations and were membrane bound. All *in vitro* assays were performed with either insect (Sf9) or yeast microsomal fractions [112]. Twelve PTs, three from *H. calycinum* (*Hc*PT 1-3) and nine from *H. perforatum* (*Hp*PT1-9) were isolated and tested for their enzymatic activities. All three *H. calycinum*-derived PTs were completely inactive in *S. cerevisiae* in this study. However, all of them could be functionally expressed in Sf9 insect cells and were identified to be xanthone-specific, i.e. accepting 1,3,7-trihydroxyxanthone (*Hc*PT1) and 1,3,6,7-tetrahydroxyxanthone (*Hc*PT, H*c*PT2) as major substrates [112]. A similar observation was made with PTs isolated from parsley, which were only active in insect cells [84]. Potential reasons might be a better mRNA stability, more closely related codon usage, appropriate glycosylation pattern and chaperon availability, lower protein toxicity, and finally a different membrane composition, which enables a better membrane fluidity in insect cells [142]. Also, synergistic effects might occur. Even omitting the PT signal peptide did not lead to a functional expression, as reported elsewhere [143].

Of all nine *H. perforatum*-derived PTs expressed in *S. cerevisiae*, three were found to be xanthone-specific (*Hp*PT1, *Hp*PT5, *Hp*PT8) and two were acylphloroglucinol-specific (*Hp*PT2, *Hp*PT6). More detailed information and further characteristics are discussed in the following sections.

4.4.1. Xanthone-specific PTs

Xanthones are plant secondary metabolites present in *Hypericum* species and others. They serve as defense compounds against microorganisms and herbivores and were identified to exhibit pharmacological properties such as antibacterial, anti-inflammatory and cytotoxic activities [34,144]. The biosynthesis starts with the condensation of benzoyl-CoA with three molecules malonyl-CoA to form 2,4,6-trihydroxybenzophenone. In the subsequent reactions, cytochrome P450 monooxygenases catalyze cyclization and subsequent 6′-hydroxylation, forming 1,3,6,7-tetrahydroxyxanthone [71,145]. Subsequent modifications might occur such as hydroxylations and/or prenylations [34,71]. *Hp*PT1 and *Hp*PT5 were identified to accept 1,3,6,7-tetrahydroxyxanthone and 1,3,7-trihydroxyxanthone as the preferred substrates using DMAPP (major) and GPP (minor) as isoprenoid donors. *Hp*PT8 was found to accept 1,3,6,7-tetrahydroxyxanthone as the most preferred substrate using exclusively DMAPP (Table 32, page 73). Besides 1,3,7-trihydroxyxanthone and 1,3,6,7-tetrahydroxyxanthone, the presence of prenylated xanthones such as 1,3,6,7-tetrahydroxy-8-prenylxanthone, 1,3,6,7-tetrahydroxy-2-prenylxanthone, 1,3,7-trihydroxy-6-methoxy-8-prenylxanthone and paxanthone was discovered in *H. perforatum* cell suspension cultures after treatment with *Agrobacterium* [144].

Furthermore, a 1,3,6,7-tetrahydroxanthone-specific PT performing a C-8 prenylation was characterized in *H. calycinum* cell cultures after elicitor treatment [34]. Therefore, the PTs identified during this study might be involved in the prenylation of the xanthone derivatives found in *H. perforatum*. The attachment of one prenyl group to the xanthone acceptor has been analyzed by MS spectrometry. Comparing the MS^2 fragmentation pattern of the *Hp*PT8 product with that of the recently published *Hc*PT product indicates identical enzymatic products [34]. However, the enzymatic products of *Hp*PT1 and *Hp*PT5 should be further analyzed by NMR spectrometry to identify the exact C-prenylation or C-geranylation positions. All xanthone-specific PTs were not further biochemically characterized in this study. Nevertheless, all enzymes show clearly plant-derived PT characteristics, such as divalent cation dependency, membrane-boundness and isoprenoid donor usage.

Membrane-bound aromatic PTs are originally localized to the envelope membranes of the chloroplasts [81,143]. Since a yeast cell does not contain any chloroplasts, the PTs have to end up in any other membranous organelle like endoplasmic reticulum, Golgi and mitochondria or enter the plasmamembrane for functional folding. A GFP_*Hp*PT5

translational fusion protein was cloned to localize *Hp*PT5. Similar to previously localized PT fusions in insect cells [112], the fluorescence of GFP_*Hp*PT5 was detected in the cytoplasm of the yeast cells. Dr. Fiesel (2017) used a *H. calycinum*-derived PT (*Hc*PT), which was expressed in insect cells [112]. Thus, the N-terminal transit peptides of PTs from different *Hypericum* species appear to function similarly in the two chloroplast-free expression systems. What remains open is the exact intracellular localization in which membranous organelle, which awaits further research.

Potential PT targets for localization might be therefore the membranes of mitochondria, endoplasmatic reticulum and Golgi. In this study, no final evidence of a specific organelle localization could be obtained. To solve the question regarding the localization of PTs within yeast cells other approaches should be realized. A co-localization expression of an active PT together with a marker protein, which has a known target organelle, may be performed. Another possibility is the separation of subcellular organelles and performing activity assays using the separated organelle fractions. In this context, a geranyl diphosphate:4hydroxybenzoate geranyltransferase from *Lithospermum erythrorhizon* could be localized to the ER in a yeast expression system [94]. However, it might also form a kind of inclusion bodies due to wrong folding events of the PT itself. GFP protein alone is expressed in its functional soluble state.

The enzymatic activity of the GFP_*Hp*PT5 protein was tested but no activity was observed (data not shown). It has been reported that tags can cause non-functional expression of a target protein [146]. This may involve a HIS-tag but also any other tag such as Strep-tag and GFP. Any tags can cause changes in the tertiary structure, thereby leading to reduced or even complete loss of activity [146,147]. Also, a HIS-tag (N- and C-terminal) was tested to purify *Hp*PT5 from solubilized membranes but no activity could be detected (data not shown). The same was observed with *Hp*IBS tested in this study, as already described before.

4.4.2. Phloroglucinol-specific PTs

Phloroglucinol derivates such as hyperforin possess a number of different pharmaceutical activities such as antidepressant properties [118]. Hyperforin is a polyprenylated acylphlorogucinol derivative with PIBP as the core structure. PIBP is formed by the condensation of three molecules of malonyl-CoA and one molecule of

isobutyryl-CoA, catalyzed by a type III polyketide synthase (IBS) [118]. A series of aromatic prenyltransferases was screened for their ability to catalyze the attachment of prenyl and geranyl side chains to PIBP. During this study, two consecutive acylphlorglucinol-specific PTs (*Hp*PT2 and *Hp*PT6) were biochemically characterized.

The biochemical investigation of *Hp*PT2 identified a substrate specificity comprising several acylphloroglucinol derivatives. The enzyme accepted the skeletons of hyperforin, adhyperforin and lupolone, namely PIBP, 2-MBP, and PIVP, respectively. Mass- and NMR-based analyses of the enzymatic products revealed the attachment of one geranyl group at the C-3 position of the aromatic ring. HPLC analysis of the *in vitro* assays did not yield further geranylated products, i.e. di-geranylated PIBP. Regardless of the prenyl-acceptor used, *Hp*PT2 did not accept DMAPP as a prenyl donor. This indicates its clear function to perform one geranylation reaction *in vivo*. Consequently, the subsequent series of prenylation reactions are expected to be performed by more prenyltransferases to obtain hyperforin and its related analogs.

The *Hp*PT2 substrate specificity was investigated using a number of *Hypericum*-derived constituents including xanthones, flavonoids, acylphloroglucinols, benzophenones and phenolic acids as prenyl acceptors as well as DMAPP and GPP as prenyl donors (Figure 11, page 43). The highest specificity was found for the hyperforin core structure PIBP (100 %), followed by the adhyperforin skeleton 2-MBP (70.6 %), 2,3',4,6-tetrahydroxybenzophenone (31.7 %), PIVP (16.9 %), PAP (16.3 %) and PBP (5 %) (Figure 33, page 82). The structural differences between the acylphloroglucinol derivatives are the acyl side chains, which originate (except for PAP, PBP and tetrahydroxybenzophneone) from the amino acids valine, isoleucine, and leucine. No further activities were observed with the other potential substrates tested in this study. *Hp*PT2 was found to have a high but somewhat broader substrate preference for acylphloglucinol derivatives compared to the xanthone-specific PTs *Hp*PT1, *Hp*PT5, and *Hp*PT8. The latter PTs were specific for a single major substrate, whereas other xanthone derivatives were accepted in the lower percentage range (<10 %). Similar observations were published for acylphloroglucinol-specific and flavonoid-specific PTs isolated from hop and *Sophora flavescens,* respectively [79,80,86,87].

Besides the substrate specificity, the effects of different divalent cations and pH variations were investigated. All PTs used in this study possess the aspartate-rich motifs (NQxxDxxxD and KDxxDxxGD), which are required for chelating the divalent

cations [112]. In contrast to plant-derived PTs, bacterial PTs do not necessarily require divalent cations [75]. Similarly to recently published plant PTs, *Hp*PT2 prefers Mg^{2+} as the best cation [34,79–81,90,94,148]. However, other cations such as Ca^{2+} and Zn^{2+} can also be accepted by a number of different plant-derived PTs [34,87]. One exception has been published for a PT from hop, which accepts exclusively Mg^{2+} as the divalent cation [87]. All PTs tested during this study failed to show any activity in the presence of EDTA, confirming the requirement of cations to perform the catalytic reaction.

The optimum pH of plant PTs has been reported to be in the alkaline range of 8.0–10.0, with one exception for a hop-derived PT, which was highly active at pH 7 [34,79,80,87]. The optimum pH of *Hp*PT2 was found to be at pH 8, which corresponds to the literature data. Also, bacterial PTs were found to exhibit their optimum catalytic efficiency at the alkaline pH values [149,150].

*Hp*PT2 exhibited the highest affinity for 2-MBP (K_M = 85 ± 15 µM), whereas that towards PIBP was somewhat lower (K_M = 124 ± 19 µM). The catalytic velocities observed with 2-MBP and PIBP were identical (V_{max} = 5.1^{-3} ± 5^{-4} nmol/mg protein/min). Relatively low differences in the kinetic parameters were found for GPP_{PIBP} [K_M = 89 ± 35 µM; V_{max} = 7.1^{-3} ± 9^{-4} nmol/mg protein/min] and $GPP_{2\text{-}MBP}$ [K_M = 60 ± 11 µM; V_{max} = 4.6^{-3} ± 3^{-4} nmol/mg protein/min]. This suggests that *Hp*PT2 is simultaneously the first enzyme involved in the biosynthesis of hyperforin and adhyperforin at the early geranylation step, which is also supported by the qPCR data analyzed by Dr. Eline Biedermann and Dr. Mariam Gaid [120]. Opposite to the proposed pathway of hyperforin biosynthesis, in which the first prenylation step is supposed to catalyze the attachment of a C_5 unit to the aromatic PIBP core, the current study revealed that the first step is the attachment of a C_{10} unit [24]. Another hint that GPP might be used as the first isoprenoid donor is the presence of 3-geranyl-PIBP in *Hypericum* species [151]. If all PTs involved in hyperforin biosynthesis would be also involved in adhyperforin biosynthesis, one would expect equal amounts of both constituents in the plant. However, the adhyperforin content within the flowering aerial part is only about 10 % of the total hyperforin content [152]. Explanations might be that the catalytic activity and affinity of PTs in the later prenylation reactions to accomplish adhyperforin biosynthesis are reduced or the steps are taken over by other enzymes. Another bottleneck might be the availability of 2-methylbutyryl-CoA for starting adhyperforin formation. To some extent, the lower availability of the core structure of adhyperfoin might be compensated by the higher affinity of *Hp*PT2 towards 2-MBP. In case of higher concentrations of PIBP in *H.*

perforatum, no such high affinity is required. However, higher catalytic activities of some enzymes may account for higher hyperforin contents compared to adhyperforin. The catalytic activity and affinity values obtained in this study are comparable with those reported for other plant PTs. K_M values were found in the range between 1 – 220 µM and catalytic activities in the range of 0.5 – 2 pmol/mg microsomal protein/min [34,76,80,83,85,87,88,148]. The affinity of *Hp*PT2 towards PIVP, which has never been reported for *Hypericum* species, might be an artificial activity due to the structural similarity compared to PIBP and 2-MBP.

A second acylphloroglucinol-specific enzyme is *Hp*PT6, which has been cloned and biochemically characterized during this study. For the first time, a PT was identified to accept only geranylated acylphloroglucinol derivatives. In addition, *Hp*PT6 shows the typical plant-derived PT characteristics regarding the divalent cation dependency, pH range, and aspartate-rich motifs. However, there are some biochemical differences compared to *Hp*PT2, which might be questionable.

If *Hp*PT6 would be located within the same chloroplast like *Hp*PT2, it could be assumed to have similar biochemical features like *Hp*PT2. Different from *Hp*PT2 and other plant PTs, which prefer Mg^{2+}, *Hp*PT6 accepts Ca^{2+} as the major divalent cation [34,79–81,90,94,148]. Typical of other plant PTs, the pH optimum of *Hp*PT6 is in the alkaline range but slightly higher (pH 8 - 9) than *Hp*PT2 (pH 7-8). This difference between *Hp*PT2 and *Hp*PT6 may be a hint that the two PTs are not located within the same organelle. It would be expected that all PTs located in the chloroplast and involved in hyperforin biosynthesis have a close pH optimum to perform the catalytic reaction with high activity. The qPCR data obtained by Dr. Eline Biedermann and Dr. Mariam Gaid for *Hp*PT6 reveal a higher expression level than for *Hp*PT2 throughout the aerial plant organs studied (fruits, flowers, buds and leaves). However, the expression of *Hp*PT6 was also relatively high in roots, which contain only traces of hyperforin and low *Hp*PT2 transcript levels.[120]. Therefore, the involvement of *Hp*PT6 in the hyperforin biosynthesis is still somewhat questionable. The lowest K_M was detected for 3-G-PIVP and 3-G-2-MBP and an approximately doubled activity was observed for 3-G-PIBP.

4.5. Genome integration of *Hp*IBCL, *Hp*IBS, *Hp*PT2, and *Hp*PT6

For the heterologous production of plant secondary metabolites like hyperforin, it is necessary to transfer the biosynthetic pathway from the native into the target host, e.g. *S. cerevisiae*. Besides the identification of the enzymes involved in the biosynthetic pathway, a number of further aspects must be considered. It is important to regulate the gene expression level and the promoter strength must be adjusted; furthermore, intracellular regulatory elements might require some modification [23].

One key element to produce the target molecules is the (over)expression of the responsible enzymes. This can be achieved by expressing the genes either plasmid-based or genome-integrated. To do so, many high copy and low copy plasmids have been designed for the successful expression in *S. cerevisiae.* However, several bottlenecks exist in case of plasmid-based expression systems. Firstly, the reproducibility of the protein expression is challenging due to the different copy numbers of the plasmids. Furthermore, a proper selection marker such as an autotrophic or antibiotic marker must be used. These types of plasmids increase the costs to produce the target protein. Auxotrophic strains must be cultivated in special selection media with (costly) supplements. During the downstream processing, the efficient antibiotic removal must be guaranteed. Another disadvantage of using episomal expression systems is the loss of plasmids during cultivation for the auxotrophic marker. This is caused by the production of the marker itself as well as cell death, releasing e.g. uracil which then is available as a complementary compound.

Consequently, due to plasmid loss, the expression level is dramatically reduced and also the reproducibility is fluctuating. Another disadvantage is the number of genes, which can be expressed at the same time. Typically, one to two genes can be expressed simultaneously, which may limit the expression of complete pathways.

Nowadays, most of the previously mentioned bottlenecks are overcome by introducing the GOIs into the genome of the target organism. Reports prove that the introduction of genes into the genome leads to a more homogeneous expression level and increases the gene stability within the cells. This guarantees that almost every cell within the cultivation population possesses all the genes introduced. Genetic instability might occur when the introduced genes share a high sequence homology with native genes. Additionally, multi tandem integrations might lead to a loss of the introduced genes due to the excision of the genes caused by chromosomal rearrangements. The

major disadvantage might be the lower expression level due to the lower gene number present within the cells.

Hyperforin biosynthesis involves 7–8 enzymes. As described previously, the plasmid-based expression of all genes might be difficult to establish. Therefore, the implementation of a genome integration protocol was developed, as described by Jensen *et. al*. (2013) during this study [103]. Besides the system used in our lab, a number of further integration strategies and examples have been published [10,18,23,98–100,102,125,153–155]. A GFP protein was chosen as an example gene to establish the protocol. The GFP gene was successfully integrated, as described elsewhere (data not shown) [119]. Afterwards, *Hp*IBCL and *Hp*IBS were successfully integrated and the product could be detected (Figure 40, page 91). However, it was not possible to quantify the product amount due to the high amount of impurities. Comparing the product amount generated by the yeast strain containing *Hp*IBCL and *Hp*IBS as integrated into the genome, a much lower product amount could be detected in the medium. The major reason might be the lower copy number, only one copy per yeast cell is present, compared to about 20 – 40 plasmid copies per cell using plasmid-based protein expression. Furthermore, the experiments must be repeated and the quantification method improved. Both PT enzymes *Hp*PT2 and *Hp*PT6 were additionally integrated into the genome to the same strain before (Figure 43, page 99). Only traces of the *Hp*PT2 product could be detected in the HPLC-DAD chromatogram (data not shown). So far, no MS data were prepared to validate the correct product formed. This needs to be confirmed in the future perspectives.

To summarize, it was possible to successfully implement the genome integration protocol in our laboratory. Both GFP and *Hp*IBCL_*Hp*IBS were actively integrated. This protocol can be further used for the implementation and improvement of further genes as well as for the cultivation.

4.6. Conclusion and Outlook

In this study, a cascade consisting of four consecutive enzymes was identified and functionally expressed in yeast, enabling the generation of the hyperforin precursor molecule 3-geranyl-5-prenyl-PIBP (Figure 44). This cascade includes the isobutyryl-CoA ligase together with an isobutyrophenone synthase for the biosynthesis of the hyperforin skeleton PIBP. The two genes were expressed both episomally and integrated into the yeast genome. By feeding isobutyric-acid, the PIBP product could be produced and was detected in both expression systems at detectable concentrations.

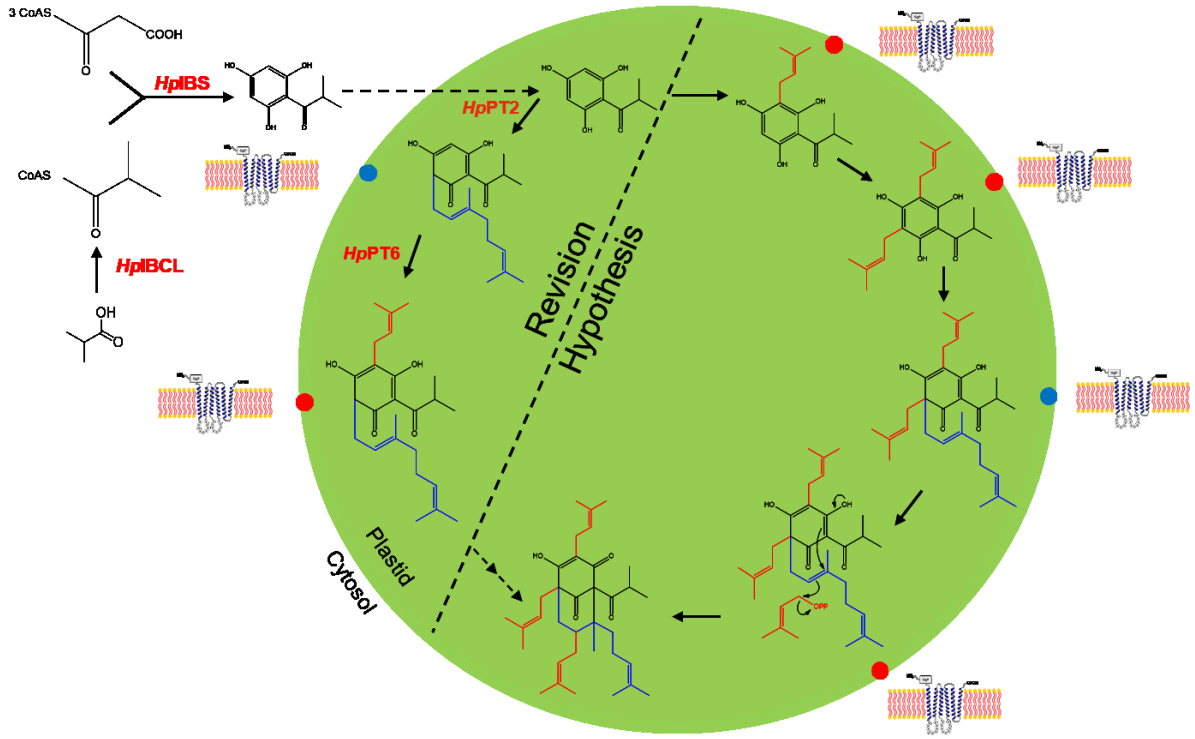

Figure 44. Enzyme cascade towards hyperforin formation, which was functionally expressed in *S. cerevisiae* and tested under *in vivo* and/or *in vitro* conditions. Modified from Beerhues (2006) [24].

In total, 12 different PTs have been investigated for their functional expression and biochemical characteristics. Finally, three xanthone-specific and two acylphlorglucinol-specific PTs were identified. Especially the latter acylphlorglucinol-specific PTs (*Hp*PT2 and *Hp*PT6) are particularly interesting for the hyperforin biosynthesis.

*Hp*PT2 transfers a geranyl side chain to the hyperforin core structure PIBP, forming 3-geranyl-PIBP. Subsequently, this product is used by *Hp*PT6 as a substrate, hereby

attaching another prenyl side chain, forming the hyperforin precursor molecule 3-geranyl-5-prenyl-PIBP. All actively expressed PTs show typical plant-specific PT characteristics. This includes dependency on divalent cations, highest activity at slightly alkaline pH values, and acceptance of geranyl and/or prenyl moieties. In addition, the two fully characterized acylphloroglucinol-specific PTs exhibited a relatively broad substrate specificity.

The kinetic data obtained for *Hp*PT2 showed the highest affinity and catalytic velocity to the basic structures of adhyperforin and hyperforin. In conclusion, it is suggested that *Hp*PT2 is involved in adhyperforin and hyperforin biosynthesis. The kinetic data of *Hp*PT6 showed the highest affinity towards the adhyperforin and colupolone precursors. A slightly lower affinity and catalytic rate were observed for the hyperforin precursor.

As an outlook, it should be mentioned that the missing PTs still have to be identified in order to complete the hyperforin biosynthesis. This is the current challenge because no PTs have so far been isolated using polyprenylated acylphloroglucinol derivatives as substrates. Also, the possibility that multiple PTs form a catalytic complex (metabolon) should be considered, finishing the hyperforin biosynthesis. Such an example has recently been published for the completion of colupolone biosynthesis [86].

In addition, it is still unclear how the last cyclization step in hyperforin biosynthesis takes place. Therefore, the corresponding enzyme still has to be identified. After the complete biosynthesis has been successfully identified, the whole pathway should be preferably integrated into the yeast genome. Moreover, the 3-geranyl-5-prenyl-PIBP product is already proved to be unstable. Therefore, it might represent another challenge to stabilize the biosynthetic hyperforin intermediates and hyperforin itself.

5. References

1. Kilbane, J. J. Future applications of biotechnology to the energy industry. *Front. Microbiol.* **7,** 4–7 (2016).
2. Belem, M. A. F. Application of biotechnology in the product development of nutraceuticals in Canada. *Trends Food Sci. Technol.* **10,** 101–106 (1999).
3. Giacomoni, P. Healing beauty? *Sci. Soc.* **9,** 7–11 (2008).
4. Berger, R. G. Biotechnology of flavours — the next generation. 1651–1659 (2009). doi:10.1007/s10529-009-0083-5
5. Leffingwell, J. C. & Leffingwell, D. Biotechnology - Conquests and Challenges in Flavors & Fragrances. **7,** 1–11 (2015).
6. Galaev, I. Y. & Mattiasson, B. 'Smart' polymers and what they could do in biotechnology and medicine. **7799,** 335–340 (1999).
7. Dragosits, M. & Mattanovich, D. Adaptive laboratory evolution – principles and applications for biotechnology. *Microb. Cell Fact.* **12,** 64 (2013).
8. Borodina, I. & Nielsen, J. Advances in metabolic engineering of yeast Saccharomyces cerevisiae for production of chemicals. 609–620 (2014). doi:10.1002/biot.201300445
9. Ida, K., Ishii, J., Matsuda, F., Kondo, T. & Kondo, A. Eliminating the isoleucine biosynthetic pathway to reduce competitive carbon outflow during isobutanol production by Saccharomyces cerevisiae. *Microb. Cell Fact.* **14,** 62 (2015).
10. Mikkelsen, M. D. *et al.* Microbial production of indolylglucosinolate through engineering of a multi-gene pathway in a versatile yeast expression platform. *Metab. Eng.* **14,** 104–11 (2012).
11. Jimenez-Garcia, S. N. *et al.* Current approaches for enhanced expression of secondary metabolites as bioactive compounds in plants for agronomic and human health purposes – a review. *Polish J. Food Nutr. Sci.* **63,** 67–78 (2013).
12. Yazaki, K., Sasaki, K. & Tsurumaru, Y. Prenylation of aromatic compounds, a key diversification of plant secondary metabolites. *Phytochemistry* **70,** 1739–1745 (2009).
13. Botta, B., Vitali, A., Menendez, P., Misiti, D. & Monache, G. Prenylated Flavonoids: Pharmacology and Biotechnology. *Curr. Med. Chem.* **12,** 713–739

(2005).

14. Dakanali, M. & Theodorakis, E. A. Polyprenylated phloroglucinols and xanthones. *Biomim. Org. Synth.* **2,** 433–467 (2011).
15. Engels, B., Dahm, P. & Jennewein, S. Metabolic engineering of taxadiene biosynthesis in yeast as a first step towards Taxol (Paclitaxel) production. *Metab. Eng.* **10,** 201–206 (2008).
16. Hansen, E. H. *et al.* De novo biosynthesis of vanillin in fission yeast (schizosaccharomyces pombe) and baker's yeast (saccharomyces cerevisiae). *Appl. Environ. Microbiol.* **75,** 2765–2774 (2009).
17. Ni, J., Tao, F., Du, H. & Xu, P. Mimicking a natural pathway for de novo biosynthesis: natural vanillin production from accessible carbon sources. *Sci. Rep.* **5,** 1–12 (2015).
18. Ro, D. K. *et al.* Production of the antimalarial drug precursor artemisinic acid in engineered yeast. *Nature* **440,** 940–943 (2006).
19. Becker, J. V. W. *et al.* Metabolic engineering of Saccharomyces cerevisiae for the synthesis of the wine-related antioxidant resveratrol. *FEMS Yeast Res.* **4,** 79–85 (2003).
20. Wang, Y. *et al.* Stepwise increase of resveratrol biosynthesis in yeast Saccharomyces cerevisiae by metabolic engineering. *Metab. Eng.* **13,** 455–463 (2011).
21. Mata-Gómez, L., Montañez, J., Méndez-Zavala, A. & Aguilar, C. Biotechnological production of carotenoids by yeasts: an overview. *Microb. Cell Fact.* **13,** 12 (2014).
22. Zhang, W. *et al.* Production of naringenin from D-xylose with co-culture of E. coli and S. cerevisiae. *Eng. Life Sci.* **17,** 1021–1029 (2017).
23. Shao, Z., Zhao, H. & Zhao, H. DNA assembler, an in vivo genetic method for rapid construction of biochemical pathways. *Nucleic Acids Res.* **37,** 1–10 (2009).
24. Beerhues, L. Hyperforin. *Phytochemistry* **67,** 2201–2207 (2006).
25. Gaid, M. *et al.* Biotechnological production of hyperforin for pharmaceutical formulation. *Eur. J. Pharm. Biophar-maceutics Eur. J. Pharm. Biopharm.* (2017). doi:10.1016/j.ejpb.2017.03.024
26. Pdbiad, C. Morphological and biochemical variations in St . John ' s wort , Hypericum perforatum L ., growing over altitudinal and UV-B radiation gradients.

110, 257–262 (2008).

27. Wölfle, U., Seelinger, G. & Schempp, C. M. Topical Application of St . John ' s Wort (Hypericum perforatum). *Planta Med* 109–120 (2014). doi:10.1055/s-0033-1351019
28. Beerhues, L. Biosynthesis of the active Hypericum perforatum constituents. *Med. Aromat. Plant Sci. Biotechnol.* 70–77 (2011).
29. Müller, W. Current St. John's wort research from mode of action to clinical efficacy. *Pharmacol. Res.* **47,** 101–109 (2003).
30. Richard, J. A. Chemistry and biology of the polycyclic polyprenylated acylphloroglucinol hyperforin. *European J. Org. Chem.* 273–299 (2014). doi:10.1002/ejoc.201300815
31. Nahrstedt, A. & Butterweck, V. Biologically active and other chemical constituents of the herb of Hypericum perforaturn L. *Pharmacopsychiat.* 129–134 (1997).
32. Crockett, S. L. Europe PMC Funders Group Essential Oil and Volatile Components of the Genus Hypericum (Hypericaceae). **5,** 1493–1506 (2010).
33. Pauli, A. & Kubeczka, K.-H. Antimicrobial properties of volatile phenylpropanes. *Nat. Prod. Commun.* **5,** 1387–94 (2010).
34. Fiesel, T. *et al.* Molecular cloning and characterization of a xanthone prenyltransferase from hypericum calycinum cell cultures. *Molecules* **20,** 15616–15630 (2015).
35. Tekelová, D., Repcak, M., Zemkova, E. & Toth, J. Quantitative changes of dianthrones, hyperforin and flavonoids content in the flower ontogenesis of Hypericum perforatum. *Planta Med.* **66,** 778–780 (2000).
36. Leuner, K. *et al.* Hyperforin--a key constituent of St. John's wort specifically activates TRPC6 channels. *FASEB J.* **21,** 4101–4111 (2007).
37. Bondy, B. Pathophysiology of depression and mechanisms of treatment. 7–20
38. Ferguson, J. M. & Ferguson, J. M. rig Pr. (2001).
39. Sell, T. S., Belkacemi, T., Flockerzi, V. & Beck, A. Protonophore properties of hyperforin are essential for its pharmacological activity. *Sci. Rep.* **4,** 7500 (2014).
40. Friedland, K. & Harteneck, C. *Hyperforin: To be or not to be an activator of TRPC(6)*. *Review in physiological Biochemistry Pharmacology* **169,** (2015).

41. Gaid, M., Haas, P., Beuerle, T., Scholl, S. & Beerhues, L. Hyperforin production in Hypericum perforatum root cultures. *J. Biotechnol.* **222,** 47–55 (2016).

42. Verotta, L., Lovaglio, E., Sterner, O., Appendino, G. & Bombardelli, E. Oxidative fragmentation of the bridged ß-triketone core of hyperforin. *European J. Org. Chem.* 1193–1197 (2004). doi:10.1002/ejoc.200300568

43. Uwamori, M. & Nakada, M. Stereoselective total synthesis of (+/-)-hyperforin via intramolecular cyclopropanation. *Tetrahedron Lett.* **54,** 2022–2025 (2013).

44. Bellavance, G. & Barriault, L. Total syntheses of hyperforin and papuaforins A-C, and formal synthesis of nemorosone through a gold(I)-catalyzed carbocyclization. *Angew. Chemie - Int. Ed.* **53,** 6701–6704 (2014).

45. Sparling, B. A., Moebius, D. C. & Shair, M. D. Enantioselective total synthesis of hyperforin. *J. Am. Chem. Soc.* **135,** 644–647 (2013).

46. Ting, C. P. & Maimone, T. J. Total synthesis of hyperforin. *J. Am. Chem. Soc.* **137,** 10516–10519 (2015).

47. Klingauf, P. *et al.* Biosynthesis of the hyperforin skeleton in Hypericum calycinum cell cultures. *Phytochemistry* **66,** 139–145 (2005).

48. Xu, H. *et al.* Characterization of the formation of branched short-chain fatty acid:CoAs for bitter acid biosynthesis in Hop glandular trichomes. *Mol. Plant* **6,** 1301–1317 (2013).

49. Adam, P., Arigoni, D., Bacher, A. & Eisenreich, W. Biosynthesis of Hyperforin in Hypericum perforatum. *J. Med. Chem.* **45,** 4786–4793 (2002).

50. Chen, Q., Fan, D. & Wang, G. Heteromeric geranyl(geranyl) diphosphate synthase is involved in monoterpene biosynthesis in arabidopsis flowers. *Molecular Plant* **8,** 1434–1437 (2015).

51. Gaid, M. *et al.* Cinnamate:CoA ligase initiates the biosynthesis of a benzoate-derived xanthone phytoalexin in Hypericum calycinum cell cultures. *Plant Physiol.* **160,** 1267–1280 (2012).

52. Open, P. M. *et al.* Four isoforms of Arabidopsis 4-coumarate:CoA ligase have overlapping yet distinct roles in phenylpropanoid metabolism. *Plant Physiol.* **169,** 2409–2421 (2015).

53. Goese, M., Kammhuber, K., Bacher, A., Zenk, M. H. & Eisenreich, W. Biosynthesis of bitter acids in hops A C-NMR and 2 H-NMR study on the building blocks of humulone. *Eur. J. Biochem.* **263,** 447–454 (1999).

54. Karppinen, K., Hokkanen, J., Tolonen, A., Mattila, S. & Hohtola, A. Biosynthesis of hyperforin and adhyperforin from amino acid precursors in shoot cultures of Hypericum perforatum. *Phytochemistry* **68,** 1038–1045 (2007).

55. Shimizu, Y., Ogata, H. & Goto, S. Type III polyketide synthases: functional classification and phylogenomics. *ChemBioChem* **18,** 50–65 (2017).

56. Zhang, Z., Pan, H.-X. & Tang, G.-L. New insights into bacterial type II polyketide biosynthesis. *F1000Research* **6,** 172 (2017).

57. Yin, Y., Cai, M., Zhou, X., Li, Z. & Zhang, Y. Polyketides in Aspergillus terreus: biosynthesis pathway discovery and application. *Appl. Microbiol. Biotechnol.* **100,** 7787–7798 (2016).

58. Thwe, A. A. *et al.* Metabolomic analysis and phenylpropanoid biosynthesis in hairy root culture of tartary buckwheat cultivars. *PLoS One* **8,** e65349 (2013).

59. Gomes, E. S., Schuch, V. & Lemos, E. G. de M. Biotechnology of polyketides: New breath of life for the novel antibiotic genetic pathways discovery through metagenomics. *Brazilian J. Microbiol.* **44,** 1007–1034 (2013).

60. Cheng, Y. Q., Coughlin, J. M., Lim, S. K. & Shen, B. Polyketide synthases that require discrete acyltransferases. *Methods Enzymol.* **459,** 165–186 (2009).

61. Hertweck, C., Luzhetskyy, A., Rebets, Y. & Bechthold, A. Type II polyketide synthases: gaining a deeper insight into enzymatic teamwork. *Nat. Prod. Rep.* **24,** 162–190 (2007).

62. Abe, I. & Morita, H. Structure and function of the chalcone synthase superfamily of plant type III polyketide synthases. *Nat. Prod. Rep.* **27,** 809–838 (2010).

63. Yu, D., Xu, F., Zeng, J. & Zhan, J. Type III polyketide synthases in natural product biosynthesis. *IUBMB Life* **64,** 285–295 (2012).

64. Huang, L. *et al.* Differential expression of benzophenone synthase and chalcone synthase in Hypericum sampsonii. *Nat. Prod. Commun.* **7,** 1–4 (2012).

65. Okada, Y. *et al.* Enzymatic reactions by five chalcone synthase homologs from hop (Humulus lupulus L.). *Biosci. Biotechnol. Biochem* **8451,** 1142–1145 (2017).

66. Shi, S. *et al.* Enzymatic synthesis of plant polyketides. *Curr. Org. Synth.* **5,** 250–266 (2008).

67. Karppinen, K. & Hohtola, A. Molecular cloning and tissue-specific expression of two cDNAs encoding polyketide synthases from Hypericum perforatum. *J. Plant Physiol.* **165,** 1079—1086 (2008).

68. Beerhues, L. & Liu, B. Biosynthesis of biphenyls and benzophenones – Evolution of benzoic acid-specific type III polyketide synthases in plants. *Phytochemistry* **70,** 1719–1727 (2009).

69. Austin, M. B. & Noel, J. P. The chalcone synthase superfamily of type III polyketide synthases. *Nat. Prod. Rep.* **20,** 79–110 (2003).

70. Liu, B., Falkenstein-Paul, H., Schmidt, W. & Beerhues, L. Benzophenone synthase and chalcone synthase from Hypericum androsaemum cell cultures cDNA cloning, functional expression, and site-directed mutagenesis of two polyketide synthases. *Plant J.* **34,** 847–855 (2003).

71. El-Awaad, I., Bocola, M., Beuerle, T., Liu, B. & Beerhues, L. Bifunctional CYP81AA proteins catalyse identical hydroxylations but alternative regioselective phenol couplings in plant xanthone biosynthesis. *Nat. Commun.* **7,** 1–12 (2016).

72. Karppinen, K., Hokkanen, J., Mattila, S., Neubauer, P. & Hohtola, A. Octaketide-producing type III polyketide synthase from Hypericum perforatum is expressed in dark glands accumulating hypericins. *FEBS J.* **275,** 4329–42 (2008).

73. Fan, A., Winkelblech, J. & Li, S. M. Impacts and perspectives of prenyltransferases of the DMATS superfamily for use in biotechnology. *Applied Microbiology and Biotechnology* **99,** 7399–7415 (2015).

74. Winkelblech, J., Fan, A. & Li, S. M. Prenyltransferases as key enzymes in primary and secondary metabolism. *Appl Microbiol Biotechnol* **99,** 7379–7397 (2015).

75. Heide, L. Prenyl transfer to aromatic substrates: genetics and enzymology. *Curr. Opin. Chem. Biol.* **13,** 171–179 (2009).

76. MUNAKATA, R. *et al.* Characterization of Coumarin-Specific Prenyltransferase Activities in *Citrus limon* Peel. *Biosci. Biotechnol. Biochem.* **76,** 1389–1393 (2012).

77. Alhassan, A. M., Abdullahi, M. I., Uba, A. & Umar, A. Prenylation of aromatic secondary metabolites: A new frontier for development of novel drugs. *Pharm Res Trop. J. Pharm. Res. J. Cit. ReportsScience Ed.* **13,** 307–307 (2014).

78. Sugiyama, A. *et al.* Metabolic engineering for the production of prenylated polyphenols in transgenic legume plants using bacterial and plant prenyltransferases. *Metab. Eng.* **13,** 629–637 (2011).

79. Sasaki, K., Tsurumaru, Y., Yamamoto, H. & Yazaki, K. Molecular characterization of a membrane-bound prenyltransferase specific for isoflavone from Sophora flavescens. *J. Biol. Chem.* **286,** 24125–24134 (2011).

80. Sasaki, K., Mito, K., Ohara, K., Yamamoto, H. & Yazaki, K. Cloning and characterization of naringenin 8-prenyltransferase, a flavonoid-specific prenyltransferase of Sophora flavescens. *PLANT Physiol.* **146,** 1075–1084 (2008).

81. Shen, G. *et al.* Characterization of an isoflavonoid-specific prenyltransferase from Lupinus albus. *PLANT Physiol.* **159,** 70–80 (2012).

82. Munakata, R. *et al.* Molecular evolution of parsnip (Pastinaca sativa) membrane-bound prenyltransferases for linear and/or angular furanocoumarin biosynthesis. *New Phytol.* **211,** 332–344 (2016).

83. Munakata, R. *et al.* Molecular Cloning and Characterization of a GDP-specific Aromatic Prenyltransferase from Citrus limon. *Plant Physiol.* **166,** 80–90 (2014).

84. Karamat, F. *et al.* A coumarin-specific prenyltransferase catalyzes the crucial biosynthetic reaction for furanocoumarin formation in parsley. *Plant J.* **77,** 627–638 (2014).

85. Akashi, T., Sasaki, K., Aoki, T., Ayabe, S. & Yazaki, K. Molecular cloning and characterization of a cDNA for pterocarpan 4-dimethylallyltransferase catalyzing the key prenylation step in the biosynthesis of glyceollin, a soybean phytoalexin. *Plant Physiol.* **149,** 683–93 (2009).

86. Li, H. *et al.* A heteromeric membrane-bound prenyltransferase complex from hop catalyzes three sequential aromatic prenylations in the bitter acid pathway. *Plant Physiol.* **167,** 650–659 (2015).

87. Tsurumaru, Y. *et al.* HlPT-1, a membrane-bound prenyltransferase responsible for the biosynthesis of bitter acids in hops. *Biochem. Biophys. Res. Commun.* **417,** 393–398 (2012).

88. Tsurumaru, Y. *et al.* An aromatic prenyltransferase-like gene HlPT-1 preferentially expressed in lupulin glands of hop. *Plant Biotechnol.* **27,** 199–204 (2010).

89. Boubakir, Z., Beuerle, T., Liu, B. & Beerhues, L. The first prenylation step in hyperforin biosynthesis. *Phytochemistry* **66,** 51–57 (2005).

90. Ohara, K., Mito, K. & Yazaki, K. Homogeneous purification and characterization

of LePGT1--a membrane-bound aromatic substrate prenyltransferase involved in secondary metabolism of Lithospermum erythrorhizon. *FEBS J.* **280,** 2572–80 (2013).

91. Ohara, K., Muroya, A., Fukushima, N. & Yazaki, K. Functional characterization of LePGT1, a membrane-bound prenyltransferase involved in the geranylation of p-hydroxybenzoic acid. *Biochem. J* **421,** 231–241 (2009).
92. Ohara, K., Yamamoto, K., Hamamoto, M., Sasaki, K. & Yazaki, K. Functional characterization of OsPPT1, which encodes p-hydroxybenzoate polyprenyltransferase involved in ubiquinone biosynthesis in Oryza sativa. *Plant Cell Physiol.* **47,** 581–590 (2006).
93. Okada, K. *et al.* The AtPPT1 gene encoding 4-hydroxybenzoate polyprenyl diphosphate transferase in ubiquinone biosynthesis is required for embryo development in Arabidopsis thaliana. *Plant Mol. Biol.* **55,** 567–77 (2004).
94. Yazaki, K., Kunihisa, M., Fujisaki, T. & Sato, F. Geranyl diphosphate:4-hydroxybenzoate geranyltransferase from Lithospermum erythrorhizon. Cloning and characterization of a ket enzyme in shikonin biosynthesis. *J. Biol. Chem.* **277,** 6240–6 (2002).
95. Kawasaki, T. *et al.* Metabolic engineering of flavonoids with prenyltransferase and chalcone isomerase genes in tomato fruits. *Plant Biotechnol.* **31,** 567–571 (2014).
96. Botta, B., Vitali, A., Menendez, P., Misiti, D. & Delle Monache, G. Prenylated flavonoids: pharmacology and biotechnology. *Curr. Med. Chem.* **12,** 717–739 (2005).
97. Sobanski, M. A. & Dickinson, J. R. No Title. **9,** 225–230 (1995).
98. Oldenburg, K. R., Vo, K. T., Michaelis, S. & Paddon, C. Recombination-mediated PCR-directed plasmid construction in vivo in yeast. *Nucleic Acids Res.* **25,** 451–452 (1997).
99. Kuijpers, N. G. A. *et al.* A versatile, efficient strategy for assembly of multi-fragment expression vectors in Saccharomyces cerevisiae using 60 bp synthetic recombination sequences. *Microb. Cell Fact.* **12,** 47 (2013).
100. Kok, S. De *et al.* Rapid and reliable DNA assembly via ligase cycling reaction. *ACS Synth. Biol.* **3,** 97–106 (2014).
101. Joska, T. M., Mashruwala, A., Boyd, J. M. & Belden, W. J. A universal cloning

method based on yeast homologous recombination that is simple, efficient, and versatile. *J. Microbiol. Methods* **100,** 46–51 (2014).

102. Bubeck, P., Winkler, M. & Bautsch, W. Rapid cloning by homologous recombination in vivo. *Nucleic Acids Research* **21,** 3601–3602 (1993).
103. Jensen, N. B. *et al.* EasyClone: method for iterative chromosomal integration of multiple genes in Saccharomyces cerevisiae. *FEMS Yeast Res.* **14,** 238–48 (2014).
104. Löoke, M., Kristjuahan, K. & Kristjuhan, A. Extraction of genomic DNA from yeasts for PCR-based applications. *Biotechniques* **50,** 325–328 (2011).
105. Cohen, S. N., Chang, A. C. Y. & Hsu, L. Nonchromosomal antibiotic resistance in bacteria: genetic transformation of Escherichia coli by R-Factor DNA. *Proc. Natl. Acad. Sci.* **69,** 2110–2114 (1972).
106. Gietz, R. D. & Schiestl, R. H. Frozen competent yeast cells that can be transformed with high efficiency using the LiAc/SS carrier DNA/PEG method. *Nat. Protoc.* **2,** 1–4 (2007).
107. Pompon, D., Louerat, B., Bronine, A. & Urban, P. in 51–64 (1996). doi:10.1016/S0076-6879(96)72008-6
108. Bradford, M. M. A rapid and sensitive method for the quantitation of microgram quantities of protein utilizing the principle of protein-dye binding. *Anal. Biochem.* **72,** 248–254 (1976).
109. Quast, D. Biosynthese der Hyperforin-Vorstufe Phlorisobutyrophenon in Saccharomyces cerevisiae. (2016).
110. Ummethum, H. Expression of Hypericum derived polyketide synthases in Saccharomyces cerevisiae. (2016).
111. Müller, A. Molekulare analyse von Prenyltransferasen aus Hypericum Arten. *Cuvillier Verlag,* **49,** (2013).
112. Fiesel, T. Tobias Fiesel (Autor) Aromatische Prenyltransferasen aus Hypericum-Arten Biosynthese (poly-)prenylierter Acylphloroglucin-Derivate im Johanniskraut. **49,** 0–16 (2017).
113. Woodside, A. B. *et al.* in *Organic Syntheses* 211–211 (John Wiley & Sons, Inc., 2003). doi:10.1002/0471264180.os066.27
114. George, J. H., Hesse, M. D., Baldwin, J. E. & Adlington, R. M. Biomimetic synthesis of polycyclic polyprenylated acylphloroglucinol natural products

isolated from hypericum papuanum. *Org. Lett.* **12,** 3532–3535 (2010).

115. Fobofou, S. A. T., Franke, K., Porzel, A., Brandt, W. & Wessjohann, L. A. Tricyclic acylphloroglucinols from Hypericum lanceolatum and regioselective synthesis of Selancins A and B. *J. Nat. Prod.* **79,** 743–753 (2016).
116. Sun, Q., Schmidt, S., Tremmel, M., Heilmann, J. & König, B. Synthesis of natural-like acylphloroglucinols with anti-proliferative, anti-oxidative and tube-formation inhibitory activity. *Eur. J. Med. Chem.* **85,** 621–628 (2014).
117. Guo, J. *et al.* Cytotoxic activities of chemical constituents from rhizomes of Anemarrhena asphodeloides and their analogues. *Arch. Pharm. Res.* **38,** 598–603 (2015).
118. Gaid, M. *et al.* Biotechnological production of hyperforin for pharmaceutical formulation. *European Journal of Pharmaceutics and Biopharmaceutics* (2017). doi:10.1016/j.ejpb.2017.03.024
119. Patz, S. Aktivitätsbasiertes Substratscreening einer episomal und genomintegrierten aromatischen Prenyltransferase aus Hypericum perforatum in Hefe. (2015).
120. Biedermann, E. Untersuchungen zur Charakterisierung von Prenyltransferasen aus Hypericum-Arten nach Expression in Nicotiana benthamiana. *Cuvillier Verlag,* **49,** 0–10
121. Jensen, N. B. *et al.* EasyClone: method for iterative chromosomal integration of multiple genes in Saccharomyces cerevisiae. *FEMS Yeast Res.* **14,** 238–48 (2014).
122. Cartwright, C. P., Li, Y., Zhu, Y.-S. Z., Kang, Y.-S. & Tipper, D. J. Use of beta lactamase as a secreted reporter of promoter function in yeast. *Yeast* **10,** 497–508 (1994).
123. Williams, T. C., Espinosa, M. I., Nielsen, L. K. & Vickers, C. E. Dynamic regulation of gene expression using sucrose responsive promoters and RNA interference in Saccharomyces cerevisiae. *Microb. Cell Fact.* **14,** 43 (2015).
124. Peng, B., Williams, T. C., Henry, M., Nielsen, L. K. & Vickers, C. E. Controlling heterologous gene expression in yeast cell factories on different carbon substrates and across the diauxic shift: a comparison of yeast promoter activities. *Microb. Cell Fact.* 1–11 (2015). doi:10.1186/s12934-015-0278-5
125. Da Silva, N. a. & Srikrishnan, S. Introduction and expression of genes for

metabolic engineering applications in Saccharomyces cerevisiae. *FEMS Yeast Res.* **12,** 197–214 (2012).

126. Adams, B. G. Induction of galactokinase in Saccharomyces cerevisiae: kinetics of induction and glucose effects. *J. Bacteriol.* **111,** 308–315 (1972).
127. Yazdani, S. S. & Gonzalez, R. Anaerobic fermentation of glycerol: a path to economic viability for the biofuels industry. *Curr. Opin. Biotechnol.* **18,** 213–219 (2007).
128. Thompson, J. C. & He, B. B. CHARACTERIZATION OF CRUDE GLYCEROL FROM BIODIESEL PRODUCTION FROM MULTIPLE FEEDSTOCKS. **22,** 261–265 (2006).
129. Aldiguier, A. S. *et al.* Synergistic temperature and ethanol effect on Saccharomyces cerevisiae dynamic behaviour in ethanol bio-fuel production. *Bioprocess Biosyst. Eng.* **26,** 217–22 (2004).
130. Swinnen, S., Ho, P. W., Klein, M. & Nevoigt, E. Genetic determinants for enhanced glycerol growth of Saccharomyces cerevisiae. *Metab. Eng.* **36,** 68–79 (2016).
131. Zambanini, T. *et al.* Efficient malic acid production from glycerol with Ustilago trichophora TZ1. *Biotechnol. Biofuels* **9,** 67 (2016).
132. Gresham, D. & Hong, J. The functional basis of adaptive evolution in chemostats. *FEMS Microbiol. Rev.* 2–16 (2014). doi:10.1111/1574-6976.12082
133. Jani, N. M. & Lopes, J. M. Regulated transcription of the Saccharomyces cerevisiae phosphatidylinositol biosynthetic gene, PIS1, yields pleiotropic effects on phospholipid synthesis. *FEMS Yeast Res.* **9,** 552–564 (2009).
134. Marques, W. L., Raghavendran, V., Stambuk, B. U. & Gombert, A. K. Sucrose and Saccharomyces cerevisiae: A relationship most sweet. *FEMS Yeast Research* **16,** (2015).
135. Da Silva, N. A. & Srikrishnan, S. Introduction and expression of genes for metabolic engineering applications in Saccharomyces cerevisiae. *FEMS Yeast Res.* **12,** 197–214 (2012).
136. Burke, C. C., Wildung, M. R. & Croteau, R. Geranyl diphosphate synthase: Cloning, expression, and characterization of this prenyltransferase as a heterodimer. *Proc. Natl. Acad. Sci.* **96,** 13062–13067 (1999).
137. Dickinson, J. R., Harrison, S. J. & Hewlins, M. J. E. An investigation of the

metabolism of valine to isobutyl alcohol in Saccharomyces cerevisiae. *J. Biol. Chem.* **273,** 25751–25756 (1998).

138. Maggio-hall, L. A., Lyne, P., Wolff, J. A. & Keller, N. P. A single Acyl-CoA dehydrogenase is required for catabolism of isoleucine, valine and short-chain fatty acids in Aspergillus nidulans. *Fungal Genet Biol.* **45,** 180–189 (2010).
139. Conrad, T. M., Lewis, N. E. & Palsson, B. Ø. Microbial laboratory evolution in the era of genome-scale science. *Mol. Syst. Biol.* **7,** 1–11 (2011).
140. Tello, M., Kuzuyama, T., Heide, L., Noel, J. P. & Richard, S. B. The ABBA family of aromatic prenyltransferases: broadening natural product diversity. *Cell. Mol. Life Sci.* **65,** 1459–1463 (2008).
141. Soelberg, J., Jorgensen, L. B. & Jäger, A. K. Hyperforin accumulates in the translucent glands of Hypericum perforatum. *Ann. Bot.* **99,** 1097–1100 (2007).
142. Marheineke, K., Grünewald, S., Christie, W. & Reilländer, H. Lipid composition of Spodoptera frugiperda (Sf 9) and Trichoplusia (Tn) insect cells used for baculovirus infection. *FEBS Lett.* **441,** 49–52 (1998).
143. Akashi, T., Sasaki, K., Aoki, T., Ayabe, S. & Yazaki, K. Molecular cloning and characterization of a cDNA for pterocarpan 4-dimethylallyltransferase catalyzing the key prenylation step in the biosynthesis of glyceollin, a soybean phytoalexin. *Plant Physiol.* **149,** 683–93 (2009).
144. Franklin, G., Conceição, L. F. R., Kombrink, E. & Dias, A. C. P. Xanthone biosynthesis in Hypericum perforatum cells provides antioxidant and antimicrobial protection upon biotic stress. *Phytochemistry* **70,** 60–68 (2009).
145. El-awaad, I. & El-awaad, I. Cytochrome P450 enzymes involved in xanthone biosynthesis in Hypericum species. (2016). doi:10.13140/RG.2.1.1741.9122
146. Rosano, G. L. & Ceccarelli, E. A. Recombinant protein expression in Escherichia coli: advances and challenges. *Front. Microbiol.* **5,** 1–17 (2014).
147. Terpe, K. Overview of tag protein fusions: from molecular and biochemical fundamentals to commercial systems. *Appl. Microbiol. Biotechnol.* **60,** 523–533 (2003).
148. Ohara, K., Mito, K. & Yazaki, K. Homogeneous purification and characterization of LePGT1-a membrane-bound aromatic substrate prenyltransferase involved in secondary metabolism of Lithospermum erythrorhizon. *FEBS J.* **280,** 2572–80 (2013).

149. Haug-Schifferdecker, E., Arican, D., Brückner, R. & Heide, L. A new group of aromatic prenyltransferases in fungi, catalyzing a 2,7-dihydroxynaphthalene 3-dimethylallyl-transferase reaction. *J. Biol. Chem.* **285,** 16487–16494 (2010).

150. Zeyhle, P. *et al.* A membrane-bound prenyltransferase catalyzes the O-prenylation of 1,6-dihydroxyphenazine in the marine bacterium streptomyces sp. CNQ-509. *ChemBioChem* **15,** 2385–2392 (2014).

151. Porzel, A., Farag, M. A., Mülbradt, J. & Wessjohann, L. A. Metabolite profiling and fingerprinting of Hypericum species: A comparison of MS and NMR metabolomics. *Metabolomics* **10,** 574–588 (2014).

152. Zemkovμ, E., Tekel, D. & Repc, M. Quantitative Changes of Dianthrones , Hyperforin and Flavonoids Content in the Flower Ontogenesis of Hypericum perforatum. **66,** 778–780 (2000).

153. Flagfeldt, D. B., Siewers, V., Huang, L. & Nielsen, J. Characterization of chromosomal integration sites for heterologous gene expression in Saccharomyces cerevisiae. *Yeast* **26,** 545–551 (2009).

154. Maury, J. *et al.* EasyCloneMulti: A set of vectors for simultaneous and multiple genomic integrations in Saccharomyces cerevisiae. *PLoS One* **11,** 1–22 (2016).

155. Sun, J. *et al.* Cloning and characterization of a panel of constitutive promoters for applications in pathway engineering in Saccharomyces cerevisiae. *Biotechnol. Bioeng.* **109,** 2082–92 (2012).

155. Chaturvedi. R. Application of Cell Culture Systems in Metabolic Engineering. Dept. of Biotechnology, Indian Institute of Technology Guwahati, Guwahati - 781039, Assam, India). [online] available at: http://nptel.ac.in/courses/102103016/31. (2012).

156. Moser G. Johanniskraut ist Arzneipflanze des Jahres. [online] available at: https://www.pharmazeutische-zeitung.de/index.php?id=54535. (2014).

157. „Weltweit leiden mehr als 320 Millionen an Depressionen“ [online] available at: http://www.fnp.de/nachrichten/wissenschaft/Weltweit-leiden-mehr-als-320-Millionen-an-Depressionen;art153,2491985 (2017). 08.07.2018

6. Appendix

6.1. List of Figures

6.2. List of Tables

6.3. List of Abbreviations and Denotation

Abbreviation	Denotation
°C	Grad Celsius
µL	Microliter
µM	Micromolar
2-MBP	2-Methylbutanoyl-phloroglucinol
3-G-X	3-geranyl-X
abs.	absolute
ADP	Adenosine diphosphate
AP	Alkaline Phosphatase
ATP	Adenosine-triphosphate
bp	Base pair(s)
BPS	Benzophenone synthase
BSA	Bovine serum albumin
BZCL	Benzoate-CoA-Ligase
$CaCl_2$	Calcium chloride
cm	centimeter
CoA	Coenzyme-A
DAD	Diode Array Detector
ddH_2O	Double-distilled water
DMAPP	Dimethylallyl pyrophosphate
DMSO	Dimethylsulfoxid
DNA	Deoxyribonucleic acid
dNTP	Deoxynucleotide triphosphate
E. coli	*Escherichia coli*
e.g.	exempli gratia (for example)
EDTA	Ethylenediaminetetraacetic acid
EPI	Enhanced Product Ion
epi.	episomal
ESI	Electrospray-Ionization

et al.	et alii
EtOAc	Ethyl acetate
EtOH	Ethanol
EV	Empty vector
Fig.	Figure
fw	forward
g	Gramm
g	Gravitational force
g/L	gram per liter
Gal	D-Galactose
GFP	Green Fluorescent Protein
gint.	genome integration
GOI	Gene of interest
GPP	Geranyl pyrophosphate
h	Hour(s)
*Ha*CHS	*Hypericum androsaemum* Chalcone synthase
*Ha*PT	*Hypericum androsaemum* Prenyltransferase
HBr	Hydrogen Bromide
HCl	hydrochloride
*Hc*PT	*Hypericum calycinum* Prenyltransferase
HIS	Histidine
*Hp*IBS	*Hypericum perforatum* Isobutyrophenone synthase
HPLC	High performance liquid chromatography
*Hp*PT	*Hypericum perforatum* Prenyltransferase
IBCL	Isobutyrate-CoA ligase
IBS	Isobutyrophenone synthase
INVSC1	Invitrogen *S. cerevisiae* No. 1
IPTG	Isopropyl β-D-1-thiogalactopyranoside
kb	Kilobase(s)
k_{cat}	Catalytic activity

K_m	Michaelis Menten constant/substrate affinity constant
KPi-buffer	Potassium phosphate buffer
LB-medium	Luria-Bertani-medium
LC	Liquid chromatography
m/z	Mass-to-charge ratio
MCS	Multiple cloning sites
MeOH	Methanol
MG	Monogeranylated
$MgCl_2$	Magnesium chloride
min	minute(s)
ml	milliliter
mL/L	milli liter per liter
mM	milli molar
mRNA	Messenger ribonucleic acid
MS	Mass spectrometry
MS^2	Tandem Mass spectrometry
MW	Molecular Weight
N_2	Nitrogen
NaCl	Sodium chloride
NaOH	Natriumhydroxid
ng	nanogram
nm	nanometer
NMR-spectrometry	Nuclear magnetic resonance spectrometry
nt	Nucleotide
OD	Optical density
OD_{600}	Optical density at a wavelength of 600 nm
PAGE	Polyacrylamide gel electrophoresis
PAP	Phloracetophenone
PBP	Phlorbenzophenone
PCR	Polymerase chain reaction

PEG	Polyethylenglycol
pH	Decimal logarithm of the reciprocal of the hydrogen ion activity
PIBP	Phlorisobutyrophenone
PIVP	Phlorisovalerophenone
PKS	Polyketide synthase
PPAP	Polycyclic polyprenylated acylphloroglucinol
PT	Prenyltransferase
Rec.	Recombinant
Ref.	Reference
RNA	Ribonukleinsäure
RP	Reverse Phase
rpm	Revolutions per minute
RT	Room temperature
rv	Reverse
s	Second(s)
S. cerevisiae	*Saccharomyces cerevisiae*
SDS-PAGE	Sodium dodecyl sulfate polyacrylamide gel electrophoresis
sec	Sekunde
SGI-medium	Synthetic minimal medium
SNP	Single Nucleotide Polymorphism
TAE	Tris-Acetate-EDTA
Taq-polymerase	Thermus aquaticus-polymerase
TBS	Tris-buffered saline
temp.	temperature
T_m	Melting Temperature
TRIS	Tris-(hydroxymethyl)-aminomethane
U	Units (enzyme activity)
URA	Uracil
USER	Uracil-Specific Excision Reagent

UV	Ultraviolet
V	Volt
v/v	volume per volume
VIS	Visible
V_{max}	Maximum Velocity
vs.	versus
w/v	weight per volume
w/w	weight per weight
wt	Wild-type
YPSE	Yeast peptone sucrose ethanol

6.4. Oligonucleotides

Oligonucleotide sequences used in this thesis are not shown to maintain confidentiality until manuscript publication.

6.5. DNA Sequences

Nucleotide sequences for enzymes used in this thesis are not shown to maintain confidentiality until manuscript publication.

6.6. Calibration Curves

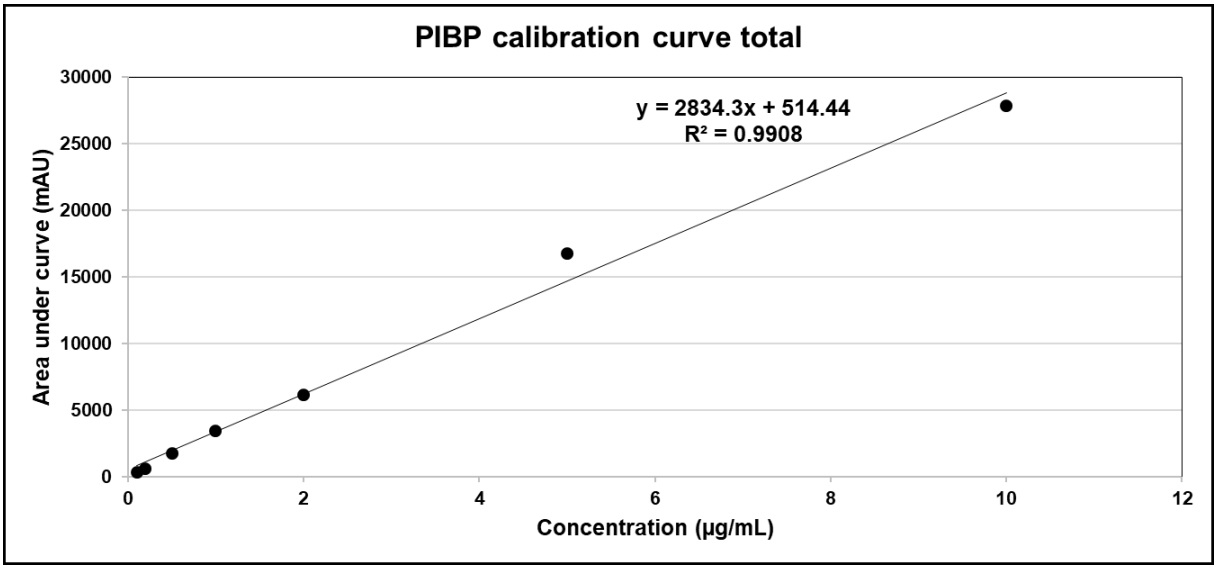

Figure 45: Calibration curve of chemically synthesized phlorisobutyrophenone. The coefficient of determination was calculated to be $R^2 = 0.9908$ from 0.1 to 10 µg phlorisobutyrophenone.

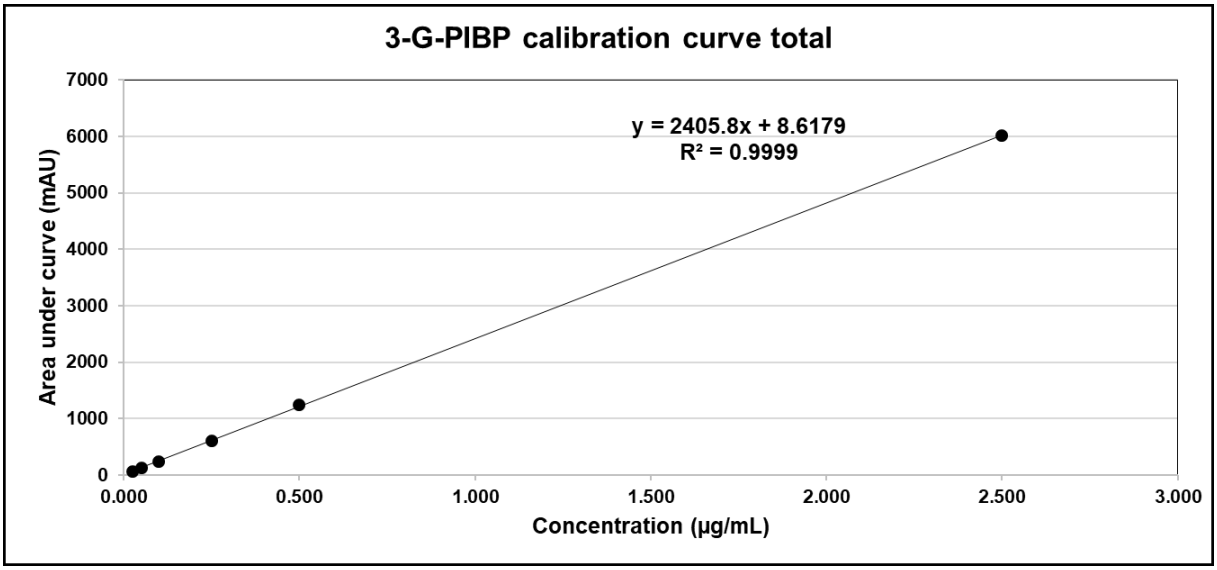

Figure 46: Calibration curve of chemically synthesized 3-geranyl-phlorisobutyrophenone. The coefficient of determination was calculated to be $R^2 = 0.9999$ from 0.1 to 10 µg 3-geranyl-phlorisobutyrophenone.

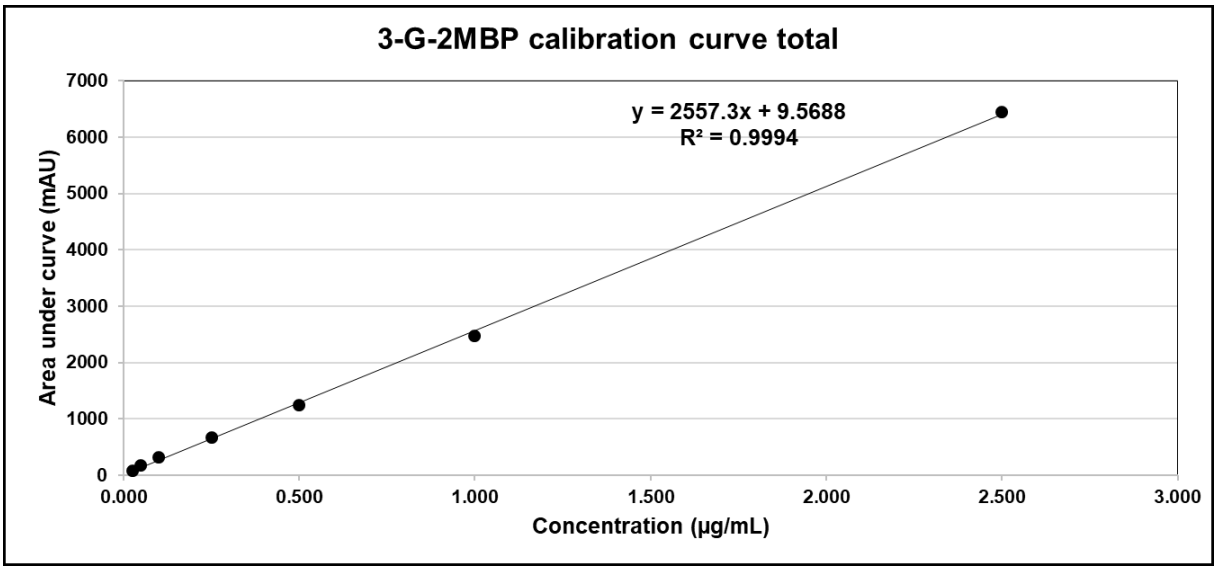

Figure 47: Calibration curve of chemically synthesized 3-geranyl-2 methylbutanoyl-phloroglucinol. The coefficient of determination was calculated to be R^2 = 0.9994 from 0.1 to 10 µg 3-geranyl-2 methylbutanoyl-phloroglucinol.

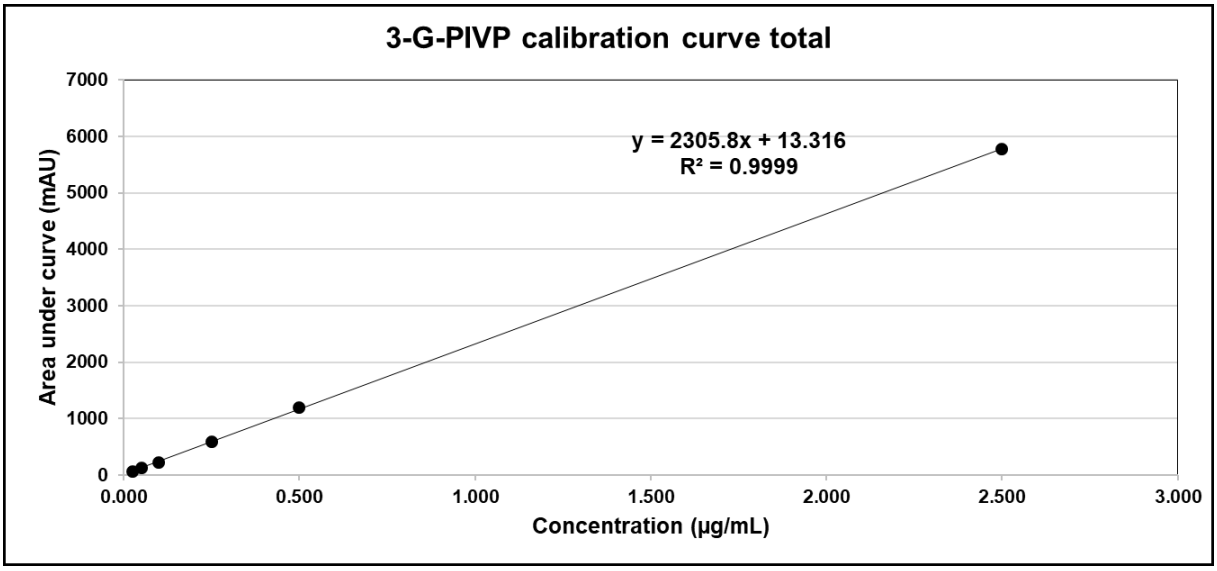

Figure 48: Calibration curve of chemically synthesized 3-geranyl-phlorisovalerophenone. The coefficient of determination was calculated to be R^2 = 0.9999 from 0.1 to 10 µg PIBP 3-geranyl-phlorisovalerophenone.

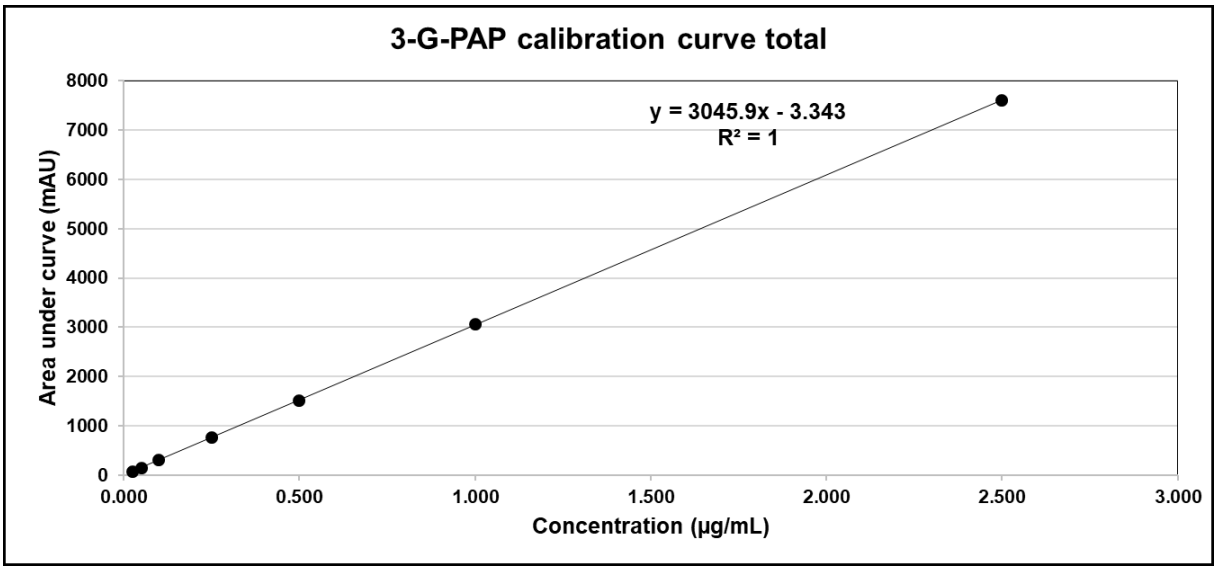

Figure 49: Calibration curve of chemically synthesized 3-geranyl-phloracetophenone. The coefficient of determination was calculated to be $R^2 = 1$ from 0.1 to 10 µg 3-geranyl-phloracetophenone.

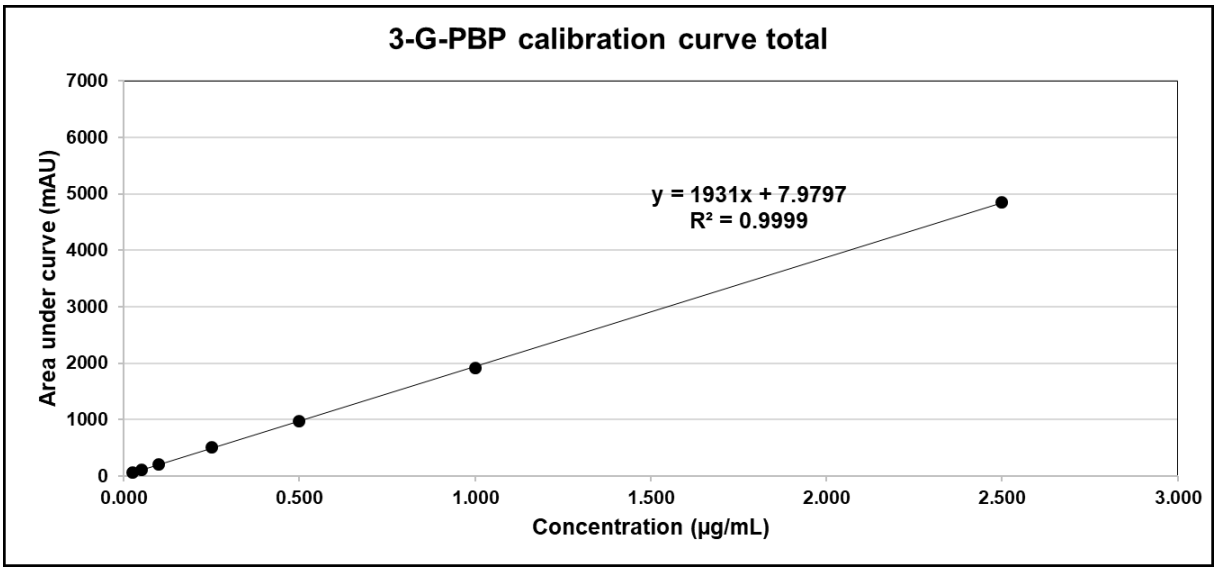

Figure 50: Calibration curve of chemically synthesized 3-geranyl-phlorbenzophenone. The coefficient of determination was calculated to be $R^2 = 0.9999$ from 0.1 to 10 µg 3-geranyl-phlorbenzophenone.

6.7. NMR Data

6.7.1. ^{1}H NMR data of chemically synthesized phlorisobutyrophenone

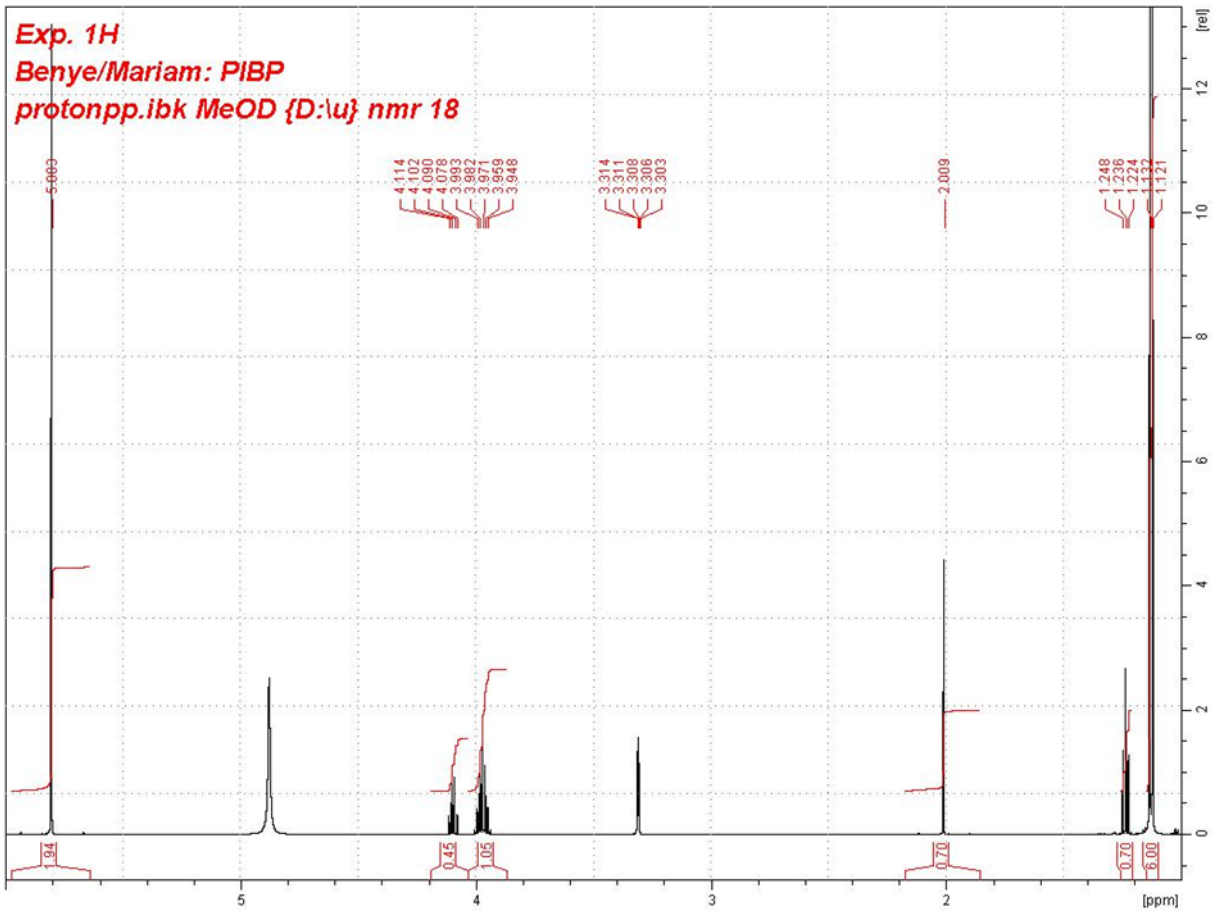

Figure 51: ^{1}H-NMR data for chemically synthesized phlorisobutyrophenone.

6.7.2. ^{1}H and ^{13}C-NMR data of chemically synthesized 2-methylbutanoyl-phloroglucinol

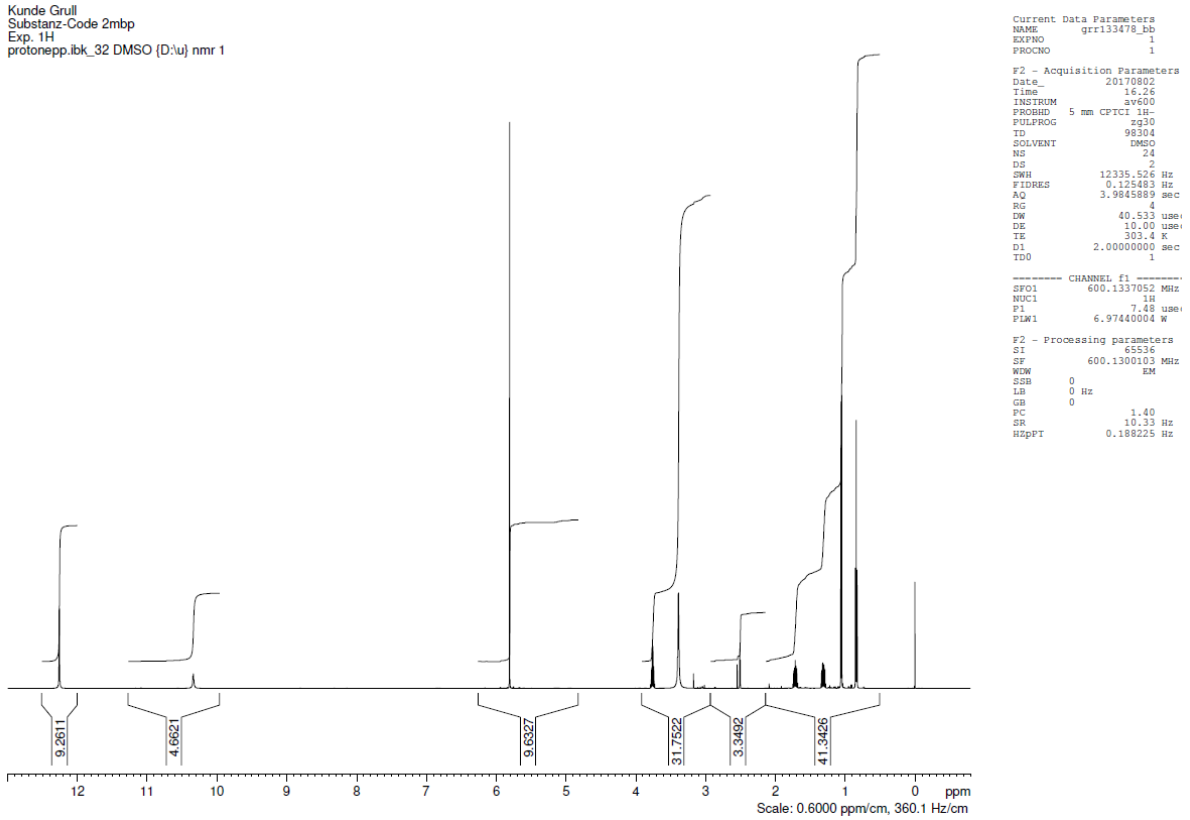

Figure 52: ^{1}H-NMR data for chemically synthesized 2-methylbutanoyl-phloroglucinol.

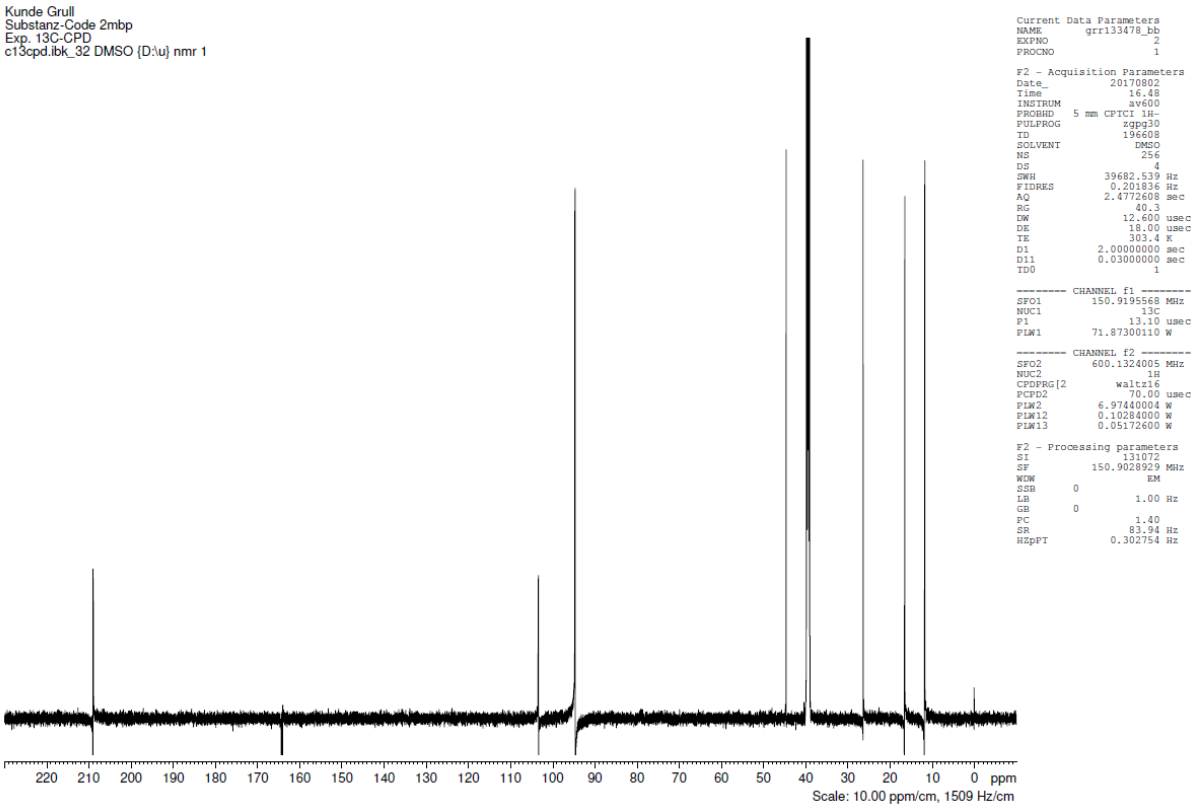

Figure 53: ^{13}C-CPD NMR data for chemically synthesized 2-methylbutanoyl-phloroglucinol.

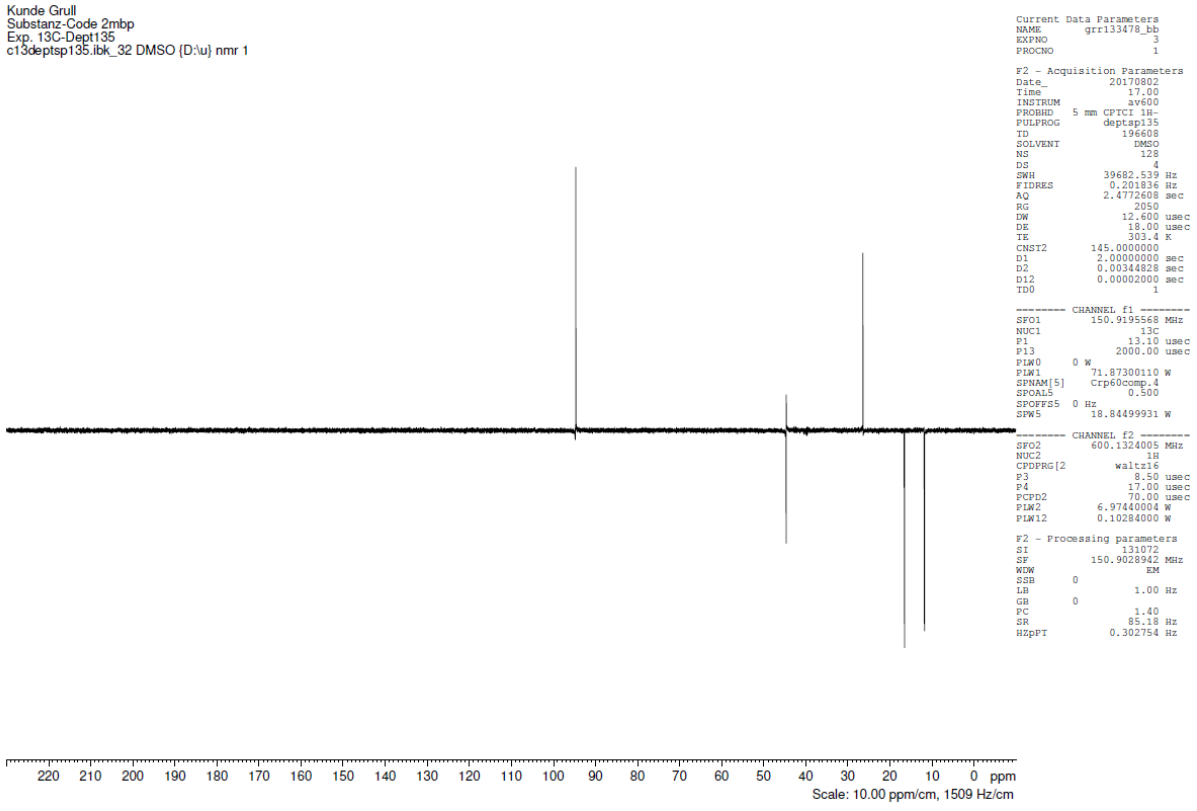

Figure 54: ^{13}C-Dept 135 NMR data for chemically synthesized 2-methylbutanoyl-phloroglucinol.

6.7.3. ^{1}H and ^{13}C-NMR data of chemically synthesized phlorisovalerophenone

Table 35: NMR data of grr133194 [CAS: 26103-97-9]

Position	^{13}C	DEPT	^{1}H
1	104.0	C_q	
2, 6	164.2	C_q	
2-, 6-OH	-	-	12.25 (s, 2 H)
3, 5	94.6	CH	5.80 (s)
4	164.5	C_q	
4-OH	-	-	10.34 (s, 1 H)
7	204.8	C_q	
8	51.9	CH_2	2.86 (d, 6.8 Hz, 2 H)
9	24.8	CH	2.14 (nonet, 6.7 Hz, 1 H)
10, 11	22.6	2 CH_3	0.91 (d, 6.7 Hz, 6 H)

[a] Measuring frequencies: 500.3 MHz (^{1}H), 125.8 MHz (^{13}C); solvent: DMSO-d_6; references: tetramethylsilane (δ_H = 0.00 ppm), solvent (δ_C = 39.50 ppm).

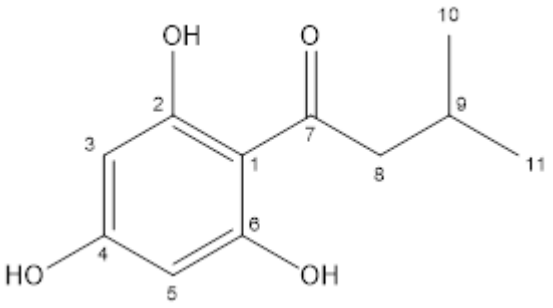

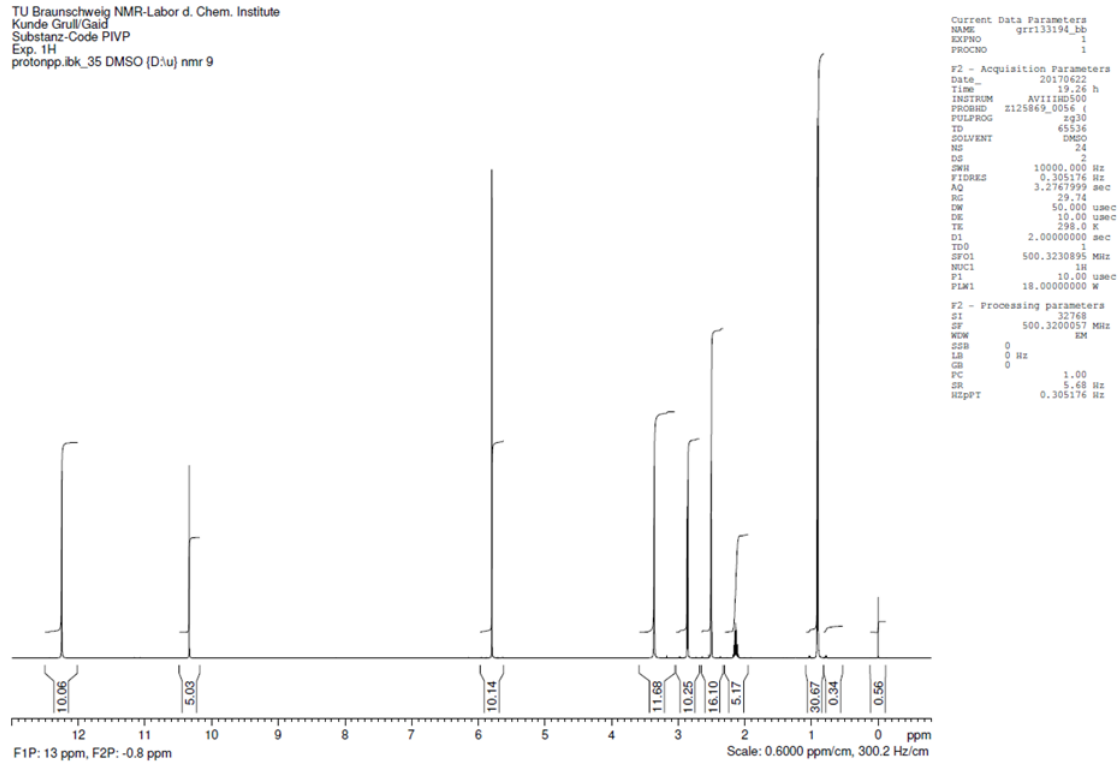

Figure 55: ^{1}H-NMR data for the chemically synthesized phlorisovalerophenone.

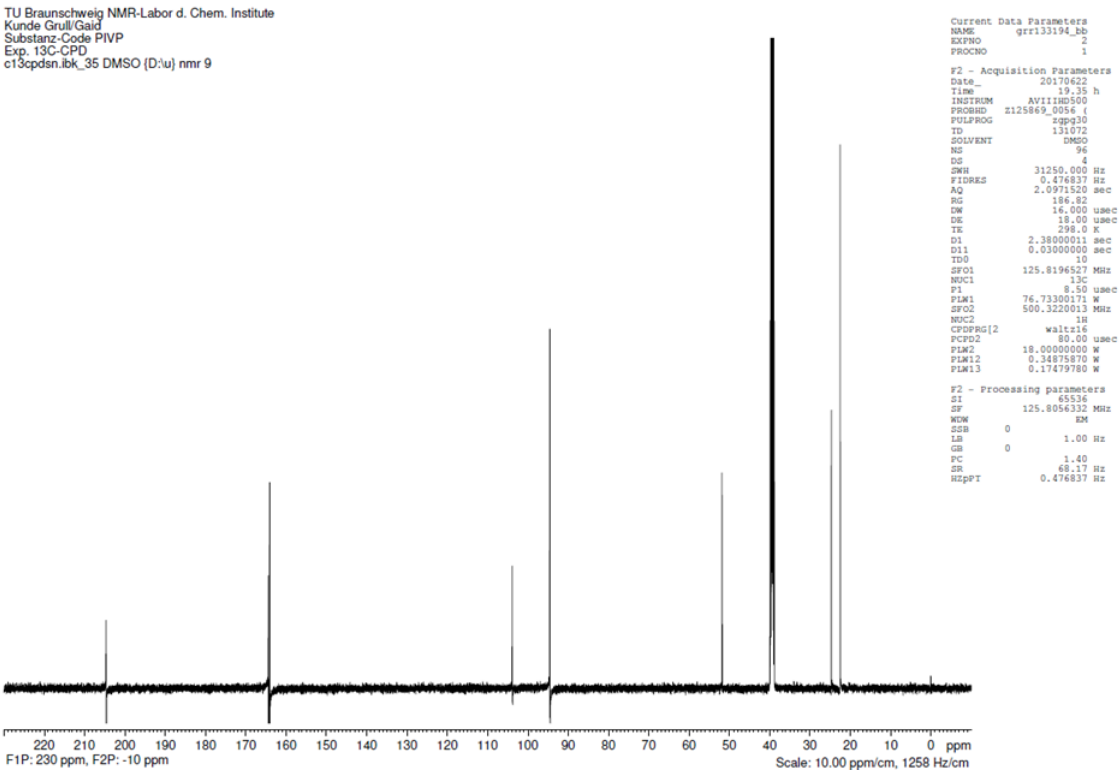

Figure 56: ^{13}C-CPD NMR data for the chemically synthesized phlorisovalerophenone.

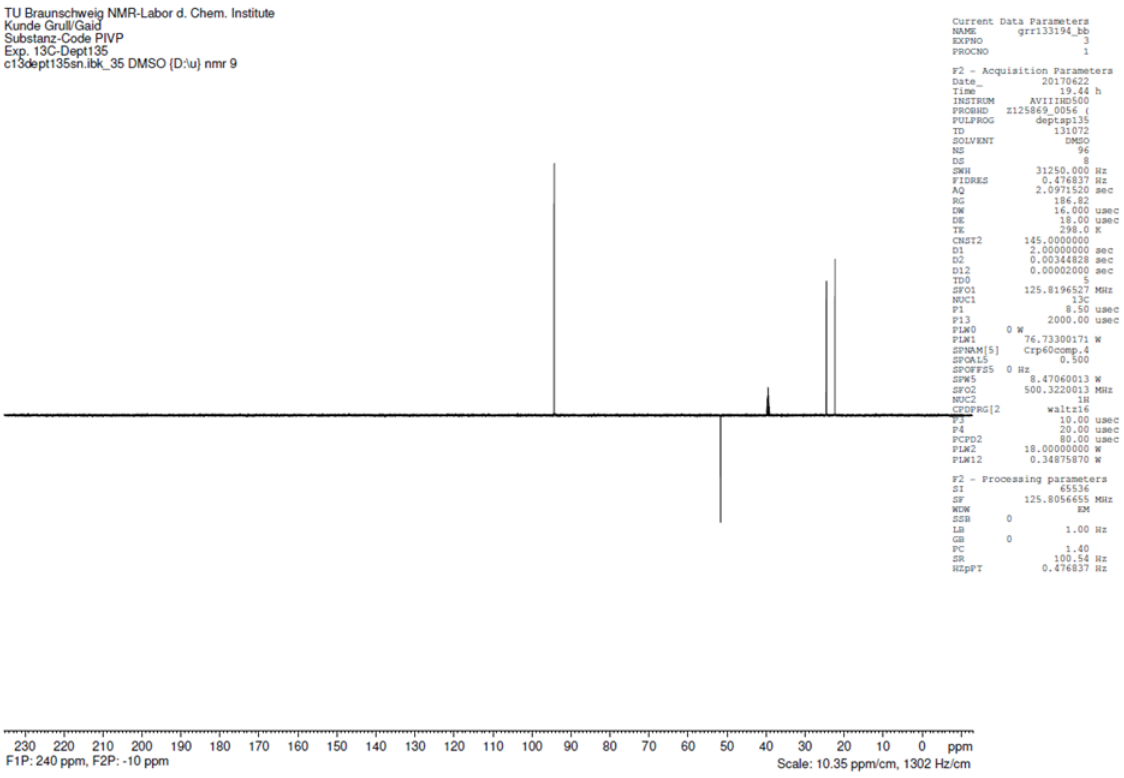

Figure 57: ^{13}C-Dept 135 NMR data for the chemically synthesized phlorisovalerophenone.

6.7.4. ^{1}H and ^{13}C-NMR data for chemically synthesized 3-prenyl-phlorisobutyrophenone

Table 36: NMR data of grr133195[a,b] [CAS No. 35932-36-6]

Position	^{13}C	DEPT	^{1}H	HMBC[c]
1	102.6	C_q		2-OH, 3, 6-OH
2	159.5	C_q		(2-OH), 3
2-OH	-	-	10.53 (s, 1 H)	
3	94.2	CH	5.99 (s, 1 H)	(2-OH), (4-OH)
4	162.1	C_q		3, 4-OH, (6-OH), 1"
4-OH	-	-	10.28 (s, 1 H)	
5	105.9	C_q		3, 4-OH, 6-OH, 1"
6	163.8	C_q		6-OH, 1"
6-OH	-	-	14.15 (s, 1 H)	
7	209.5	C_q		8, 9, 10
8	38.1	CH	3.90 (sept, 6.7 Hz, 1 H)	9, 10
9, 10	19.3	2 CH_3	1.07 (d, 6.7 Hz, 6 H)	8, 9, 10
1"	21.0	CH_2	3.07 (br. d, 7.1 Hz, 2 H)	
2"	123.4	CH	5.11 (t x sept, 7.1, 1.4 Hz, 1 H)	1", 4"$_E$, 4"$_Z$
3"	129.5	C_q		1", 4"$_E$, 4"$_Z$
4"$_E$	25.5	CH_3	1.59 (br. d, 1.3 Hz, 3 H)	2", 4"$_Z$
4"$_Z$	17.6	CH_3	1.68 (br. d, 1.2 Hz, 3 H)	2", 4"$_E$

[a] Measuring frequencies: 500.3 MHz (^{1}H), 125.8 MHz (^{13}C); solvent: DMSO-d_6; references: tetramethylsilane (δ_H = 0.00 ppm), solvent (δ_C = 39.50 ppm).

[b] For previous NMR data, see Boubakir et al. (2005). The present data and assignments are more complete.

[c] Entries in the HMBC column indicate ^{1}H nuclei showing long-range correlations with the ^{13}C chemical shift in the second column. Weak correlations in parentheses.

Z. Boubakir, T. Beuerle, B. Liu, L. Beerhues (2005) *Phytochemistry 66*, 51–57.

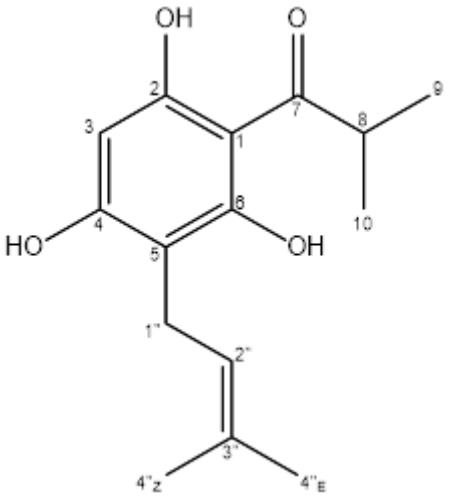

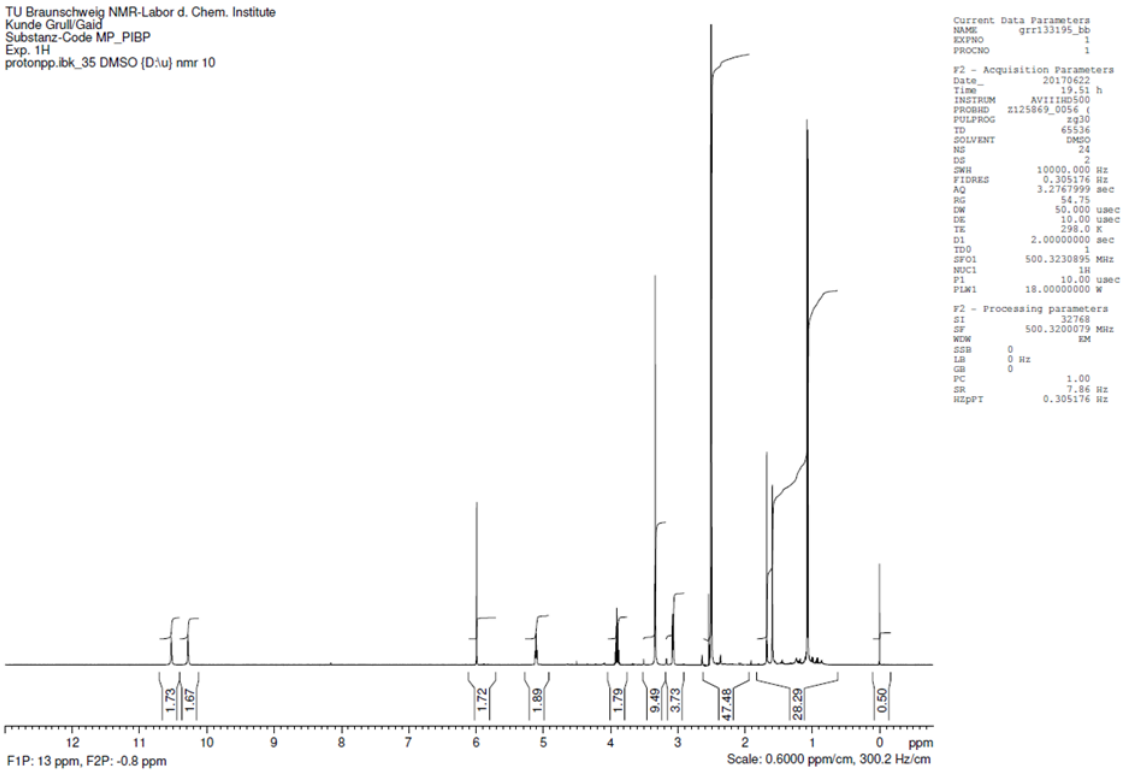

Figure 58: ^{1}H-NMR data for the chemically synthesized 3-prenyl-phlorisobutyrophenone.

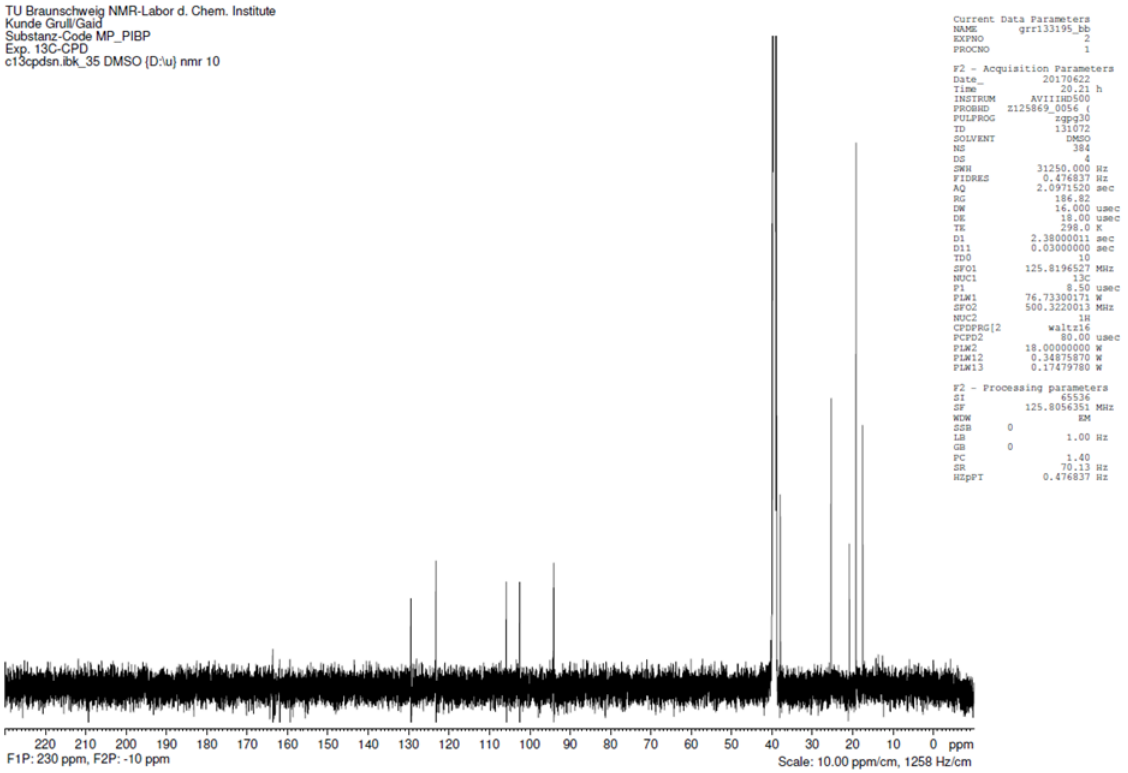

Figure 59: ^{13}C-CPD NMR data for the chemically synthesized 3-prenyl-phlorisobutyrophenone

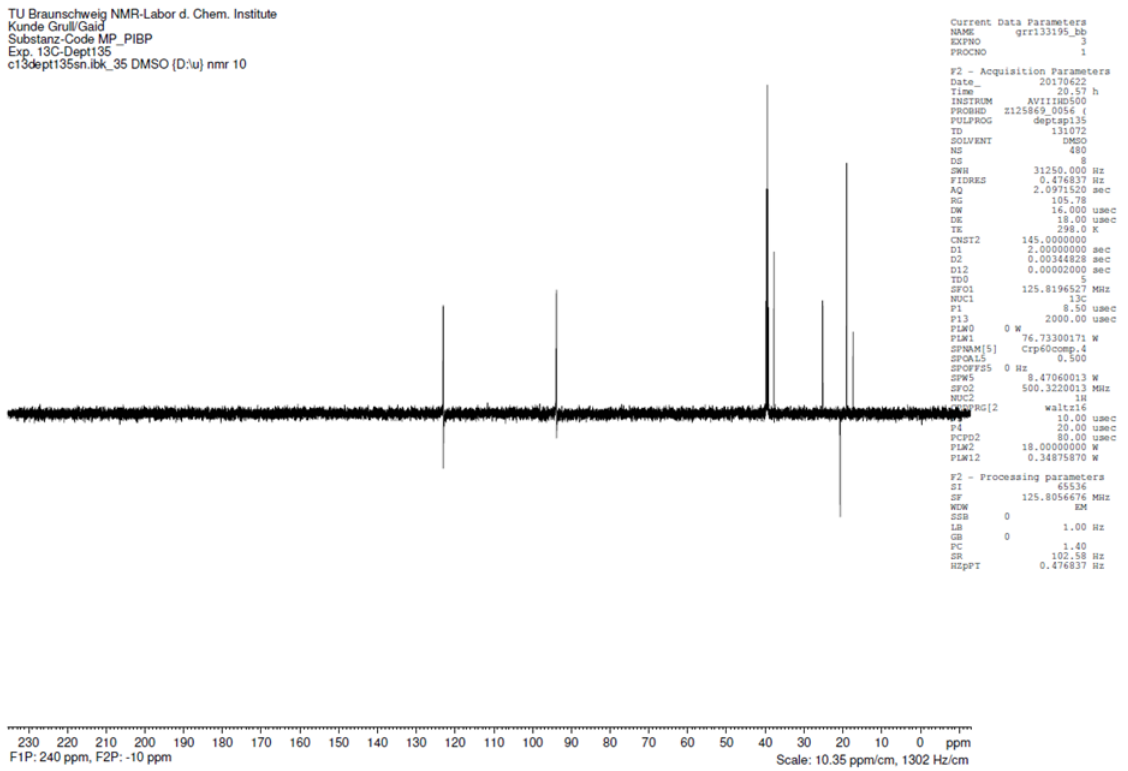

Figure 60: ^{13}C-Dept 135 NMR data for the chemically synthesized 3-prenyl-phlorisobutyrophenone

6.7.5. ^{1}H and ^{13}C-NMR data of chemically synthesized 3-geranyl-2-methylbutanoyl-phloroglucinol

Table 37: NMR data of grr133479[a, b] [CAS No. 72008-04-9]

Position	^{13}C	DEPT	^{1}H[c]	HMBC[d]
1	103.1	C_q		5, 2-OH, 6-OH
2	163.7	C_q		2-OH, (4-OH), (6-OH), 1'
2-OH	-	-	14.21 (s, 1 H)	
3	105.9	C_q		2-OH, 4-OH, 5, 1'
4	162.0	C_q		(2-OH), 4-OH, 1'
4-OH	-	-	10.27 (s, 1 H)	
5	94.1	CH	5.99 (s, 1 H)	4-OH, 6-OH
6	159.5	C_q		5, 6-OH
6-OH	-	-	10.50 (s, 1 H)	
7	209.1	C_q		(5), 8, 9 (both H), 11
8	44.6	CH	3.79 (sext, 6.7 Hz, 1 H)	9 (both H), 10, 11
9	26.4	CH_2	1.72 (dqd, 13.3, 7.4, 6.4 Hz, 1 H) 1.31 (dqd, 13.3, 7.4, 6.9 Hz, 1 H)	8, 10, 11
10	11.8	CH_3	0.84 (t, 7.4 Hz, 3 H)	8, 9 (both H)
11	16.7	CH_3	1.06 (d, 6.8 Hz, 3 H)	8, 9 (both H)
1'	20.8	CH_2	3.08 (br. d, 7.1 Hz, 1')	(5), 2'
2'	123.1	CH	5.12 (t x sext, 7.1, 1.3 Hz, 1 H)	1', 4', 9'
3'	133.0	C_q		1', 4', (5'), 9'
4'	39.2	CH_2	1.89 ("t", ca. 7.6 Hz, 1 H)	2', 5', 9'
5'	26.1	CH_2	1.98 ("q", ca. 7.2 Hz, 1 H)	4', (6')
6'	124.1	CH	5.03 (t x sept, 7.1, 1.4 Hz, 1 H)	4', 5', $8'_E$, $8'_Z$
7'	130.5	C_q		5', $8'_E$, $8'_Z$
$8'_E$	25.4	CH_3	1.59 (br. d, 1.3 Hz, 3 H)	6', $8'_Z$
$8'_Z$	17.4	CH_3	1.52 (br. d, 0.9 Hz, 3 H)	6', $8'_E$
9'	15.8	CH_3	1.69 (br. d, 1.3 Hz, 3 H)	2', 4'

[a] Measuring frequencies: 600.1 MHz (^{1}H), 150.9 MHz (^{13}C); solvent: DMSO-d_6; references: tetramethylsilane (δ_H = 0.00 ppm), solvent (δ_C = 39.50 ppm).
[b] For previous NMR data, see Schmidt et al. (2012): good data, solvent $CDCl_3$.
[c] Some important H,H-NOEs: 1'-9'; 2'-1', 4'; 4'-9'; 5'-4', $8'_Z$, 9'; 6'-(5'), $8'_E$.
[d] Entries in the HMBC column indicate ^{1}H nuclei showing long-range correlations with the ^{13}C chemical shift in the second column. Weak correlations in parentheses.
S. Schmidt, G. Jürgenliemk, H. Skaltsa, J. Heilmann (2012) *Phytochemistry* *77*, 218–225

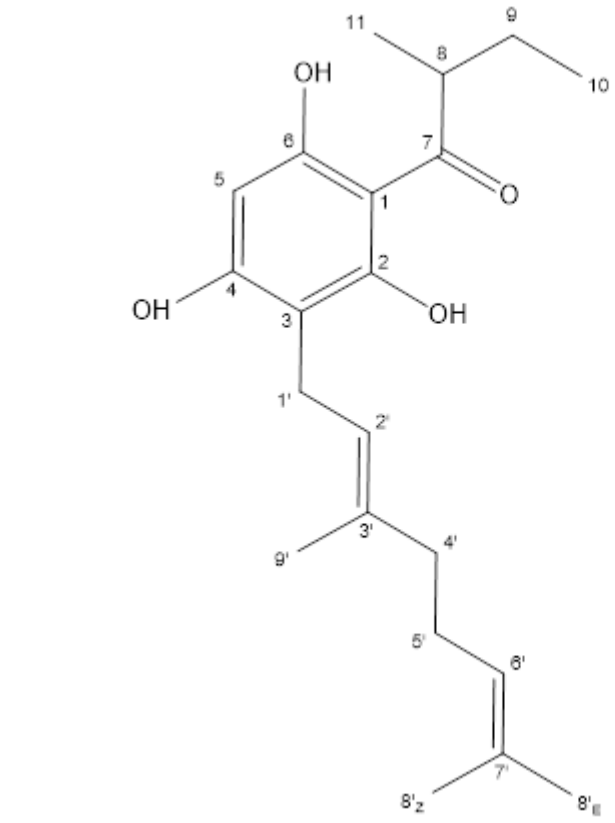

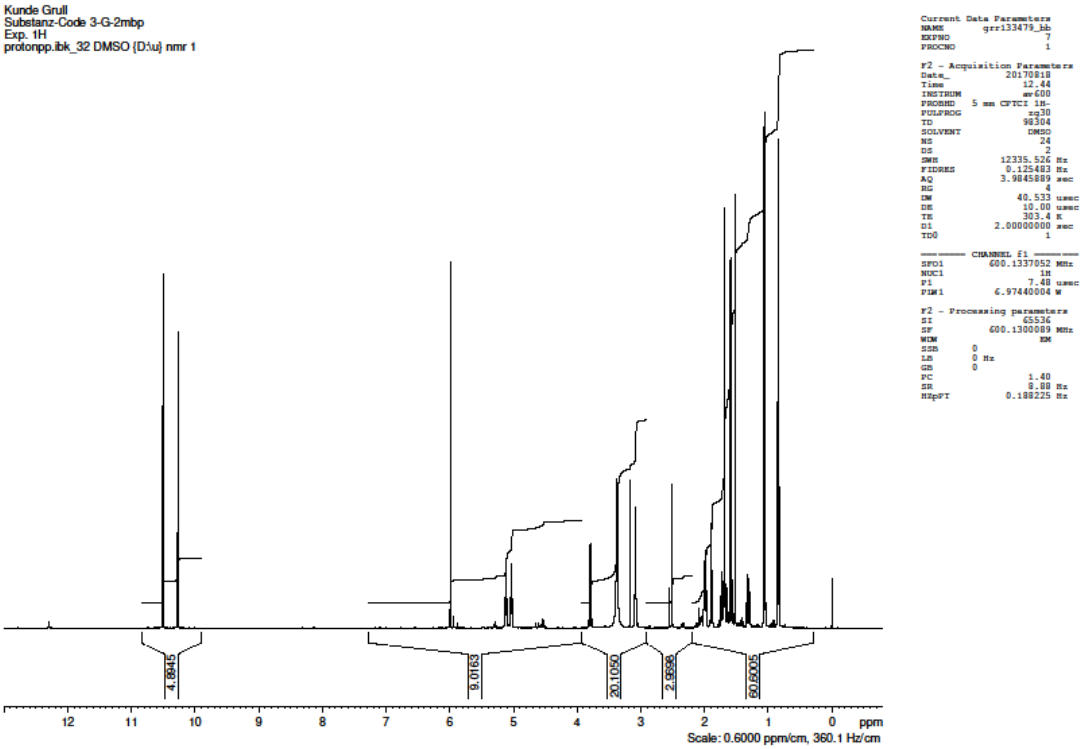

Figure 61: ^{1}H-NMR data for the chemically synthesized 2-methylbutanoyl-phloroglucinol.

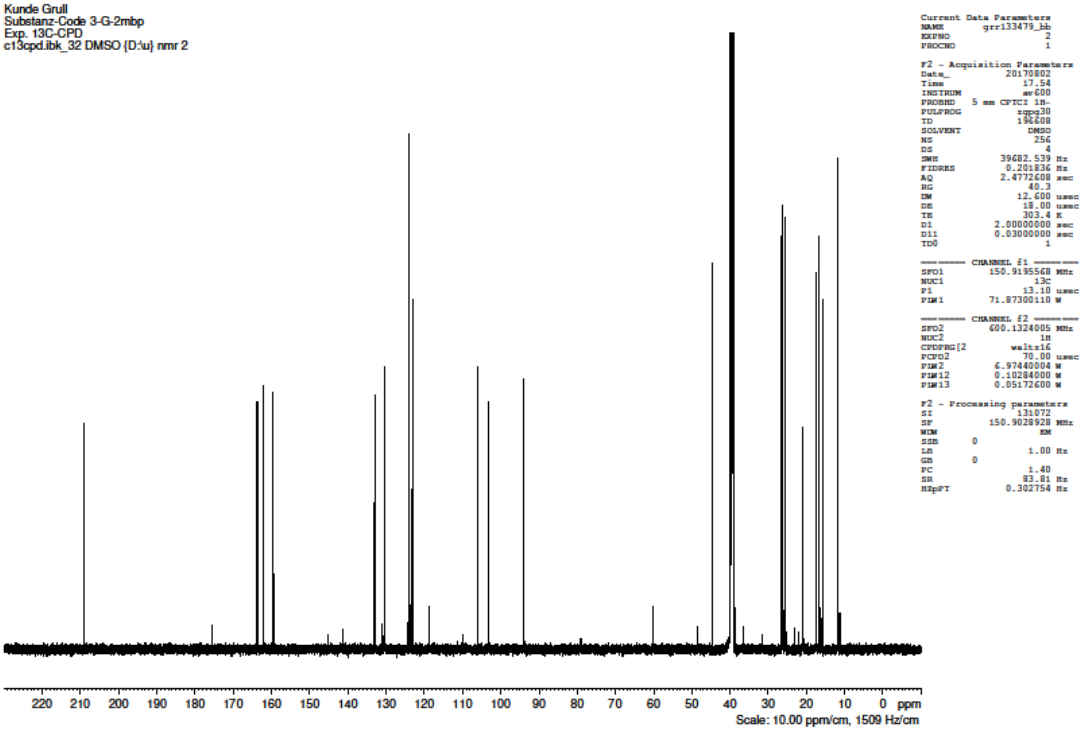

Figure 62: ^{13}C-CPD NMR data for the chemically synthesized 2-methylbutanoyl-phloroglucinol.

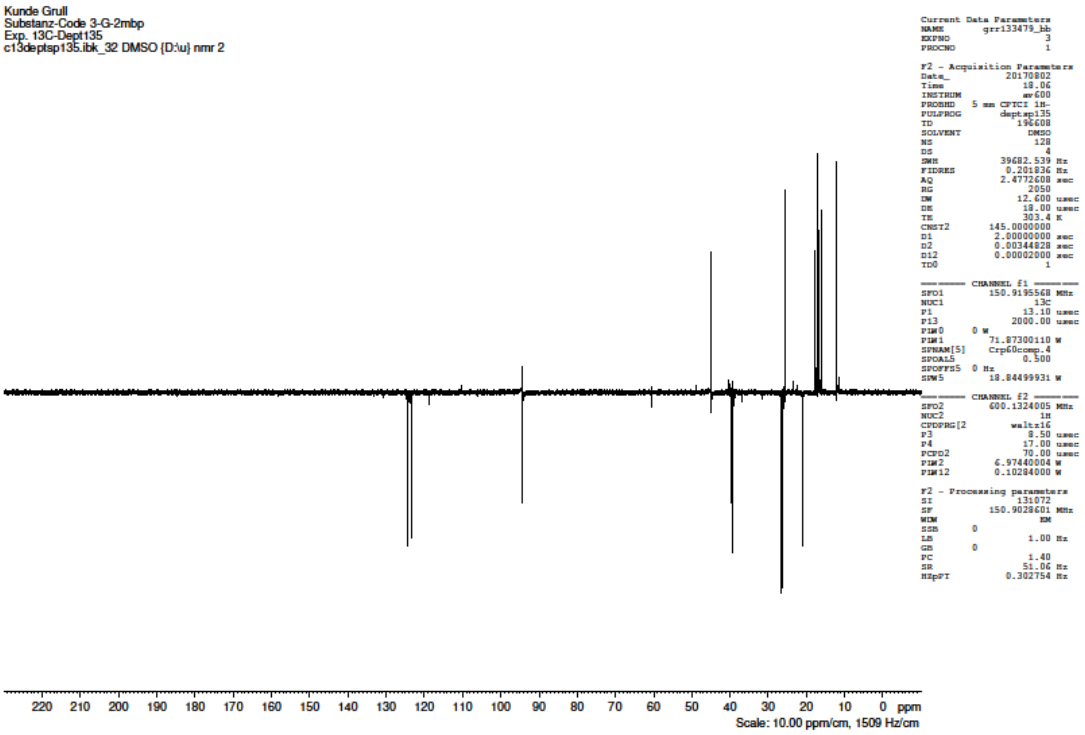

Figure 63: ^{13}C-Dept 135 NMR data for the chemically synthesized 2-methylbutanoyl-phloroglucinol.

6.7.6. ^{1}H and ^{13}C-NMR data for chemically synthesized 3-geranyl-phlorisovalerophenone

Table 38: NMR data of grr133197[a, b] [CAS No. 144785-80-8]

Position	^{13}C	DEPT	^{1}H	HMBC[c]
1	105.1	C_q		5
2	162.5	C_q		1'
3	105.5	C_q		5, 1'
4	160.8	C_q		5, 1'
5	95.3	CH	5.83 (s, 1 H)	-
6	160.0	C_q		5
7	205.9	C_q		8
8	52.9	CH_2	2.94 (d, 6.7 Hz, 2 H)	9, 10, 11
9	25.2	CH	2.26 (nonet, 6.7 Hz, 1 H)	8, 10, 11
10, 11	22.8	CH_3	0.97 (d, 6.7 Hz, 6 H)	8, 9, 10, 11
1'	21.6	CH_2	3.37 (br. d, 7.2 Hz, 2 H)	(2')
2'	121.5	CH	5.25 (t x sext, 7.2, 1.3 Hz, 1 H)	1', 4'/5', 9'
3'	140.1	C_q		1', 4'/5', 9'
4'	39.7	CH_2	2.14-2.06 (m, 2 H)	2', 5', 9'
5'	26.3	CH_2	2.14-2.06 (m, 2 H)	4'
6'	123.6	CH	5.05 (t x sept, 6.9, 1.4 Hz, 1 H)	4'/5', $8'_E$, $8'_Z$
7'	132.2	C_q		4'/5', $8'_E$, $8'_Z$
$8'_E$	25.7	CH_3	1.68 (br. d, 1.2 Hz, 3 H)	(6'), $8'_Z$
$8'_Z$	17.7	CH_3	1.60 (br. d, 0.9 Hz, 3 H)	(6'), $8'_E$
9'	16.2	CH_3	1.82 (q, 1.3 Hz, 3 H)	2', 4'/5'

[a] Measuring frequencies: 500.3 MHz (^{1}H), 125.8 MHz (^{13}C); solvent: $CDCl_3$; references: tetramethylsilane (δ_H = 0.00 ppm), solvent (δ_C = 77.01 ppm).
[b] For previous NMR data, see Rios and Delgado (1992). Their ^{1}H NMR data are incomplete and the ^{13}C NMR spectrum was taken from a 3:3:1-mixture of three compounds.
[c] Entries in the HMBC column indicate ^{1}H nuclei showing long-range correlations with the ^{13}C chemical shift in the second column. Weak correlations in parentheses. 4'/5' stands for 4' and/or 5'.
M. Y. Rios, G. Delgado (1992) *Phytochemistry 31*, 3491–3494

Figure 64: ^{1}H-NMR data for the chemically synthesized 3-geranyl-phlorisovalerophenone.

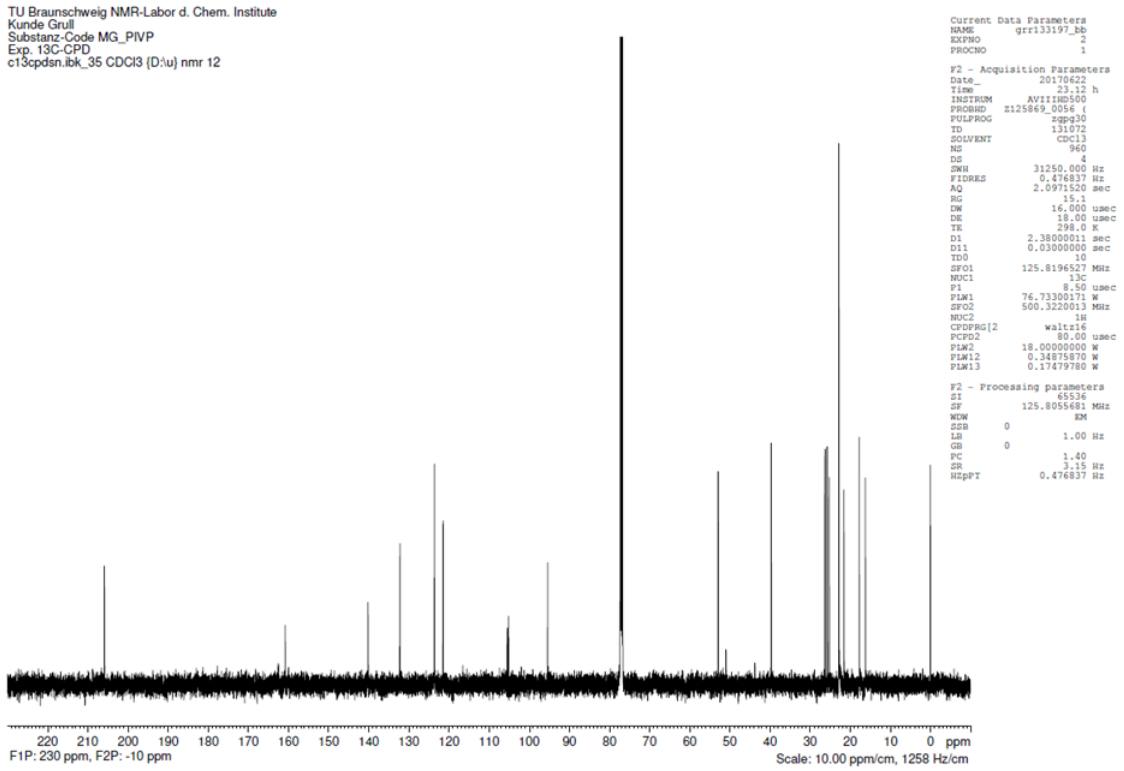

Figure 65: ^{13}C-CDP NMR data for the chemically synthesized 3-geranyl-phlorisovalerophenone.

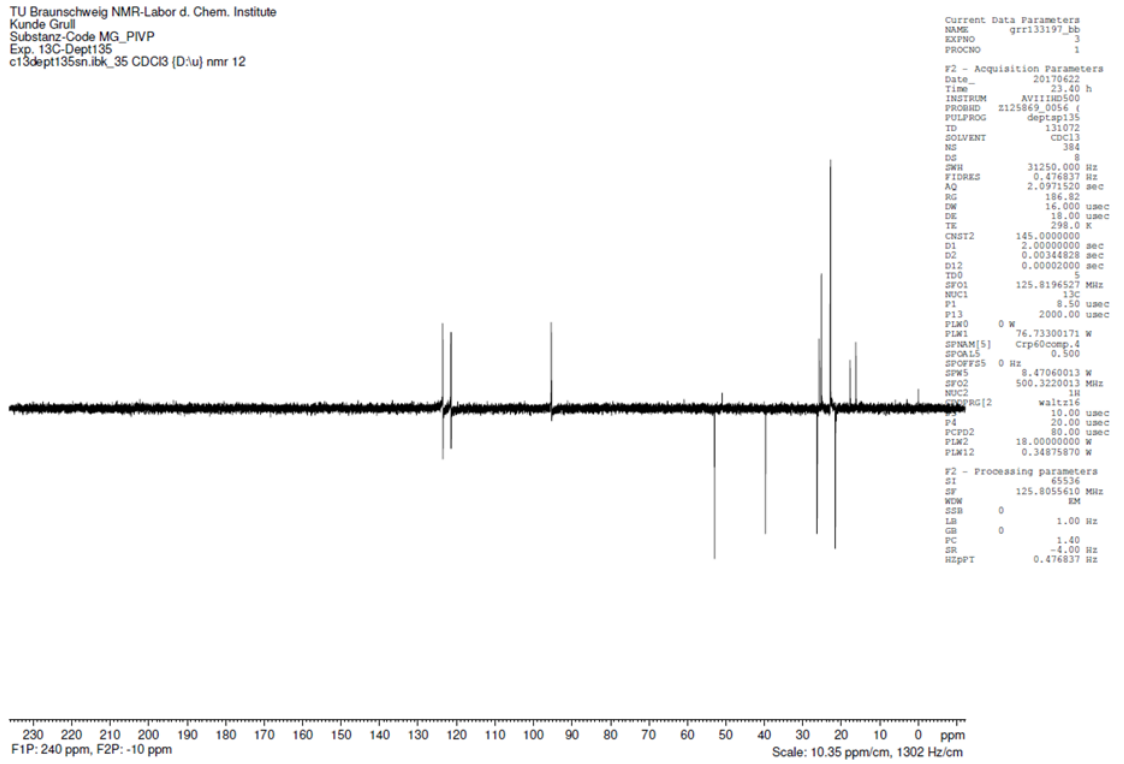

Figure 66: ^{13}C-Dept 135 NMR data for the chemically synthesized 3-geranyl-phlorisovalerophenone.

6.7.7. ^{1}H and ^{13}C-NMR data for chemically synthesized 3-geranyl-phloracetophenone

Table 39: NMR data of grr133196[a, b] [CAS No. 43230-43-9]

Position	13C	DEPT	1H	HMBC[c, d]
1	105.2	C_q		5, 8
2	162.4	C_q		1'
3	105.4	C_q		5, 1', (2')
4	161.2	C_q		5, 1'
5	95.3	CH	5.86 (s, 1 H)	
6	160.4	C_q		5
7	203.6	C_q		(5), 8
8	32.9	CH_3	2.67 (s, 3 H)	
1'	21.5	CH_2	3.37 (dd, 7.2, 0.4 Hz, 2 H)	(5), 2'
2'	121.4	CH	5.25 (t x sext, 7.2, 1.3 Hz, 1 H)	1', 4'/5', 9'
3'	140.1	C_q		1', 4'/5', 9'
4'	39.7	CH_2	2.13-2.07 (m, 2 H)	2', 5', (6'), 9'
5'	26.2	CH_2	2.13-2.07 (m, 2 H)	4', 6'
6'	123.6	CH	5.05 (t x sept, 7.0, 1.4 Hz, 1 H)	4'/5', $8'_E$, $8'_Z$
7'	132.2	C_q		4'/5', $8'_E$, $8'_Z$
$8'_E$	25.7	CH_3	1.68 (br. d, 1.2 Hz, 3 H)	6', $8'_Z$
$8'_Z$	17.7	CH_3	1.60 (br. d, 0.9 Hz, 3 H)	6', $8'_E$
9'	16.2	CH_3	1.81 (br. d, 1.3 Hz, 3 H)	2', 4'/5'

[a] Measuring frequencies: 500.3 MHz (^{1}H), 125.8 MHz (^{13}C); solvent: $CDCl_3$; references: tetramethylsilane (δ_H = 0.00 ppm), solvent (δ_C = 77.01 ppm).
[b] For previous NMR data, see Basabe et al. (2010). Their ^{13}C NMR spectrum is unassigned and has inconsistencies in the C_{ar}–O region, similarly in Lee et al. (2008).
[c] Entries in the HMBC column indicate ^{1}H nuclei showing long-range correlations with the ^{13}C chemical shift in the second column. Weak correlations in parentheses. 4'/5' etc. stands for 4' and/or 5'.
[d] Experiment carried out with NUS (non-uniform sampling with a data sample of 50 per cent).
P. Basabe, M. de Román, I. S. Marcos, D. Diez, A. Blanco, O. Bodero, F. Mollinedo, B. G. Sierra, J. G. Urones (2010) *Eur. J. Med. Chem. 45*, 4258–4269. Y. R. Lee, X. Li, J. H. Kim (2008) *J. Org. Chem. 73*, 4313–4316.

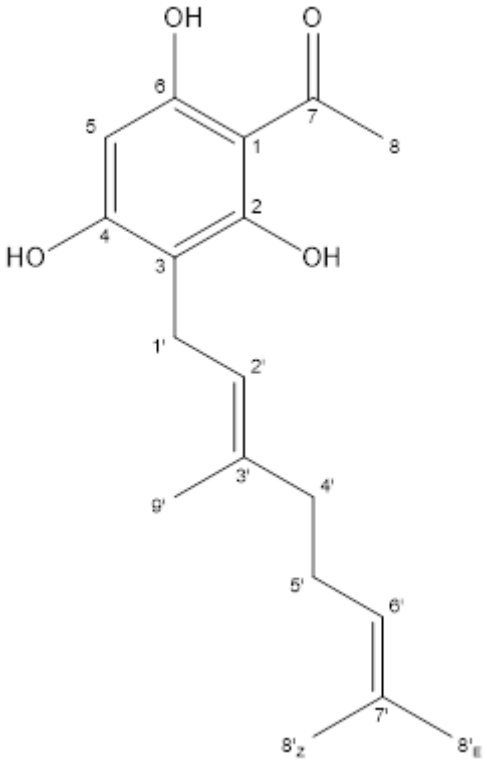

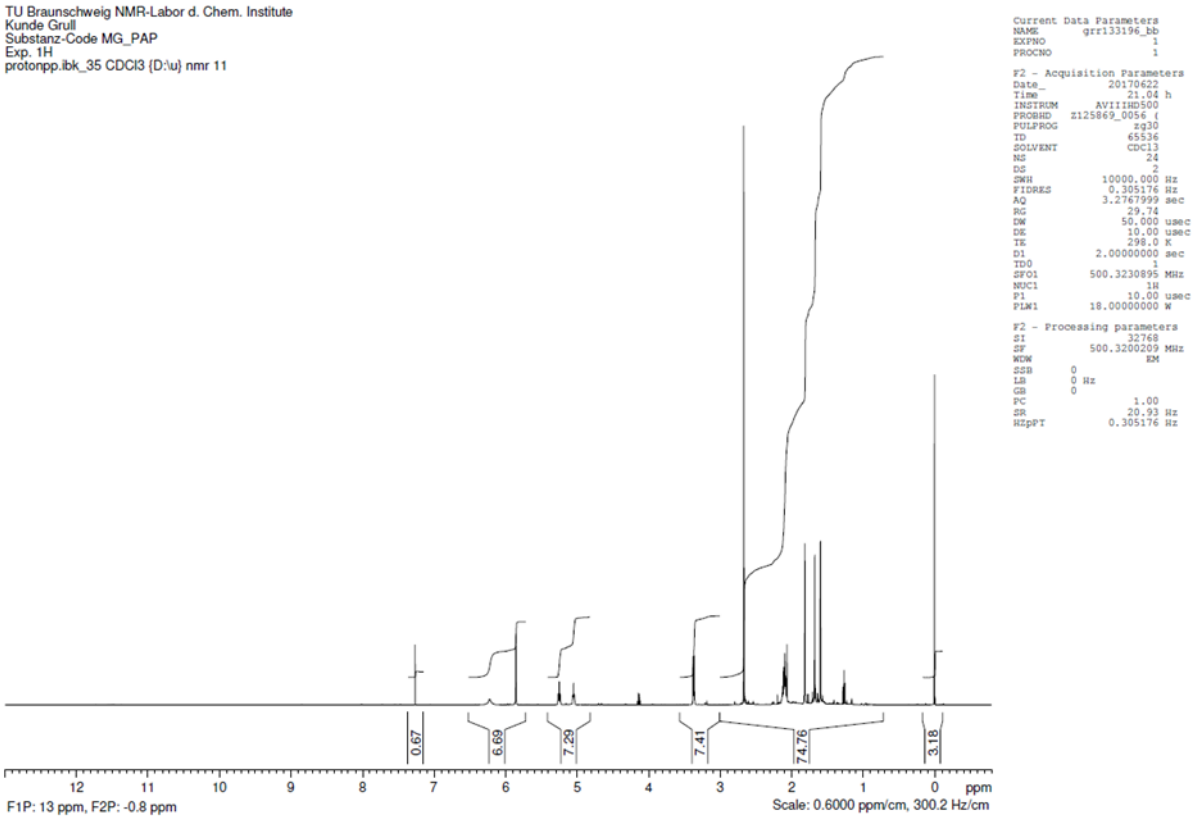

Figure 67: ^{1}H-NMR data for the chemically synthesized 3-geranyl-phloracetophenone.

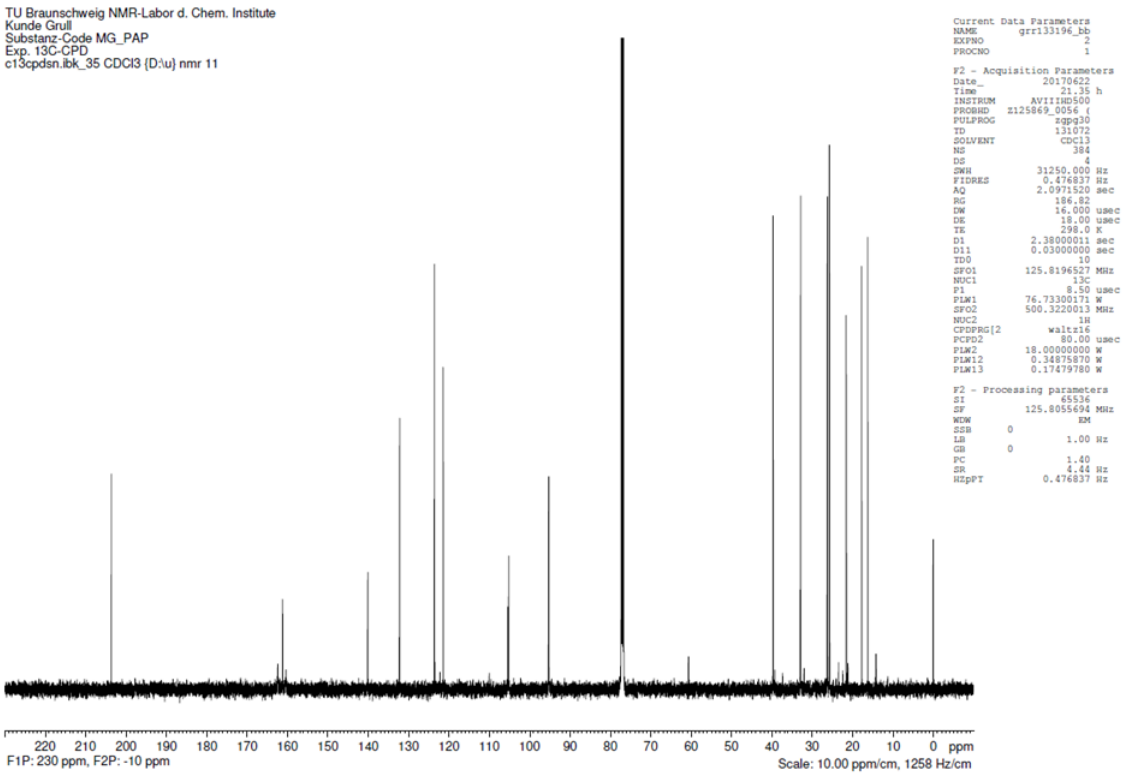

Figure 68: ^{13}C-CPD NMR data for the chemically synthesized 3-geranyl-phloracetophenone.

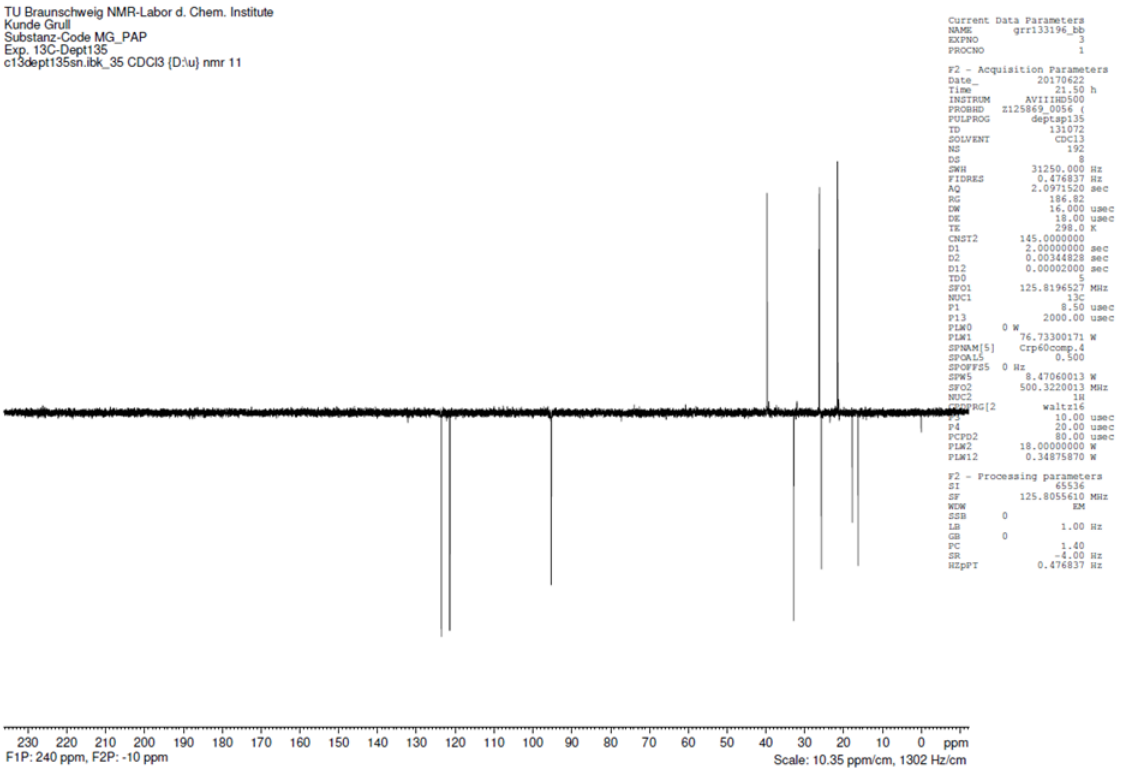

Figure 69: ^{13}C-Dept 135 NMR data for the chemically synthesized 3-geranyl-phloracetophenone.

6.7.8. ^{1}H and ^{13}C-NMR data for chemically synthesized 3-geranyl-phlorbenzophenone

Table 40: NMR data of grr133480[a, b] [CAS No. 70219-87-3]

Position	^{13}C	DEPT	^{1}H[c]	HMBC[d]
1	104.5	C_q	-	2-OH, 5
2	160.8	C_q	-	(2-OH), 1'
2-OH			10.28 (s, 1 H)	
3	106.5	C_q	-	2-OH, 5, 1'
4	162.8	C_q	-	5, 1'
5	96.2	CH	5.94 (s, 1 H)	-
6	159.4	C_q	-	5
7	197.8	C_q	-	(5), 9, 13
8	140.1	C_q	-	10, 12
9, 13	127.9	2 CH	7.64 ("d", 2 H)	9, (10), (11), (12), 13
10, 12	129.0	2 CH	7.50 ("t", 2 H)	10, 12
11	132.1	CH	7.57 ("t", 1 H)	9, 13
1'	21.6	CH_2	3.37 (br. d, 7.1 Hz, 2 H)	(5), 2'
2'	121.5	CH	5.26 (t x sext, 7.1, 1.4 Hz, 1 H)	1', (4'), 9'
3'	139.2	C_q	-	1', 4', 9'
4'	39.7	CH_2	2.07 (m, 2 H)	(1'), 2', 5', 9'
5'	26.3	CH_2	2.10 (m, 2 H)	4', (6')
6'	123.7	CH	5.05 (t x sept, 6.8, 1.4 Hz, 1 H)	(5'), $8'_E$, $8'_Z$
7'	132.1	C_q	-	$8'_E$, $8'_Z$
$8'_E$	25.7	CH_3	1.66 (br. d, 1.2 Hz, 3 H)	6', $8'_Z$
$8'_Z$	17.7	CH_3	1.59 (br. d, 0.9 Hz, 3 H)	6', $8'_E$
9'	16.2	CH_3	1.79 (br. d, 1.3 Hz, 3 H)	2', 4'

[a] Measuring frequencies: 600.1 MHz (^{1}H), 150.9 MHz (^{13}C); solvent: $CDCl_3$; references: tetramethylsilane (δ_H = 0.00 ppm), solvent (δ_C = 77.01 ppm).
[b] For previous ^{1}H NMR data, see Bohlmann and Suwita (1980). Their assignments of protons $8'_E$ and $8'_Z$ should be interchanged.
[c] Some important H,H-NOEs: 1'-9'; 2'-1', 4', (5'); 4'-9'; 5'-$8'_Z$, 9'; 6'-4', 5', $8'_E$.
[d] Entries in the HMBC column indicate ^{1}H nuclei showing long-range correlations with the ^{13}C chemical shift in the second column. Weak correlations in parentheses.

F. Bohlmann, A. Suwita (1980) *Phytochemistry 19*, 683–684

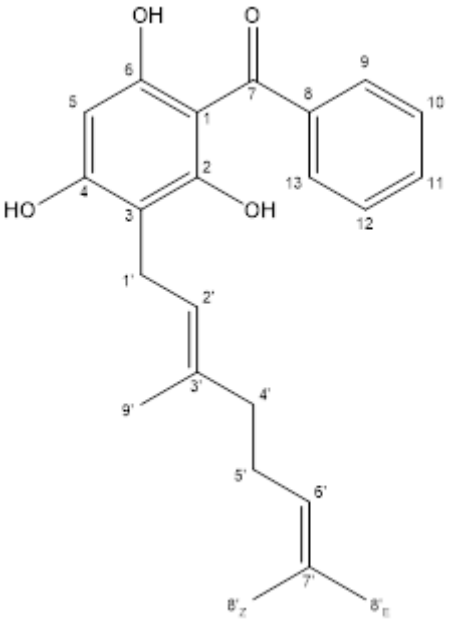

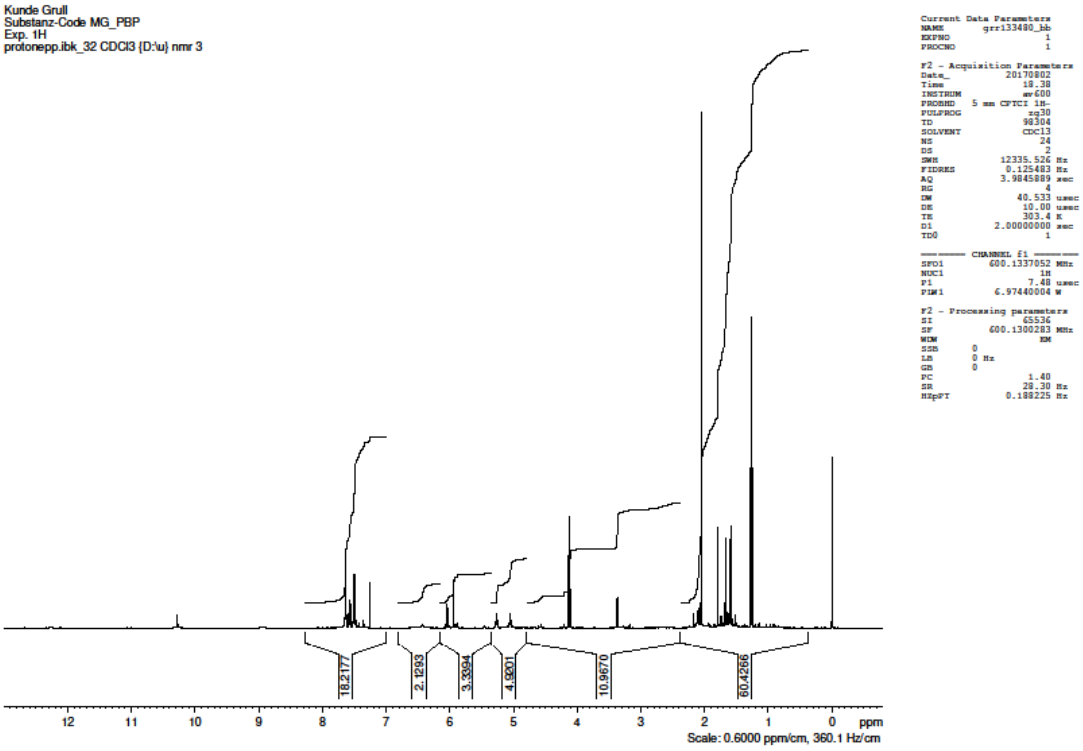

Figure 70: ^{1}H-NMR data for the chemically synthesized 3-geranyl-phlorbenzophenone.

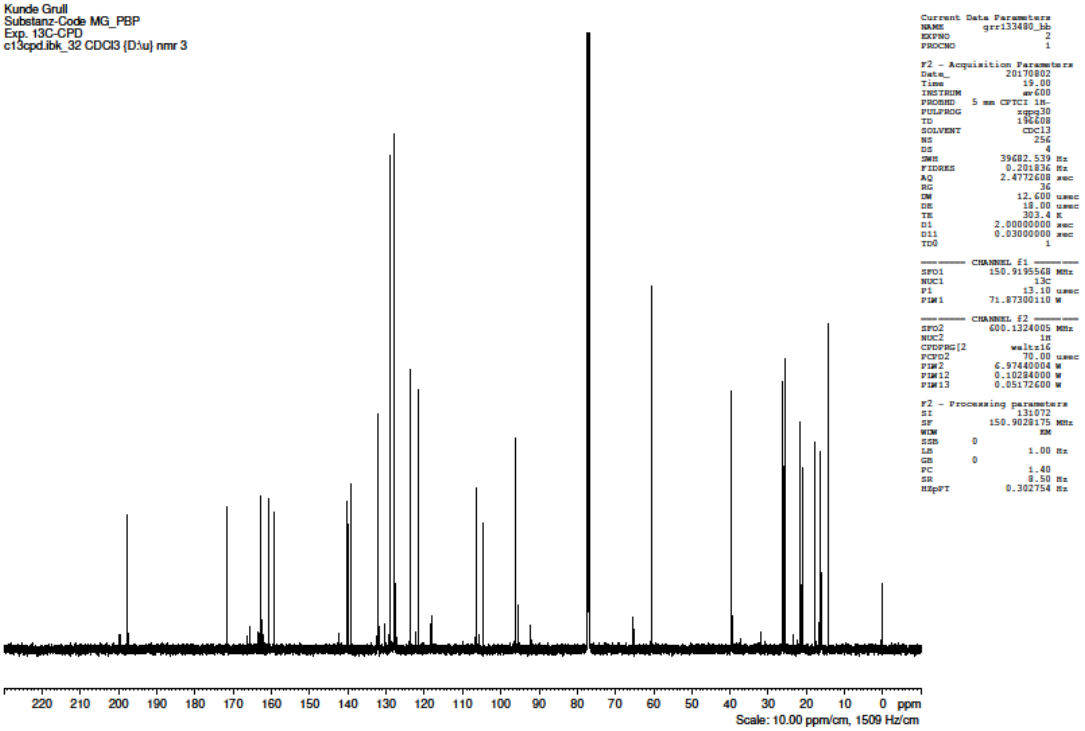

Figure 71: ^{13}C-CPD NMR data for the chemically synthesized 3-geranyl-phlorbenzophenone.

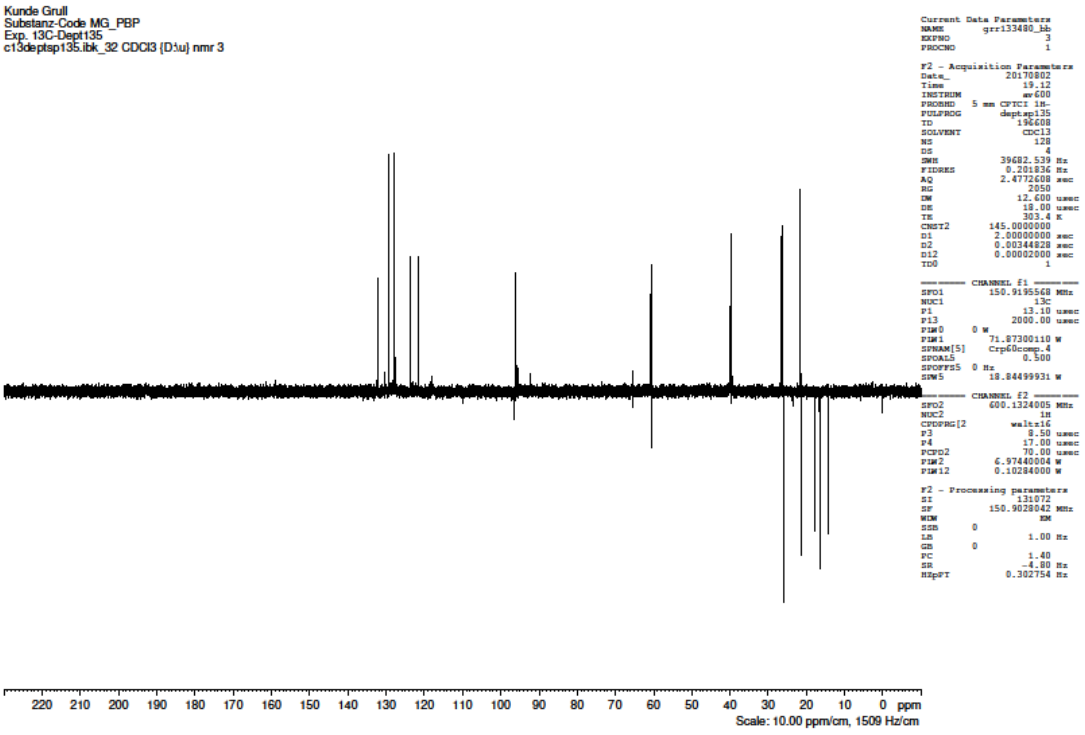

Figure 72: ^{13}C-Dept 135 NMR data for the chemically synthesized 3-geranyl-phlorbenzophenone.

6.7.9. ^{1}H and ^{13}C-NMR data of the *Hp*PT2 product from incubation with phlorisobutyrophenone and GPP

Table 41: ^{1}H and ^{13}C nuclear magnetic resonance (NMR) data of 3-geranyl-2,4,6-trihydroxyisobutyrophenone (**1**) in $CDCl_3$

Position	^{13}C[a]	^{1}H[a,b]	HMBC[c,d]
1	104.1	-	(5)
2	162.8	-	11
3	105.8	-	(5), 11, 12, (20)
4	160.8	-	(5), 11
5	95.3	5.89 (s, 1 H)	-
6	159.8	-	(5)
7	210.6	-	8, 9/10
8	39.2	3.89 (sept, *J* = 6.7 Hz, 1 H)	9/10
9, 10	19.3	1.17 (d, *J* = 6.7 Hz, 6 H)	8, 9/10
11	21.6	3.36 (d, *J* = 7.2 Hz, 2 H)	12
12	121.6	5.25 (t x sext, *J* = 7.2, ≈1.2 Hz, 1 H)	11, (14), 20
13	139.5	-	11, 14, 20
14	39.7	2.10 (m, 2 H)	12, 15, 20
15	26.3	2.06 (m, 2 H)	14, 16
16	123.7	5.05 (t x sept, *J* = 6.8, ≈1.4 Hz, 1 H)	15, 18, 19
17	132.1	-	(15), 18, 19
18	25.7	1.67 (d, *J* ≥1.1 Hz, 3 H)	16, 19
19	17.7	1.59 (br. s, 3 H)	(16), 18
20	16.2	1.81 (br. s, 3 H)	12, 14

[a] Chemical shifts in ppm: δ_C relative to $CDCl_3$ (δ = 77.01 ppm) and δ_H relative to TMS (δ = 0.00 ppm).

[b] δ_H of OH protons at 11.9, 8.7 and 6.5 ppm, broad signals, unassigned.

[c] Entries in the HMBC column indicate ^{1}H nuclei showing long-range correlations with the ^{13}C chemical shift in the second column.

[d] Weak correlations in parentheses.

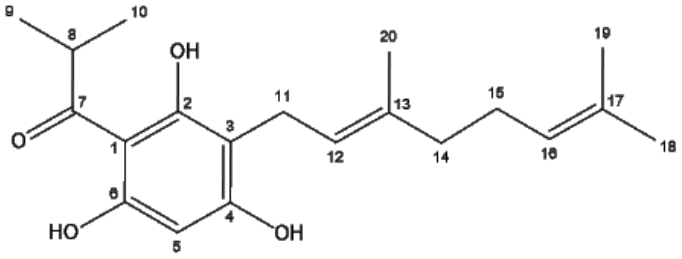
9
10
8
OH
20
19
7
2
11
13
15
17
O
3
1
12
14
16
18
6
4
HO
OH
5

6.7.10. ^{1}H and ^{13}C-NMR data of the *Hp*PT2 product from incubation with phlorisobutyrophenone and DMAPP

Table 42: NMR data of gam129944[a, b] ("DP_PiBP4") [CAS No. 72008-03-8]

Position	^{13}C	DEPT	^{1}H[c]	HMBC[d]
1	104.2	C_q	-	5
2	162.6	C_q	-	1'
3	105.6	C_q	-	1', 5
4	160.7	C_q	-	1', 5
5	95.5	CH	5.83 (s, 1 H)	-
6	159.7	C_q	-	5
7	210.5	C_q	-	(8), 9, 10
8	39.3	CH	3.88 (sept, 6.7 Hz, 1 H)	9, 10
9, 10	19.3	2 CH_3	1.18 (d, 6.7 Hz, 6 H)	8, 9, 10
1'	21.6	CH_2	3.38 (br. d, 7.2, 2 H)	(2')
2'	121.4	CH	5.26 (t x sext, 7.2, 1.2 Hz, 1 H)	1, 4', 9'
3'	140.2	C_q	-	1, 4', 9'
4'	39.7	CH_2	2.09 (m, 2 H)	(2'), 5', 9'
5'	26.3	CH_2	2.11 (m, 2 H)	4'
6'	123.6	CH	5.05 (t x sept, 7.2, 1.2 Hz, 1 H)	5', 8'$_E$, 8'$_Z$
7'	132.2	C_q	-	(5'), 8'$_E$, 8'$_Z$
8'E	25.7	CH_3	1.68 (q, 1.1 Hz, 3 H)	(6'), 8'$_Z$
8'Z	17.7	CH_3	1.60 (br. "s", 3 H)	8'$_E$
9'	16.2	CH_3	1.82 (q, 1.1 Hz, 3 H)	(2'), (4')

[a] Measuring frequencies: 600.1 MHz (^{1}H), 150.9 MHz (^{13}C); solvent: $CDCl_3$; references: tetramethylsilane (δ_H = 0.00 ppm), solvent (δ_C = 77.01 ppm).

[b] For previous ^{1}H NMR data, see Bohlmann and Zdero (1979); their δ_H values differ by 0.05–0.06 ppm from ours and their 8'$_E$/8'$_Z$-assignments should be interchanged.

[c] H,H-COSY cross-peaks: 8 – 9, 10; 1' – 4', 9'; 2' – 1', 4', 9'; 4' – (9'); 5' – 8'$_E$, 8'$_Z$; 6' – 5', 8'$_E$, 8'$_Z$.

[d] Entries in the HMBC column indicate ^{1}H nuclei showing long-range correlations with the ^{13}C chemical shift in the second column. Weak correlations in parentheses.

F. Bohlmann, C. Zdero (1979) *Phytochemistry 18*, 641–644.

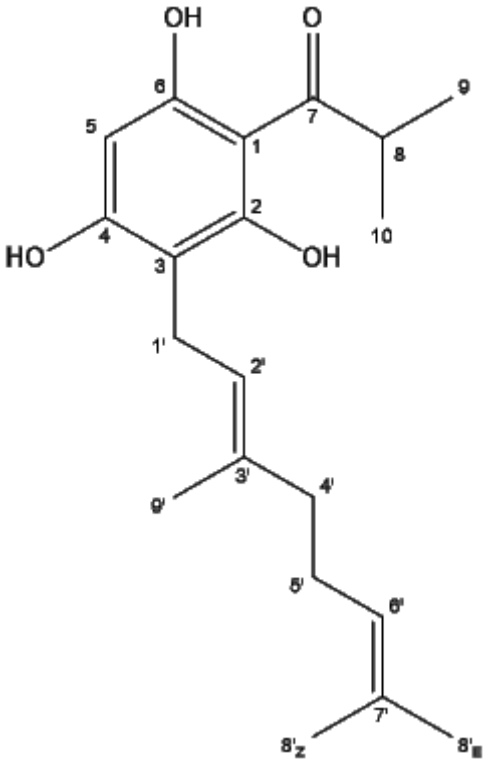
OH
O
6
9
7
5
1
8
2
10
4
HO
3
OH
1'
2'
3'
4'
9'
5'
6'
7'
8'Z
8'E

6.7.11. ^{1}H and ^{13}C-NMR data of the *Hp*PT6 product from incubation with 3-geranyl-phlorisobutyrophenone and DMAPP

Table 43: NMR data of grr132394[a]

Position	^{13}C[b]	DEPT[c]	^{1}H[d]	HMBC[e]
1		C_q	-	
2		C_q	-	
2-OH	-	-		
3		C_q	-	
4		C_q	-	
4-OH	-	-		
5		C_q	-	
6		C_q	-	
6-OH	-	-		
7	210.6	C_q	-	8, 9, 10
8	38.4	CH	3.98 (sept, 6.8 Hz, 1 H)	9, 10
9, 10	19.5	2 CH_3	1.09 (d, 6.8 Hz, 6 H)	8, 9, 10
1', 1''	21.5	2 CH_2	3.24 (br. d, 6.7 Hz, 4 H)	(2, 2'')
2'	123.0	CH	5.05 (m, 1 H)	1', 4', 9'
3'	133.7	C_q	-	1', 4', 9'
4'	39.3	CH_2	1.90 (m, 2 H)	(2'), (9')
5'	26.1	CH_2	1.99 (m, 2 H)	4'
6'	124.1	CH	5.04 (m, 1 H)	4', 5', 8'$_E$, 8'$_Z$
7'	130.6	C_q	-	5', 8'$_E$, 8'$_Z$
8'$_E$	25.46	CH_3	1.59 (br. d, 1.3 Hz, 3 H)	8'$_Z$
8'$_Z$	17.5	CH_3	1.52 (br. d, 1.1 Hz, 3 H)	6', 8'$_E$
9'	16.0	CH_3	1.70 (br. d, 1.3 Hz, 3 H)	2', 4'
2''	123.3	CH	5.04 (m, 1 H)	1'', 4''$_E$, 4''$_Z$
3''	130.1	C_q	-	1'', 4''$_E$, 4''$_Z$
4''$_E$	25.51	CH_3	1.61 (br. d, 1.3 Hz, 3 H)	4''$_Z$
4''$_Z$	17.8	CH_3	1.69 (br. d, 1.1 Hz, 3 H)	2'', 4''$_E$

[a] Measuring frequencies: 600.1 MHz (^{1}H), 150.9 MHz (^{13}C); solvent: DMSO-d_6; references: tetramethylsilane (δ_H = 0.00 ppm), solvent (δ_C = 39.50 ppm).
[b] Due to lack of material ^{13}C chemical shifts had to be taken from the 2D HSQC and HMBC spectra.
[c] DEPT information from a multiplicity-edited HSQC spectrum.
[d] Some important H,H-COSY crosspeaks: 2' - 1', 9'; 6'/2'' - 1'', 4''$_E$, 4''$_Z$, 8'$_E$, 8'$_Z$; 8 - 9, 10; 1'/1'' - 4', 4''$_E$, 4''$_Z$; 5' - 4', 8'$_E$, 8'$_Z$; 4' - (9'); 8 - 9, 10.
[e] Entries in the HMBC column indicate ^{1}H nuclei showing long-range correlations with the ^{13}C chemical shift in the second column. Weak correlations in parentheses.

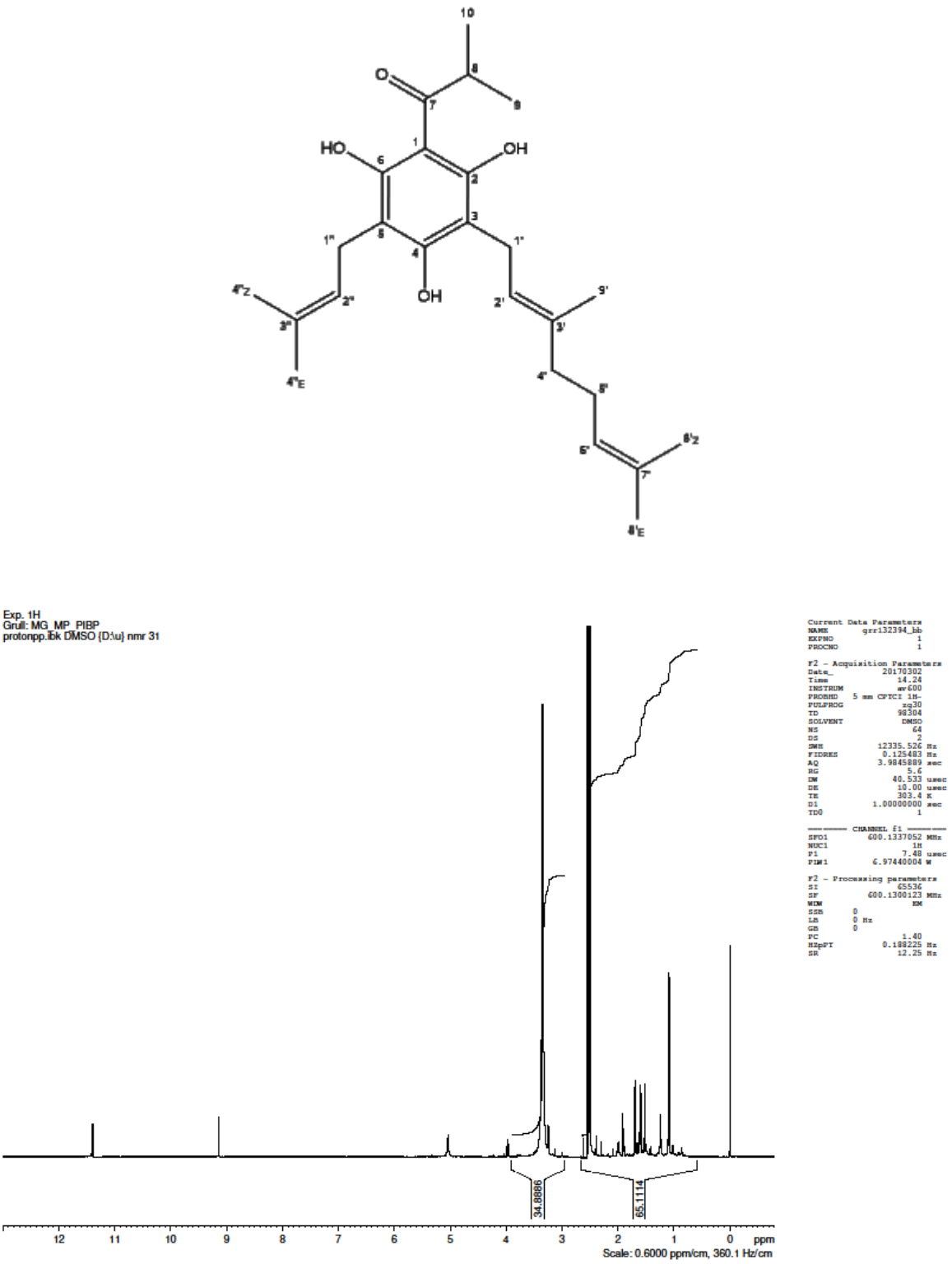

Figure 73: ^{1}H-NMR data of the enzymatic product 3-geranyl-5-prenyl-phlorisobutyrophenone.

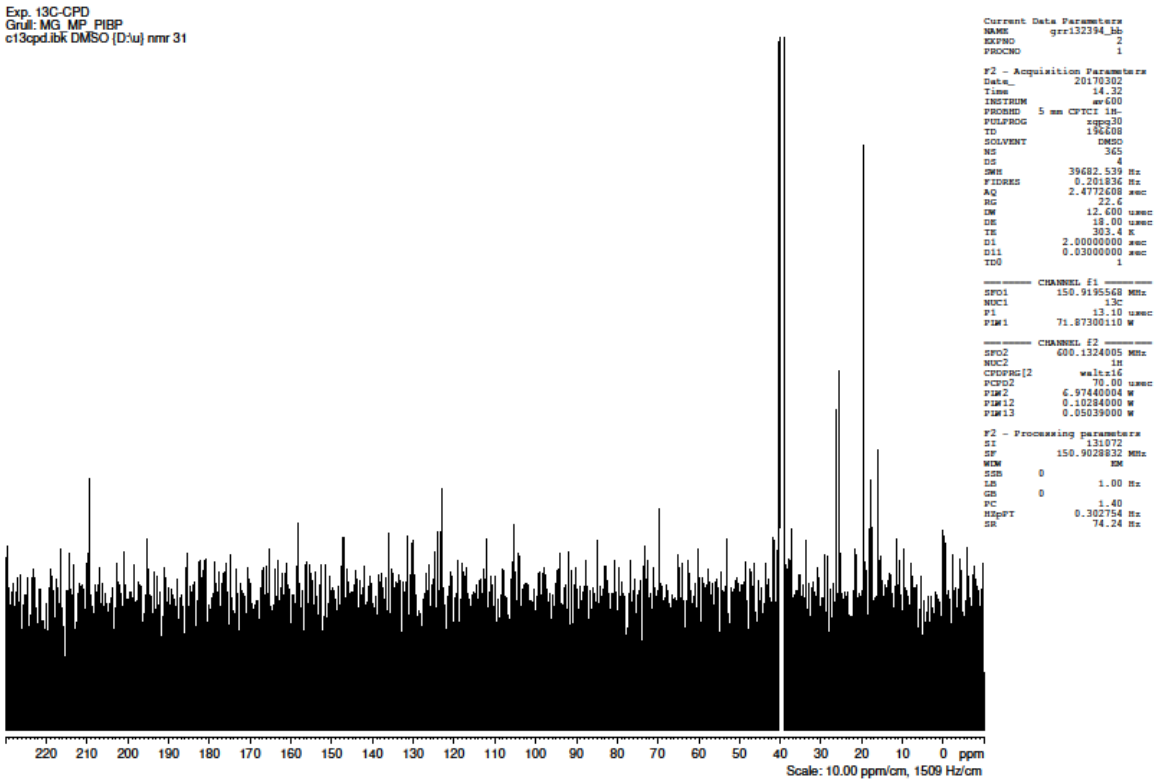

Figure 74: ^{13}C-CPD NMR data data of the enzymatic product 3-geranyl-5-prenyl-phlorisobutyrophenone.

Curriculum Vitae

Personal information:

Name:	Marco Grull
Date of Birth:	21.08.1986
Place of birth:	Eberswalde – Finow
Nationality:	German

Education:

Nov. 2014 – Oct. 2017	**TU - Braunschweig (GER)** Ph.D. in the Institute of Pharmaceutical Biology (Georg-Christoph-Lichtenberg-Stipendium)
Oct. 2012 – Oct. 2014	**RWTH Aachen University (GER)** M.Sc. Biology; Major: Microbiology and Genetics, White/Red Biotechnology
Sep. 2009 – Sep. 2012	**University of Applied Science, Bonn Rhine Sieg (GER)** Degree: B.Sc. Applied Biology Major: Human Biology, Microbiology, and Molecular Genetics
Sep. 2004 – Jul. 2007	**Rhine Academy e.V. Cologne (GER)** Degree: State-approved biological technical assistant
Aug. 1998 – Jul. 2004	**Secondary School: Realschule Bopfingen (GER)**